A NUMERICAL STUDY OF RUPTURE PROPAGATION AND EARTHQUAKE SOURCE MECHANISM

by

SHAMITA DAS

B.Sc., University of Calcutta (1965)

M.Sc., University of Calcutta (1968)

M.S., Boston College (1972)

SUBMITTED IN

PARTIAL FULFILLMENT

OF THE REQUIREMENTS FOR THE

DEGREE OF DOCTOR OF SCIENCE

at the

MASSACHUSETTS INSTITUTE OF TECHNOLOGY

July, 1976

Signature of Author.....

Department of Earth and Planetary Sciences, July , 1976.....

Certified by..... .....
Thesis Supervisor

Accepted by.....
Chairman, Departmental Committee on Graduate Students

ABSTRACT

A Numerical Study of Rupture Propagation

And Earthquake Source Mechanisms

by

Shamita Das

Submitted to the Department of Earth
and Planetary Sciences in July 1976
in partial fulfillment of the
requirements for the degree of
Doctor of Science

Rupture propagation in an elastic medium represents an important aspect of seismic source mechanism of an earthquake. In this thesis, we present a numerical technique to determine the displacement and stress fields due to propagation of two-dimensional shear cracks in an infinite, homogeneous medium which is linearly elastic everywhere off the crack-plane. Starting from the representation theorem, an integral equation for the displacements inside the crack is found. This integral equation is solved for various initial and boundary conditions on the crack surface. Tests of the numerical method are made against the analytical solution of Kostrov and the numerical solution of Madariaga. A critical stress-jump across the tip of a crack is used as a fracture

criterion and shown to be equivalent to Irwin's fracture criterion based upon the critical stress-intensity factor. For an in-plane shear crack starting from the Griffith's critical length, the terminal velocity of the crack-tip is found to be sub-Rayleigh or super-shear depending on the strength of the material measured by the critical stress-jump. Observed sub-Rayleigh rupture velocities for large earthquakes imply that the apparent specific surface energies for actual earthquakes are many orders of magnitudes greater than the values measured in the laboratory on small rock samples. For large earthquakes, they may be of the order of 10^{10} ergs/cm^2.

Our numerical technique is used to study (1) spontaneous unilateral propagation of a finite shear crack,(2) effect of obstacles (part of fault plane with greater strength) on the near- and far-field displacements and their spectra (3) and, the arrest mechanisms for stopping rupture. We find that the difference in dynamic displacement field for unilateral and bilateral crack propagation are more than what may be expected from different geometries. We show also that the corner frequency may not be significantly different between ruptures with and without obstacles, but the corresponding far-field wave-forms are distinctly different between the two. The high-frequency spectra decay as ω^{-2}, for most cases, but at stations located near the plane of rupture propagation, segments of the spectral curve decaying as $\omega^{-3/2}$ or ω^{-1} are found. Our

results for rupture propagation in the fault plane with obstacles show good agreement with observations of rockbursts in a deep mine.

We can predict how the arrest of a propagating shear crack occurs for a given distribution of strength of the medium along the fault-plane. Finally, for the case when the prestressed region is limited, the crack-tip is found to "overshoot" into the unstressed region before coming to a stop. The amounts of overshoot are calculated for finite in-plane shear cracks under various conditions of initial stress. When the rupture stops abruptly, the high frequency asymptote of the spectra fall off as ω^{-2}. When the tip stops gradually, we found a wide intermediate range in which the spectrum decays as ω^{-1}.

Thesis Supervisor: Keiiti Aki

Professor of Geophysics

Acknowledgements

I would like to express my deepest gratitude to my advisor Professor Keiiti Aki for suggesting the thesis topic and being a constant source of inspiration and encouragement. Working with Kei has been a rewarding experience due to his limitless supply of patience, great physical insight, and continued confidence in me.

I would like to thank all the people who, directly and indirectly, helped in the writing of this thesis. In particular, I would like to thank Gerry LaTorraca and Mike Fehler for innumerable discussions and moral support. Also, I gratefully acknowledge the helpful discussions with Raul Madariaga and Yed Angoran.

I am grateful to Dr. John Filson for advice and assistance, both scientific and human, and to Lincoln Laboratory for supporting me during part of my stay at M.I.T. Dr. Joe Andrews of the U.S.G.S., Menlo Park, was kind enough to let me use one of his figures (Figure 3.6 of this thesis) before it was published.

Finally, I would like to thank my parents and my husband for the many sacrifices they have made for me.

This research was supported by the National Science Foundation under grant DES74-22025.

TABLE OF CONTENTS

CHAPTER I

Introduction

A recent trend in seismology has been to model earthquakes as propagating shear cracks with various geometries. A shear crack is a surface S_1, say, of a body, subjected to an initial stress field, over which the shear tractions fall below their initial values resulting in a displacement discontinuity across S_1. The slip motion on a propagating crack can be determined by the shape, size, and orientation of S_1, the initial stress field acting on S_1 and the distribution of strength parameter corresponding to an adopted fracture criterion on S_1. Once the slip motion across S_1 is determined, we can compute the far-field seismograms using the Green function representation theorem.

1.1 Summary of recent works

The problem of finding the time-history of crack-tip location from a knowledge of the cohesive-force distribution on the crack plane was first studied by Kostrov in 1966, in a paper entitled "Unsteady Propagation of Longitudinal Shear Cracks". Following a method similar to one developed originally in the field of aerodynamics by Evvard (1947) (and described in detail by Ward (1950)), Kostrov solved the dynamic problem of a semi-infinite, instantaneous, anti-plane shear crack in an infinite medium by reducing the problem to a mixed boundary value problem in a half-space. He found closed form expressions for the displacements inside the

crack and the stresses outside the crack both on the plane of the crack. Kostrov determined the actual motion of the crack tip by using Griffith's fracture criterion in which γ, the energy required to create unit area of the crack surface is a material constant. In principle, Kostrov's method is also applicable to finite cracks. In practice, however, the multiple integrals resulting from the repeated wave diffractions at the crack tips cannot be obtained in closed form for even simple cases.

In spite of this limitation, Kostrov's work gave insight into the process of how energy is consumed at the crack-tip as the crack-tip advances. It led to the work of Burridge (1969) who used a numerical technique to solve the problem of anti-plane as well as in-plane finite shear cracks. He studied the case when the crack-tip moves at a fixed velocity.

In 1974, Hamano extended the analyses of Kostrov and Burridge to the case of finite, two-dimensional cracks in an infinite medium where the time history of crack-tip location need not be assumed a priori. Instead, he determined the rupture velocity from the conditions of strength distribution on the crack-plane. He used a critical stress-jump fracture criterion which is easily incorporated into the scheme of numerical computation. Hamano's technique is applicable to all three modes of two-dimensional crack extension: the tensile crack and the in-plane and antiplane shear cracks.

In 1976, Andrews combined a finite difference technique

with Griffith's fracture criterion, given in terms of Ida's (1973) cohesive force diagram, to solve for the rupture propagation of a finite, two-dimensional shear crack in an infinite medium. He showed the maximum rupture velocity for the in-plane shear crack to be sub-Rayleigh or super-shear depending on the strength of the material on the fault plane. Richards (1976) solved analytically the problem of a three-dimensional elliptical self-similar shear crack in an infinite medium. In this case, the crack dimension grows linearly with time and never stops. Madariaga (1976) calculated, by a finite difference technique, the slip motion for a circular shear crack which grows at a fixed velocity and stops suddenly. Later, in this thesis, we shall compare results obtained by Hamano's method with those of Kostrov, Andrews, Richards and Madariaga.

In addition, we shall compare our theoretical results with the model experiment of Archuleta and Brune (1975) who studied unilateral propagation of a shear crack in foam rubber. One of the interesting results is that the normal component of displacement across the fault, in both our calculation and foam rubber experiment, does not show an impulsive form predicted by a propagating step-like dislocation and observed at station #2 for the Parkfield, California, earthquake of 1966.

A study of arrest mechanisms for propagating cracks was made by Husseini et al. (1975). They suggested two stopping

mechanisms. One is called the "fracture energy barrier" arrest mechanism for which a fault encounters a region of greater strength and stops. The other is called the "seismic gap" arrest mechanism. In this case, only a finite region of the fault is prestressed so that the crack-tip propagates into unstressed regions, slows down and eventually stops. Husseini et al. studied these arrest mechanisms for the case of semi-infinite, instantaneous, antiplane shear crack in an infinite medium. In this thesis, we shall apply these two arrest mechanisms to the more complicated cases of finite, shear cracks in an infinite medium and shall determine the stopping positions of the crack-tip under various conditions of initial stress and strength distribution on the crack plane.

1.2 Outline of thesis

In Chapter II, we provide a physical description of the crack propagation problem and derive an integral equation, which is common to all the crack configurations studied in this thesis. The integral equation is solved numerically to determine the displacements on the crack plane. We compare our results with available analytic and numerical solutions.

In Chapter III, we introduce the fracture criterion and frictional arrest of fault slip. We briefly review existing fracture criteria and find the relation between these fracture criteria and Hamano's criterion based on the stress jump

across the crack tip. We calculate the terminal velocity of anti-plane and in-plane shear cracks using Hamano's criterion and compare the results with those of Kostrov and Andrews. We find an estimate for the apparent specific surface energy for earthquakes by observing that the rupture velocity is sub-Rayleigh for most large earthquakes.

In Chapter IV, we consider spontaneous propagation of two-dimensional, unilateral, in-plane shear cracks and compare our results with the experimental results of Archuleta and Brune. We simulate obstacles to rupture propagation by regions of greater strength on the crack-plane and find their effect on the near- and far-field displacements and their spectra. We compare our results with observations made by Spottiswoode and McGarr (1975) on rockbursts in deep mines. Finally, we discuss the possible mechanisms by which a finite propagating crack can stop.

In Appendix I we derive an equation for the balance of rates of energies at the tip of a crack.

Chapter II

Formulation of the Problem and Method of Solution.

In this chapter, we shall first describe the physical set-up of the problem for the case of in-plane shear crack and anti-plane shear crack, such as the initial conditions, boundary conditions and the symmetries of stress and displacement components. Next, we shall give a mathematical formulation of the problem and derive the integral equation for the displacements on the crack surface. The numerical technique used to solve this integral equation for given initial and boundary conditions will be described. Finally, we shall make some comparisons of our solution with available analytical or other numerical techniques to find the accuracy of our numerical method.

Glossary of Symbols

(in alphabetical order)

d	= grid length along x_1-direction in numerical method
F_{ni}	= discretized values of g_{ni}
$G_{ni}(\vec{x},t;\vec{y},s)$	= Green's function for general elastodynamic problems
$g_{ni}(\vec{x},t;\vec{y},s)$	= Green's function for a homogeneous half-space
k	= stress-intensity factor
$H(\ )$	= Heaviside unit step function
n_j	= direction - cosines of normal to surface
t,s	= time
t	= grid-length in time in numerical method
Tp	$= \alpha t/d$
Ts	$= \beta t/d$
S_1	= crack region on $x_2 = 0$ plane
S_2	= region outside crack on plane of crack
$\dot{U}$	= velocity intensity factor
X	$= x_1/d$
x_1,x_2,x_3	= Cartesian coordinates
x_1	= axis along which crack tip propagates
x_2	= normal to crack plane
Yp	= X/Tp
Ys	= X/Ts
$u_i(x,t)$	= displacements

α = compressional wave velocity

β = shear wave velocity

τ_{ij} = stress components

τ_o = initial stress

τ_f = dynamic friction stress on crack

ξ = s/x_1

§2.1 Description of the problem and derivation of initial and boundary conditions.

We shall model the earthquake source as a two-dimensional propagating shear crack in an infinite, isotropic homogeneous elastic solid. Figure 2.1 shows the geometry of the crack. Let $x_2 = 0$ be the plane on which the slip occurs, the crack being infinitely long in the x_3 direction. Initially the infinite body is under a uniform shear stress which has only one non-zero component acting on the plane $x_2 = 0$. The direction of the initial shear stress determines the mode of crack propagation. For an in-plane shear crack, the non-zero shear component of prestress is τ_{21} and for the antiplane shear crack, it is τ_{23}. Let us assume that the initial shear stress is increased so that the crack extends along the plane $x_2 = 0$, in the direction x_1. We shall take the origin of time $s = 0$ as the time when the crack starts extending. The extension of the crack may be rapid enough to generate elastic waves. The tip of the crack may move at some predetermined velocity or the position of the crack-tip as a function of time may be found using the state of stress near the crack-tip and appropriate fracture criterion. As the crack extends, there is relative motion between the regions $x_2 < 0$ and $x_2 > 0$ and a displacement discontinuity is set up across the $x_2 = 0$ plane. This

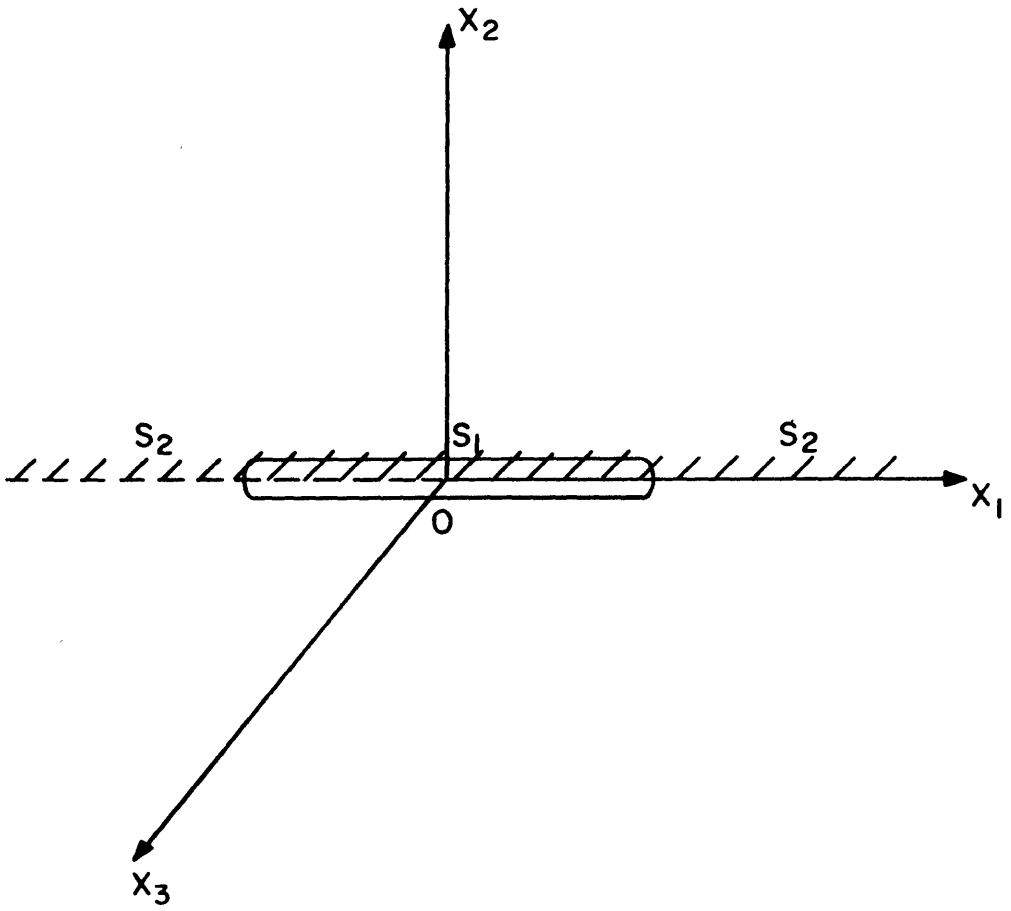

Figure 2.1. Geometry of the crack and the coordinate axes. x_1 is the direction of crack-propagation and $x_2 = 0$ is the plane of the crack. The crack is infinitely long in the x_3-direction. S_1 is the crack region and S_2 is the region outside the crack on the plane of the crack.

discontinuity in displacement is a function only of the coordinate x_1 and time s. For the in-plane crack, the displacement discontinuity is the difference of the x_1 component of displacement between the positive ($x_2 > 0$) and negative ($x_2 < 0$) sides of the fault-plane and for the anti-plane crack, it is the difference in the x_3 component of displacement between the positive and negative sides of the plane $x_2 = 0$. The stress on the crack surface is zero if there is complete stress release or equal to some constant value corresponding to the dynamic frictional stress on the crack surface. Using the principle of superposition, we can subtract the initial static state of stress from the subsequent dynamic state of stress. Then, the problem will reduce to one for zero initial stress and the stress assigned on the crack is the dynamic friction stress (τ_f) minus the initial stress τ_0. We can assign the stress on the crack as a function of position and time, if necessary. Thus, before rupture occurs, the body is in equilibrium with zero initial prestress. We shall assume that initially the displacements and velocities are zero everywhere in the medium. This gives the initial conditions for the problem. We discuss next the symmetry of the displacements and stresses across the plane $x_2 = 0$.

Let us first consider the case of the in-plane shear crack. For the two-dimensional case, there are two compo-

nents of displacement $u_1(x_1,x_2,s)$ and $u_2(x_1,x_2,s)$ and three components of stress

$$\tau_{21} = \mu[\frac{\partial u_1(x_1,x_2,s)}{\partial x_2} + \frac{\partial u_2(x_1,x_2,s)}{\partial x_1}]$$

$$\tau_{22} = \lambda\Delta + 2\mu\frac{\partial u_2(x_1,x_2,s)}{\partial x_2}$$

$$\tau_{11} = \lambda\Delta + 2\mu\frac{\partial u_1(x_1,x_2,s)}{\partial x_1}$$

The displacements $u_1(x_1,x_2,s)$ and $u_2(x_1,x_2,s)$ satisfy the equations of motion

$$\rho\frac{\partial^2 u_1}{\partial s^2} = (\lambda + \mu)\frac{\partial\Delta}{\partial x_1} + \mu\nabla^2 u_1$$

$$\rho\frac{\partial^2 u_2}{\partial s^2} = (\lambda + \mu)\frac{\partial\Delta}{\partial x_2} + \mu\nabla^2 u_2 \qquad 2.1$$

where $\Delta = \frac{\partial u_1}{\partial x_1} + \frac{\partial u_2}{\partial x_2}$, λ, μ being Lame's parameters and ρ the density of the medium. The equations of motion are satisfied by

$$u_1 = \frac{\partial\phi}{\partial x_1} - \frac{\partial\psi}{\partial x_2} \quad \text{and} \quad u_2 = \frac{\partial\phi}{\partial x_2} + \frac{\partial\psi}{\partial x_1}$$

provided ϕ and ψ satisfy the following wave-equations:

$$\frac{\partial^2\phi}{\partial x_1^2} + \frac{\partial^2\phi}{\partial x_2^2} = \frac{1}{\alpha^2}\frac{\partial^2\phi}{\partial s^2}$$

and

$$\frac{\partial^2\psi}{\partial x_1^2} + \frac{\partial^2\psi}{\partial x_2^2} = \frac{1}{\beta^2}\frac{\partial^2\psi}{\partial s^2}$$

where $\alpha = \sqrt{(\lambda + 2\mu)/\rho}$ and $\beta = \sqrt{\mu/\rho}$ are the P and S wave velocities respectively. ϕ and ψ are called the scalar potentials. The above wave-equations have solutions of the form

$$\phi = e^{i\omega s + ikx_1 \pm \nu_1 x_2}$$

$$\psi = e^{i\omega s + ikx_1 \pm \nu_2 x_2}$$

where $\nu_1 = \sqrt{k^2 - \omega^2/\alpha^2}$ and $\nu_2 = \sqrt{k^2 - \omega^2/\beta^2}$, k being the wave-number and ω the frequency. We require ϕ and ψ to satisfy the "radiation condition" of Sommerfeld, i.e. there is no wave source at infinity, so that ϕ and ψ tend to zero as $x_2 \to \pm\infty$.

Thus, for the region $x_2 > 0$, we have

$$\phi = \phi^+ e^{i\omega s + ikx_1 - \nu_1 x_2}$$

$$\psi = \psi^+ e^{i\omega s + ikx_1 - \nu_2 x_2}$$

and for $x_2 < 0$, we have

$$\phi = \phi^- e^{i\omega s + ikx_1 + \nu_1 x_2}$$

$$\psi = \psi^- e^{i\omega s + ikx_1 + \nu_2 x_2}$$

The boundary conditions are that the tractions τ_{21} and τ_{22}, and the normal component displacement u_2 are continuous across the crack-plane $x_2 = 0$, and u_1 is continuous outside the crack across $x_2 = 0$ but discontinuous across the portion

of $x_2 = 0$ which contains the crack. The continuity of u_2 and τ_{21} across $x_2 = 0$ leads to the conditions

$$-\nu_1(\phi^+ + \phi^-) + ik(\psi^+ - \psi^-) = 0$$

$$2ik\nu_1(\phi^+ + \phi^-) + (k^2 + \nu_2^2)(\psi^+ - \psi^-) = 0$$

The determinant of coefficients here does not vanish as long as $\frac{\omega}{k} \neq \alpha$, so that we must have

$$\phi^+ + \phi^- = 0$$

and

$$\psi^+ - \psi^- = 0$$

Therefore $\phi^+ = -\phi^-$ and $\psi^+ = \psi^-$

Substituting these relationships in the equations for u_1 and u_2, i.e.,

$$u_1 = \frac{\partial \phi}{\partial x_1} - \frac{\partial \psi}{\partial x_2}$$

and $$u_2 = \frac{\partial \phi}{\partial x_2} + \frac{\partial \psi}{\partial x_1}$$

we find that $u_1(x_1,x_2,s)$ and τ_{22} are odd functions of x_2 and $u_2(x_1,x_2,s)$ and τ_{21} are even functions of x_2. Now τ_{22} is odd in x_2 but it is also continuous across $x_2 = 0$. Hence $\tau_{22} = 0$ at $x_2 = 0$. Since $u_1(x_1,x_2,s)$ is odd in x_2, and discontinuous across that part of $x_2 = 0$ which contains the crack, we can write for the cracked region of plane $x_2 = 0$, $u_1(x_1,+0,s) = -u_1(x_1,-0,s) = \frac{1}{2}\Delta u_1$, where Δu_1 is the relative

displacement in the x_1-direction across the plane $x_2 = 0$.

For the antiplane case, we have one component of displacement $u_3(x_1,x_2,s)$ and two components of stress

$$\tau_{13} = \mu\frac{\partial u_3}{\partial x_1}(x_1,x_2,s) \quad \text{and} \quad \tau_{23} = \mu\frac{\partial u_3}{\partial x_2}(x_1,x_2,s) \ .$$

The displacement $u_3(x_1,x_2,s)$ satisfies the equation of motion

$$\rho\frac{\partial^2 u_3}{\partial s^2}(x_1,x_2,s) = \frac{\partial \tau_{13}}{\partial x_1} + \frac{\partial \tau_{23}}{\partial x_2}$$

which reduces to the wave-equation

$$\frac{\partial^2 u_3}{\partial s^2}(x_1,x_2,s) = \beta^2\left[\frac{\partial^2 u_3}{\partial x_1^2}(x_1,x_2,s) + \frac{\partial^2 u_3}{\partial x_2^2}(x_1,x_2,s)\right] \quad 2.2$$

β being the shear-wave velocity. Assume a solution of the form

$$u_3 = e^{i\omega s + ikx_1 \pm \nu_2 x_2}$$

where

$$\nu_2 = \sqrt{k^2 - \omega^2/\beta^2} \ ,$$

k is the wave-number and ω the frequency. $u_3(x_1,x_2,s)$ has to satisfy the "radiation condition" so that u_3 tends to zero as $x_2 \to \pm\infty$.

For the region $x_2 > 0$,

$$u_3 = u_3^+ \, e^{i\omega s + ikx_1 - \nu_2 x_2}$$

and for the region $x_2 < 0$,

$$u_3 = u_3^- e^{i\omega s + ikx_1 + \nu_1 x_2}$$

The boundary conditions are that u_3 is continuous outside the region of the crack across $x_2 = 0$ but discontinuous across the part of $x_2 = 0$ containing the crack and τ_{23} is continuous across $x_2 = 0$. (The stress component τ_{13} does not act on the plane $x_2 = 0$). The continuity of τ_{23} across the plane $x_2 = 0$ gives $u_3^+ = -u_3^-$ so that u_3 is odd in x_2 and τ_{23} is even in x_2. Since $u_3(x_1, x_2, s)$ is odd in x_2 and discontinuous across the broken part of the plane $x_2 = 0$, we can write, for the broken region of $x_2 = 0$, $u_3(x_1, +0, s) = -u_3(x_1, -0, s) = 1/2\ \Delta u_3$, where Δu_3 is the relative displacement in the x_3-direction across the $x_2 = 0$ plane.

Thus, we have shown that both in the case of the in-plane shear crack and the antiplane shear crack, there is a symmetry in the problem about the plane $x_2 = 0$. Due to this symmetry, it will be sufficient to solve the problem in a half-space bounded by the plane containing the crack, i.e. the plane $x_2 = 0$.

Let us divide the plane $x_2 = 0$ into two regions, S_1 and S_2 where S_1 is the region occupied by the crack and S_2 is the region outside the crack on the plane of the crack. In S_1, the stress has some known value. We shall solve the problem in the upper half-plane $x_2 \geq 0$. The initial conditions for the case of the plane shear crack are

$$u_1(x_1, 0, s) = 0$$

$$u_2(x_1, 0, s) = 0$$

$$\text{for } s \leq 0 \qquad 2.3$$

$$\frac{\partial u_1}{\partial s}(x_1, 0, s) = 0$$

$$\frac{\partial u_2}{\partial s}(x_1, 0, s) = 0$$

and for the case of antiplane shear crack are $u_3(x_1, 0, s) = 0$ and $\frac{\partial u_3}{\partial s}(x_1, 0, s) = 0$, $s \leq 0$. 2.4

Next, we discuss the boundary conditions. For the plane shear crack, the component of motion $u_1(x_1, x_2, s)$ is anti-symmetric in x_2 but continuous across $x_2 = 0$ outside the crack region, i.e. in S_2. Hence $u_1 = 0$ in S_2.

Thus, the boundary conditions are:

(i) In S_1, $\tau_{21} = \tau_f - \tau_o$, where τ_f is the dynamic frictional stress and τ_o the initial stress.

(ii) In S_1 and S_2, $\tau_{22} = 0$ 2.5

(iii) In S_2, $u_1(x_1, O, s) = 0$

For the antiplane case, we get, by a similar argument, the boundary conditions as

(i) In S_1, $\tau_{23} = \tau_f - \tau_o$ 2.6

(ii) In S_2, $u_3(x_1, 0, s) = 0$

(2.5) and (2.6) define two mixed boundary-value problems.

We have thus reduced the problem of a crack in an infinite medium to the problem of a half-space bounded by the plane $x_2 = 0$. The advantage of this is that we will be able to use the Green's function for a half-space in the formulation of relatively simple integral equations. The displacement discontinuity (slip) between the two faces of fault plane will be twice the surface displacement determined for the half-space problem. In later discussions, the parallel component of displacement on the crack will always refer to the displacement determined for the half-space. In the next section, we deduce the integral equation for the displacement on the crack.

2.2 The mathematical formulation of the problem.

Let us start with the general case of the three dimensional elasto-dynamic problem and consider a volume V of an elastic body bounded by the surface S. Let $u_i(\vec{x},t)$ be the i-th component of the displacement vector, $c_{ijpq}(\vec{x})$ the elastic constants of the medium and $f_i(\vec{x},t)$ the i-th component of the body forces at $\vec{x} = (x_1,x_2,x_3)$ and time t. $u_i(\vec{x},t)$ satisfies the equation of motion

$$\left(c_{ijpq}(\vec{x})\, u_{p,q}(\vec{x},t)\right)_{,j} - \rho(\vec{x})\, \ddot{u}_i(\vec{x},t) = -f_i(\vec{x},t)$$

Let $v_i(\vec{x},t)$ be another motion due to body force $g_i(\vec{x},t)$. Then $v_i(\vec{x},t)$ satisfies

$$\left(c_{ijpq}\, v_{p,q}\right)_{,j} - \rho \ddot{v}_i = -g_i$$

Let $\bar{v}_p(\vec{x},t) = v_p(\vec{x},-t)$ and $\bar{g}_i(\vec{x},t) = g_i(\vec{x},-t)$

Betti's theorem says that

$$\int_{-\infty}^{\infty} dt \int_V (u_i \bar{g}_i - \bar{v}_i f_i)\, dV = \int_{-\infty}^{\infty} dt \int_S n_j dS \left(\bar{v}_i\, c_{ijpq}\, u_{p,q} - u_i\, c_{ijpq}\, \bar{v}_{p,q}\right)$$

Let $g_i(\vec{x},t) = \delta_{ni}\, \delta(x_1-y_1)\, \delta(x_2-y_2)\, \delta(x_3-y_3)\, \delta(t+s)$,

where $\vec{y} = (y_1,y_2,y_3)$ is a point in V, δ_{ni} is the Kronecker delta and $\delta(x)$ is the Dirac delta function. Then

$$\bar{g}_i(\vec{x},t) = \delta_{ni}\,\delta(\vec{x},t;\vec{y},s).$$

Let $G_{in}(\vec{x},t;\vec{y},s)$ be the impulse response corresponding to $g_i(\vec{x},t)$ so that the impulse response corresponding to $\bar{g}_i(\vec{x},t)$ is $G_{in}(\vec{x},-t;\vec{y},-s)$. $G_{in}(\vec{x},t;\vec{y},s)$ is the displacement in the x_i-direction at $(\vec{x},t)$ due to an impulsive point force of unit amplitude in the y_n-direction at $(\vec{y},s)$. Substituting this form of $\bar{g}_i(\vec{x},t)$ into Betti's theorem, we get the representation theorem

$$u_n(\vec{y},s) = \int_{-\infty}^{\infty} dt \int_V G_{in}(\vec{x},-t;\vec{y},-s)\, f_i(\vec{x},t)\, dV_x$$
$$+ \int_{-\infty}^{\infty} dt \int_S n_j \left\{ G_{in}(\vec{x},-t;\vec{y},-s)\, c_{ijpq}(\vec{x})\, u_{p,q}(\vec{x},t) \right.$$
$$\left. - u_i(\vec{x},t)\, c_{ijpq}(\vec{x})\, G_{pn,q}(\vec{x},-t;\vec{y},-s) \right\} dS_x$$

If there is no body force or $f_i(\vec{x},t) = 0$, we have

$$u_n(\vec{y},s) = \int_{-\infty}^{\infty} dt \int_S n_j \left\{ G_{in}(\vec{x},-t;\vec{y},-s)\, c_{ijpq}(\vec{x})\, u_{p,q}(\vec{x},t) \right.$$
$$\left. - u_i(\vec{x},t)\, c_{ijpq}(\vec{x})\, G_{pn,q}(\vec{x},-t;\vec{y},-s) \right\} dS_x$$

The last term of the right hand side of the above equation can be eliminated, if our Green's function gives tractions which vanish on the surface S, because then

$$n_j \, c_{ijpq} \, G^{free}_{pn,q} \, (\vec{x}, -t \, ; \, \vec{y}, -s) = 0$$

Furthermore, for the homogeneous boundary conditions, the Green's function satisfies the following reciprocity (Knopoff and Gangi, 1959),

$$G_{np} \, (\vec{y}, s \, ; \, \vec{y}', s') = G_{pn} \, (\vec{y}', -s' \, ; \, \vec{y}, -s)$$

Therefore, we get

$$u_n \, (\vec{y}, s) = \int_{-\infty}^{\infty} dt \int_S n_j \, G^{free}_{in} \, (\vec{y}, s \, ; \, \vec{x}, t) \, c_{ijpq} \, (\vec{x}) \, u_{p,q}(\vec{x}, t) \, dS_x$$

If $\vec{y}$ is also on S, which is the case we encounter in this paper, we cannot eliminate the surface integral containing $\tau_{ij} = c_{ijpq} \, G_{pn,q} \, (\vec{x}, -t; \vec{y}, -s)$, because it does not vanish for $\vec{y}$ on S. In fact, the surface traction $\tau_{ij} n_j$ at $\vec{y}$ is equivalent to the δ-function body force that we put in the form of $g(\vec{x}, t) = \delta_{ni} \, \delta(\vec{x}, t; \vec{y}, s)$.
If we include this point force in the surface integral as traction then we must eliminate it from the volume integral in the representation theorem. Thus, Betti's theorem will give

$$0 = \int_{-\infty}^{\infty} dt \int_S n_j \left\{ G_{in} \, (\vec{x}, -t \, ; \, \vec{y}, -s) \, c_{ijpq} \, (\vec{x}) \, u_{p,q} \, (\vec{x}, t) \right\} dS_x$$

$$- u_i \, (\vec{y}, s)$$

which reduces to the same equation as for the case of $\vec{y}$ inside S. For a homogeneous half-space, we write the Green's function

$$G_{ni}(\vec{y}, s; \vec{x}, t) = g_{ni}(\vec{y}-\vec{x}, s-t), \text{ and}$$

$$u_n(\vec{y}, s) = \int_{-\infty}^{\infty} dt \int_S n_j \, g_{ni}(\vec{y}-\vec{x}, s-t) \, c_{ijpq}(\vec{x}) \cdot u_{p,q}(\vec{x}, t) \, dS_x$$

gives the x_n-component of displacement at $\vec{y}$ at time s due to an impulsive point force of unit magnitude applied at $\vec{x}$ at time t, $\vec{x}$ and $\vec{y}$ both being on S.

In the two-dimensional problem described in the preceding section, putting both of $\vec{x} = (x,0)$ and $\vec{y} = (x_1,0)$ on the plane $x_2 = 0$, we get

$$u_n(x_1, s) = \int_{-\infty}^{\infty} dt \int_{-\infty}^{\infty} g_{ni}(x_1-x, 0, s-t) \, \tau_{i2}(x,t) \, dx \qquad \ldots\ldots (2.7)$$

where

$$\tau_{ij} = \mu \left(\frac{\partial u_i}{\partial x_j} + \frac{\partial u_j}{\partial x_i} \right).$$

2.3 The integral equation for the antiplane shear crack

In the problem of anti-plane shear crack, we assume that the initial stress is constant and has the only non-zero component τ_{23}. The only component of displacement will be in the x_3-direction and will be independent of x_3. Let it be $u_3(x_1,x_2,s)$. The non-zero components of stress are

$$\tau_{13} = \mu \frac{\partial u_3(x_1,x_2,s)}{\partial x_1} \qquad \text{and} \qquad \tau_{23} = \mu \frac{\partial u_3(x_1,x_2,s)}{\partial x_2}$$

u_3 is odd in x_2 and τ_{23} is even in x_2. The geometry of the crack and the directions of the surface tractions are shown in Fig. 2.2.

The displacement $u_3(x_1,x_2,s)$ satisfies the equation of motion (2.2). The wave motions set up by the movement along the crack will be of the SH type, travelling with the shear wave velocity. The Green's function for the half-space $x_2 \geq 0$ is given in this case, by (cf. Achenbach, 1973)

$$g_{33}(x-x_1,\ x_2,\ s-t) = \beta H\left(\beta(s-t) - \sqrt{(x-x_1)^2 + x_2^2}\right) \Big/ \pi\mu R$$

where $$R^2 = \beta^2(s-t)^2 - (x-x_1)^2 - x_2^2$$

and $H(\ \ )$, is the Heaviside unit-step function. The Green's function is non-zero only in the cone defined by

$$\beta(s-t) - \sqrt{(x-x_1)^2 + x_2^2} \geq 0\ , \qquad s \geq t \geq 0 \qquad (2.8)$$

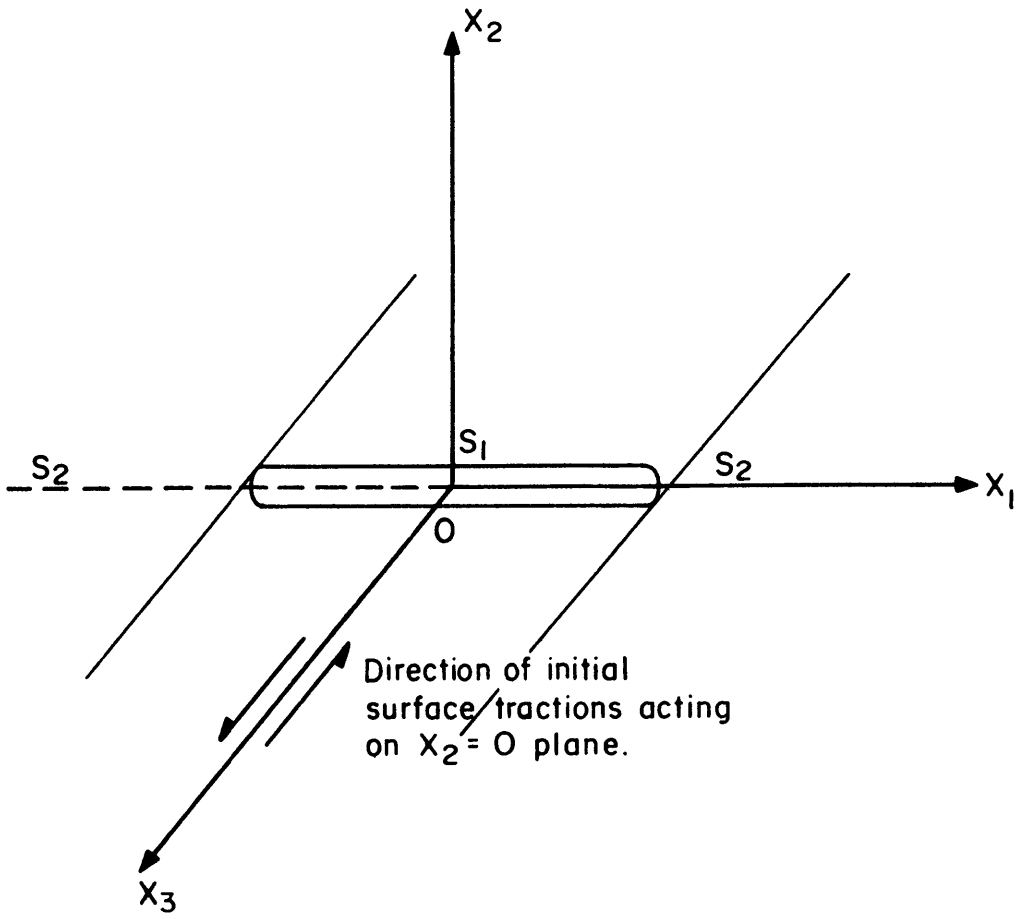

Figure 2.2. Geometry of the crack for the antiplane shear crack. The direction of the initial stress in the regions $x_2 > 0$ and $x_2 < 0$ are shown by arrows. S_1 is the broken region and S_2 is the unbroken region.

From equation (2.7) we get

$$u_3(x_1,0,s) = \frac{\beta}{\pi\mu} \iint_S \frac{\tau_{23}(x,t)}{R}\, dx\, dt \qquad (2.9)$$

S being that part of the x-t plane that lies inside the cone defined by Equation (2.8). On $x_2 = 0$, the region of integration reduces to a triangle in the x-t plane, given by the pair of straight lines $\beta^2(s-t)^2-(x-x_1)^2 \geq 0$, $s \geq t \geq 0$. If $\tau_{23}(x,t)$ were known in the entire region of integration, then integration of (2.9) will uniquely determine the solution. However, $\tau_{23}(x,t)$ is known in the region S_1 but not in S_2, so that we must first determine $\tau_{23}(x,t)$ in S_2 before we can carry out the integration in equation (2.9). The initial conditions under which (2.9) has to be solved are given by equation (2.4) and the boundary conditions are given by equation (2.6).

2.32 The Integral Equation for the In-Plane Shear Crack

We consider the same two-dimensional geometry of a plane crack as in the anti-plane case, but now the only non-zero component of the initially applied stress is τ_{21} (Fig. 2.3). There are two components of displacement, both in the plane (x_1-x_2) given by $u_1(x_1,x_2,s)$ and $u_2(x_1,x_2,s)$. As shown before, u_1 is anti-symmetric in x_2 and u_2 and τ_{21} are

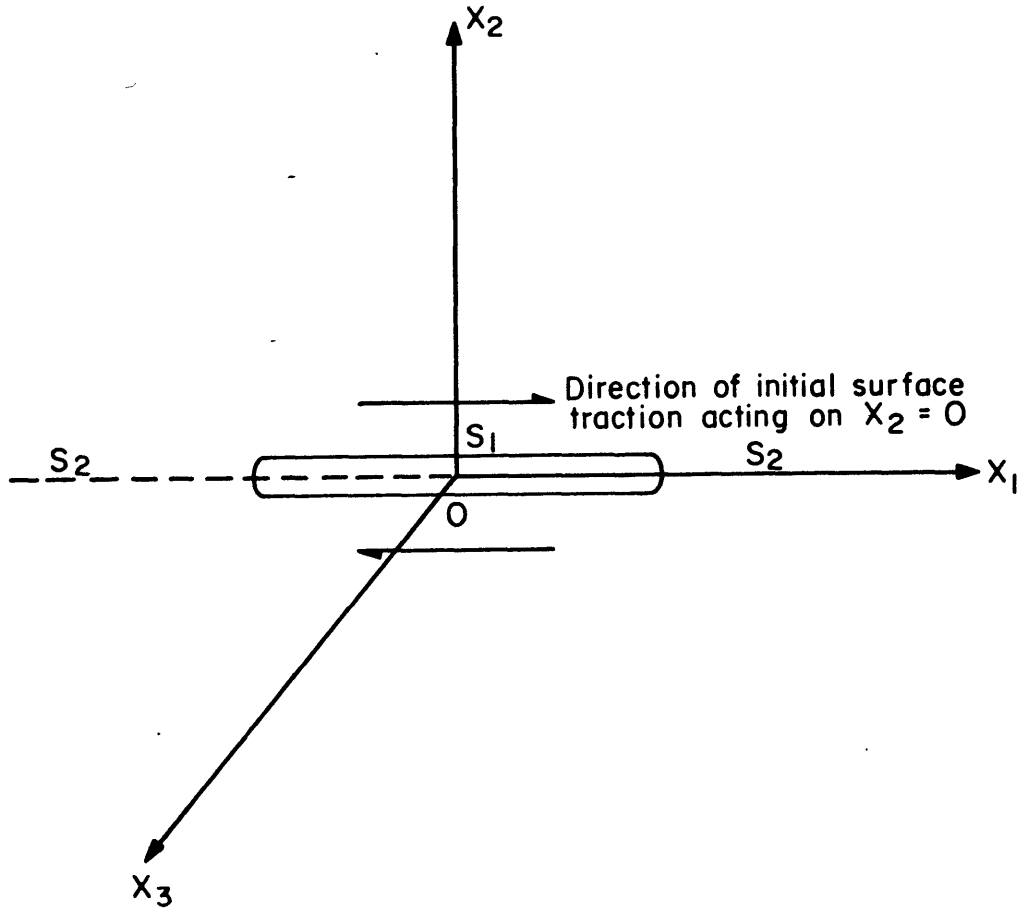

Figure 2.3. Geometry of the crack for the in-plane shear crack. Arrows indicate the direction of the initial stress in the regions $x_2 > 0$ and $x_2 < 0$.

symmetric in x_2. The displacements u_1 and u_2 satisfy the equations of motion given by equation (2.1).

Let $g_{11}(x-x_1,0,s-t)$ and $g_{21}(x-x_1,0,s-t)$ be the x_1 and x_2 components of the Green's functions for the half-space $x_2 \geq 0$. g_{11} and g_{21} were given by Lamb (1904).

Writing $g_{11} = g_{11}^{P} + g_{11}^{S}$, we find we have on $x_2 = 0$,

$$g_{11}^{P}(x_1, 0, s) = \frac{1}{\pi\mu x_1 \beta^2} \cdot \frac{4\xi^2 (\xi^2 - 1/\beta^2) \sqrt{\xi^2 - 1/\alpha^2}}{h(\xi^2)} \quad , \xi > \frac{1}{\alpha} \tag{2.10}$$

$$g_{11}^{S}(x_1, 0, s) = \frac{1}{\pi\mu x_1 \beta^2} \cdot \frac{(2\xi^2 - 1/\beta^2)^2 \sqrt{\xi^2 - 1/\beta^2}}{h(\xi^2)} \quad , \xi > \frac{1}{\beta}$$

where $\xi = s/x_1$, α and β are the compressional and shear wave velocities respectively, and

$$h(\xi^2) = (2\xi^2 - \frac{1}{\beta^2})^4 - 16\xi^4 (\xi^2 - 1/\alpha^2)(\xi^2 - 1/\beta^2) \tag{2.11}$$

is proportional to the Rayleigh equation. Lamb also gives

$$g_{21}(x_1, 0, s) = \frac{K'}{\mu} \delta(s - x_1/c) + \frac{2}{\pi\mu\beta^2 x_1} \cdot \left(\frac{1}{\alpha} < \xi < \frac{1}{\beta}\right)$$
$$\left\{ \frac{\xi(2\xi^2 - 1/\beta^2)\sqrt{(\xi^2 - 1/\alpha^2)(1/\beta^2 - \xi^2)}}{h(\xi^2)} \right\} \tag{2.12}$$

where c is the Rayleigh wave velocity.

The constant K' in the above expression depends on the elastic constants of the medium and can be written as

$$K' = \frac{\left(2\beta^2/c^2 - 1\right)^3}{16\frac{\beta^2}{c^2}\left\{1 - \left(6 - 4\beta^2/\alpha^2\right)\beta^2/c^2 + 6\left(1-\beta^2/\alpha^2\right)\frac{\beta^4}{c^4}\right\}}$$

For $\lambda = \mu$, i.e. $\alpha^2 = 3\beta^2$, $K' = .125\ 000$. Using equation 2.7, we can deduce the integral equations to determine u_1 and u_2 on $x_2 = 0$ as

$$u_1(x_1, 0, s) = \iint_S \tau_{21}(x,t)\, g_{11}(x_1 - x, 0, s-t)\, dx\, dt \tag{2.13a}$$

$$u_2(x_1, 0, s) = \iint_S \tau_{21}(x,t)\, g_{21}(x_1 - x, 0, s-t)\, dx\, dt \tag{2.13b}$$

the region of integration S being the triangle in the (x-t) plane given by

$$\alpha^2(s-t)^2 - (x - x_1)^2 \geq 0 \quad , s \geq t \geq 0$$

If $\tau_{21}(x,t)$ were known in S, we could carry out the integrations in equation 2.13 to find u_1 and u_2. Since we know $\tau_{21}(x,t)$ only inside the crack region S_1, we have to determine it in S_2 before we can integrate equation 2.13. The initial conditions under which 2.13 has to be solved are given by equation 2.3 and the boundary conditions are given by equation 2.5.

2.4 Numerical method of solving the integral equation

The integral equations that we have to solve in the case of the plane and the antiplane shear crack are both of the form

$$u(x_1, 0, s) = \iint_S \tau(x,t)\, g\,(x_1 - x,\ 0,\ s - t)\, dx\, dt \qquad (2.14)$$

where u is the appropriate component of displacement, g the appropriate component of the Green's function and $\tau(x,t)$ the traction on the crack.

In order to solve the integral equation 2.14 numerically, we divide the $(x_1\text{-}t)$ plane into small sections called "grids" each having length Δx along the x_1-direction and Δt along the t direction. The ratio of $\Delta t/\Delta x$ is a constant called the "grid ratio". The grid points are the points given by $x_1 = l\Delta x$ and $s = n\Delta t$ where $l = 0, \pm 1, \pm 2, \pm 3, \ldots$ and $n = 0, 1, 2, 3\ldots$ The stresses and the displacements are assumed to be constant within each grid element. The kernel g has to be discretized so that the integrals in equations 2.14 can be replaced by summations over grids. Now, g is the appropriate component of the surface displacement due to a surface point source. Following Hamano (1974), we shall discretize g by averaging it over a grid interval centered at the observation point as well as at source point. Then the discretized green function is:

$$F(x_j, t) = \frac{1}{d} \int_{x_j - d/2}^{x_j + d/2} g_1(x, t)\, dx \qquad (2.15)$$

where we average over a grid of length $d = \Delta x$, whose center is at x_j, and

$$g_1(x, t) = \frac{1}{d} \int_{x - d/2}^{x + d/2} g(y, t)\, dy$$

is the displacement at (x,t) due to a distribution of point forces in the segment (-d/2, + d/2).

Discretizing the integral equation (2.14), we obtain the matrix equation

$$u_n(x_i, t_k) = \Delta t\, \Delta x \sum_{j,l} F(x_i - x_j, t_k - t_l)\, \tau(x_j, t_l) \qquad (2.16)$$

where (x_i, t_k) refer to the observation point and the summation extends over the source points and times. The component of the stress tensor used in equation (2.16) is τ_{21} for the in plane shear crack and τ_{23} for the anti-plane shear crack. From equation 2.16 and the boundary condition that the parallel component of displacement vanishes outside the crack, we have

$$u_n(x_i, t_k) = 0 \qquad \text{in} \quad S_2$$

$$\text{i.e. } \Delta t\,\Delta x \sum_{j,l} F(x_i - x_j, t_k - t_l)\,\tau(x_j, t_l) = 0 \quad , \qquad (x_i, t_k) \in S_2$$

$$\text{or } \sum_{\substack{j \neq i \\ k \neq l}} F(x_i - x_j, t_k - t_l)\,\tau(x_j, t_l) = -F(0,0)\,\tau(x_i, t_k) \qquad (2.17)$$

This gives $\tau(x_i, t_k)$ in S_2 from the value of τ in S_1. Knowing τ on S_1 and S_2, we can substitute it in equation 2.16 to get $u_n(x_i, t_k)$. To identify the regions S_1 and S_2, the position of the crack-tip as a function of time must be known, either a priori or must be found using the state of stress near the crack-tip and an appropriate fracture criterion.

Fig. 2.4 shows the trajectory of the crack-tip as a function of time in the $(x_1\text{-}s)$ plane. From the principle of causality, the region of integration in the (x-s) plane when finding the displacement at (x_1, t_1) is the rectangle OABC which has one corner at (x_1, t_1). To find the stress at (x_o, t_o), the region of integration is over the rectangle $OA_1B_1C_1$, but excluding the point (x_o, t_o). For a crack half-length of unity and assuming the fastest wave speed to be unity, the number of computational operations we would need up to a time T is proportional to $(\frac{\Delta x_1}{\Delta t})N^3T^4$, where N is the number of grids in the x_1-direction.

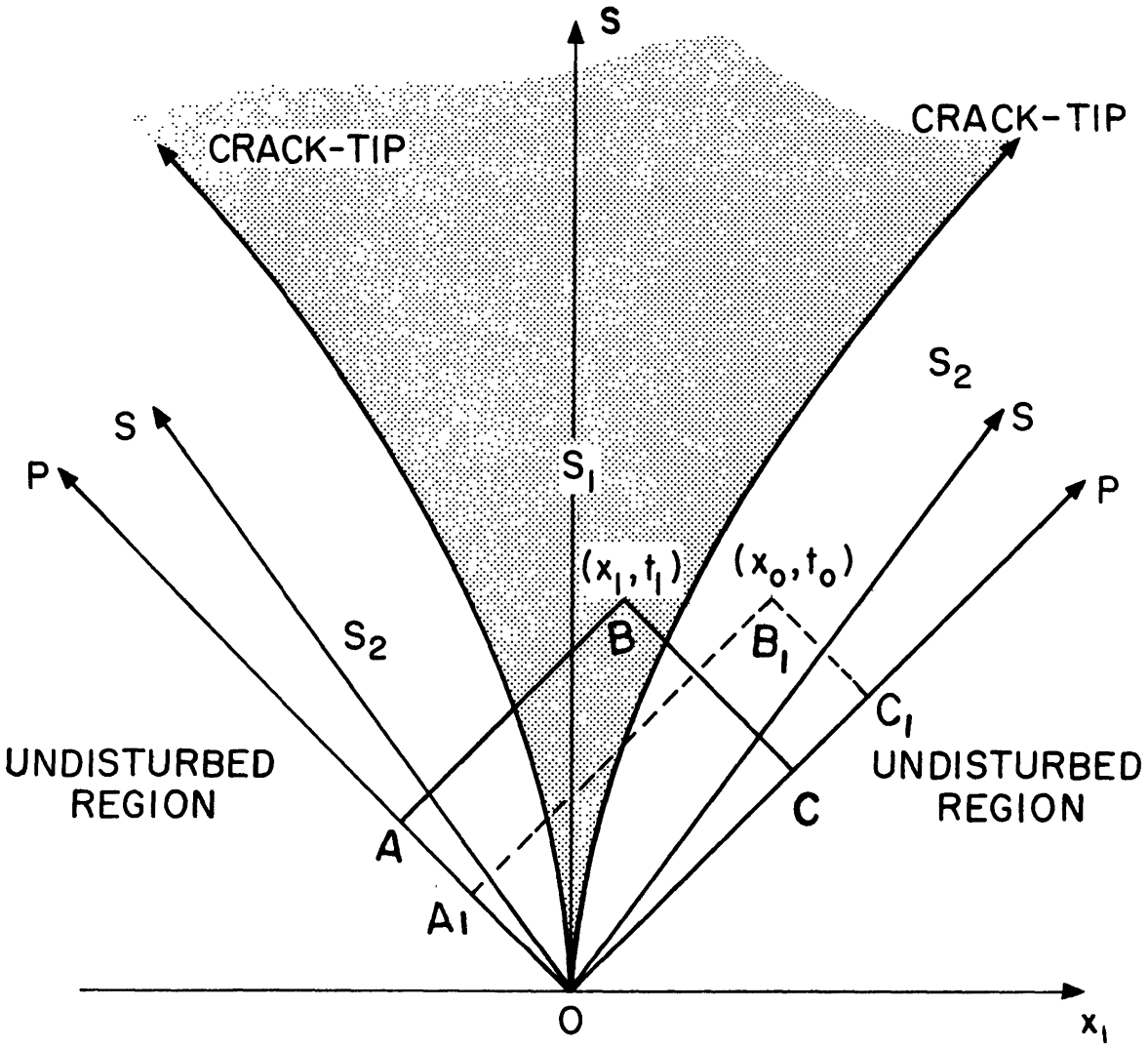

Figure 2.4. Trajectory of the crack-tip in the (x-s) plane. S_1 is the crack region and S_2 is the region outside the crack.
P and S denote the P and S waves from the initial point of break.

Discretized kernels for the in-plane and anti-plane shear crack

Using equation (2.15), we can discretize the kernels g_{11}, g_{21}, g_{33} so as to be able to use them in equation 2.16. For the antiplane case, the discretized kernel is given by

$$F_{33}(\bar{X}, T_s) = \frac{\beta}{\pi \mu d} T_s \, D_x^2 \, \mathcal{J}_1(Y_s) \qquad (2.18)$$

where $\bar{X} = x_1/d$, $T_s = s\beta/d$, $Y_s = \bar{X}/T_s$,

d is the grid length in the space dimension (X and T_s are thus dimensionless distance and time), and

$$D_x^2 \mathcal{J}(Y) = \mathcal{J}(Y+1) - 2\mathcal{J}(Y) + \mathcal{J}(Y-1) ,$$

$$\mathcal{J}_1(Y_s) = -Y_s \sin^{-1} Y_s + \sqrt{1 - Y_s^2} \quad , \quad Y_s < 1$$

$$= \frac{\pi}{2} Y_s \quad , \quad Y_s \geq 1$$

Note that the shape of $F_{33}(X,Ts)$ does not depend explicitly on X but only on the ratio X/Ts. The discretized kernel $F_{33}(X,Ts)$ is shown in Figure 2.5.

For the in-plane shear crack, we get

$$F_{11} = F_p + F_s$$

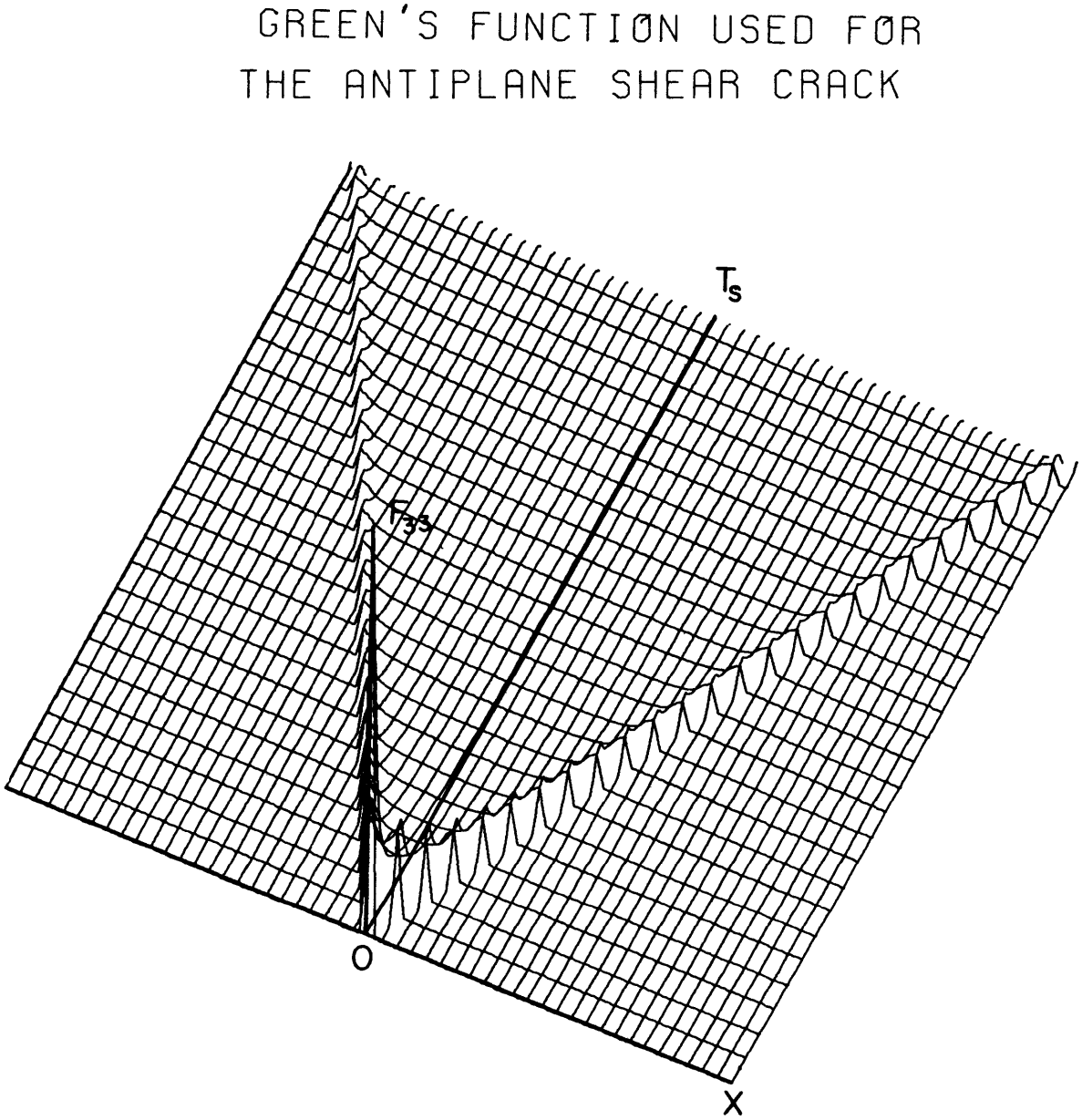

Figure 2.5. Composite plot showing the discretized kernel $F_{33}(X,Ts)$ giving the Green's function, for the antiplane problem. $F_{33}(X,Ts)$ is symmetric about X = 0.

where

$$F_p(\bar{X}, T_p) = \frac{\beta^2}{\pi\mu d}\, 4T_p \left[\sum_{i=1}^{3} a_i^p\, D_x^2\, \mathcal{J}_2^p(Y_p; z_i)\right] \tag{2.19}$$

$$F_s(\bar{X}, T_s) = \frac{\beta}{\pi\mu d}\, T_s \left[-D_x^2\, \mathcal{J}_1(Y_s) - \sum_{i=1}^{3} a_i^s\, D_x^2\, \mathcal{J}_2^s(Y_s; z_i)\right]$$

where

$\bar{X} = x_1/d$, $T_s = t\beta/d$, $Y_{p,s} = \bar{X}/T_{p,s}$

$d = \Delta x$ being the grid length in the x_1-direction, and $1/z_i$'s are β^2 times the roots of the Rayleigh equation $h(\xi^2) = 0$ and

$$\mathcal{J}_2^{p,s}(Y; z) = \frac{Y}{\sqrt{z^{p,s}(z^{p,s}-1)}} \tan^{-1}\left[\frac{\sqrt{z^{p,s}(z^{p,s}-1)}\; Y}{-z^{p,s}\sqrt{1-Y^2}}\right]$$

$$-\frac{1}{\sqrt{z^{p,s}-1}} \tan^{-1}\sqrt{\frac{1-Y^2}{z^{p,s}-1}}, \quad \begin{matrix} Y<1 \\ z>1 \end{matrix}$$

$$= \frac{y}{2\sqrt{z^{P,S}(1-z^{P,S})}} \log \left| \frac{\sqrt{z^{P,S}(1-z^{P,S})}\, y - z^{P,S}\sqrt{1-y^2}}{\sqrt{z^{P,S}(1-z^{P,S})}\, y + z^{P,S}\sqrt{1-y^2}} \right|$$

$$- \frac{1}{2\sqrt{1-z^{P,S}}} \log \left| \frac{\sqrt{1-y^2} - \sqrt{1-z^{P,S}}}{\sqrt{1-y^2} + \sqrt{1-z^{P,S}}} \right| ,$$

$$y < 1$$
$$z < 1 ,$$

$$= -\frac{\pi}{2} \frac{y}{\sqrt{z^{P,S}(z^{P,S}-1)}} , \qquad \begin{matrix} y \geq 1 \\ z > 1 \end{matrix}$$

$$= 0 , \qquad \begin{matrix} y > 1 \\ z \leq 1 \end{matrix} .$$

where $z^P = \frac{\beta^2}{\alpha^2} z^S$

and $z^S = x^2/\beta^2 t^2$

$$a_1 = \frac{1}{(z_1 - z_2)(z_1 - z_3)} \left(z_1^2 A_2 + z_1 B_2 + C_2 \right)$$

$$a_2 = \frac{1}{(z_2 - z_1)(z_2 - z_3)} \left(z_2^2 A_2 + z_2 B_2 + C_2 \right)$$

$$a_3 = \frac{1}{(z_3 - z_2)(z_3 - z_1)} \left(z_3^2 A_2 + z_3 B_2 + C_2 \right)$$

$$A_2^P = \beta^2/\alpha^2 \quad , \quad B_2^P = -(1 + \beta^2/\alpha^2) \quad , \quad C_2^P = 1$$

$$A_2^S = 3 \quad , \quad B_2^S = -16(1 - \beta^2/\alpha^2) \quad , \quad C_2^S = 4(3 - 4\beta^2/\alpha^2)$$

If we assume Poisson's condition, i.e. $\lambda = \mu$, then

$$1/z_1, 1/z_2, 1/z_3 = \frac{1}{4}, \frac{1}{4}(3-\sqrt{3}), \frac{1}{4}(3+\sqrt{3})$$

The discretized kernel $F_{11}(X,Tp)$ is shown in Figure 2.6.

PARALLEL COMPONENT OF GREEN'S FUNCTION USED FOR PLANE SHEAR CRACK

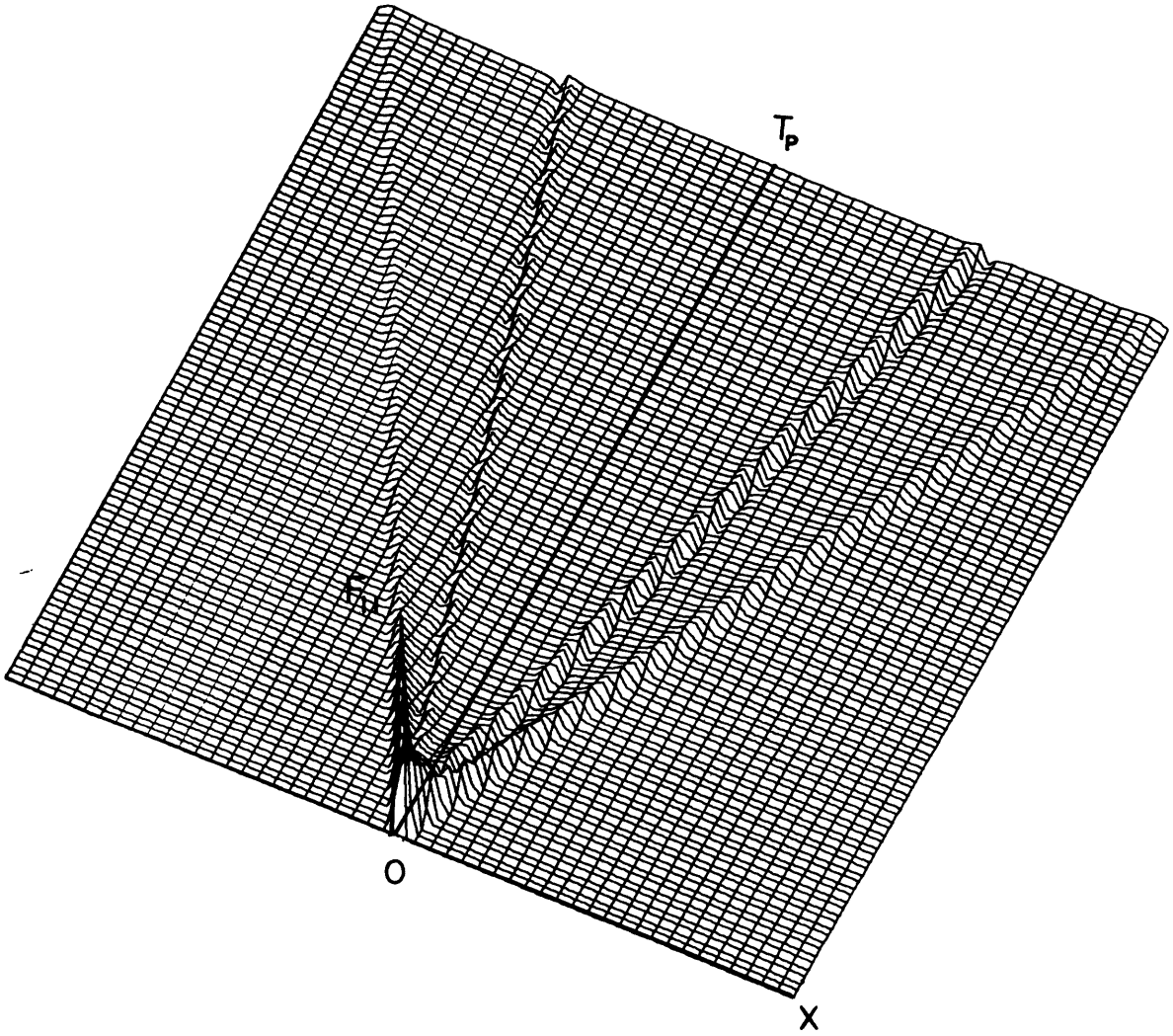

Figure 2.6. Composite plot showing the discretized kernel $F_{11}(X,Tp)$ giving the parallel component of the Green's function for the in-plane problem. The P-waves and Rayleigh waves are clearly visible. $F_{11}(X,Tp)$ is symmetric about X = 0.

For the component $g_{21}(x_1,s)$ of the Green's function the discretized kernel F_{21} cannot be evaluated analytically since the integrals obtained by using equation 2.15 reduce to elliptic integrals. Hence, in this case, the integrals are evaluated numerically at each grid point, and $F_{21}(X,Tp)$ is shown in Figure 2.7.

Substituting these discretized kernels in equation 2.16 we can solve the integral equations for $u_1(x_1,s)$, $u_2(x_1,s)$, $u_3(x_1,s)$ provided we know the location of the crack-tip as a function of time.

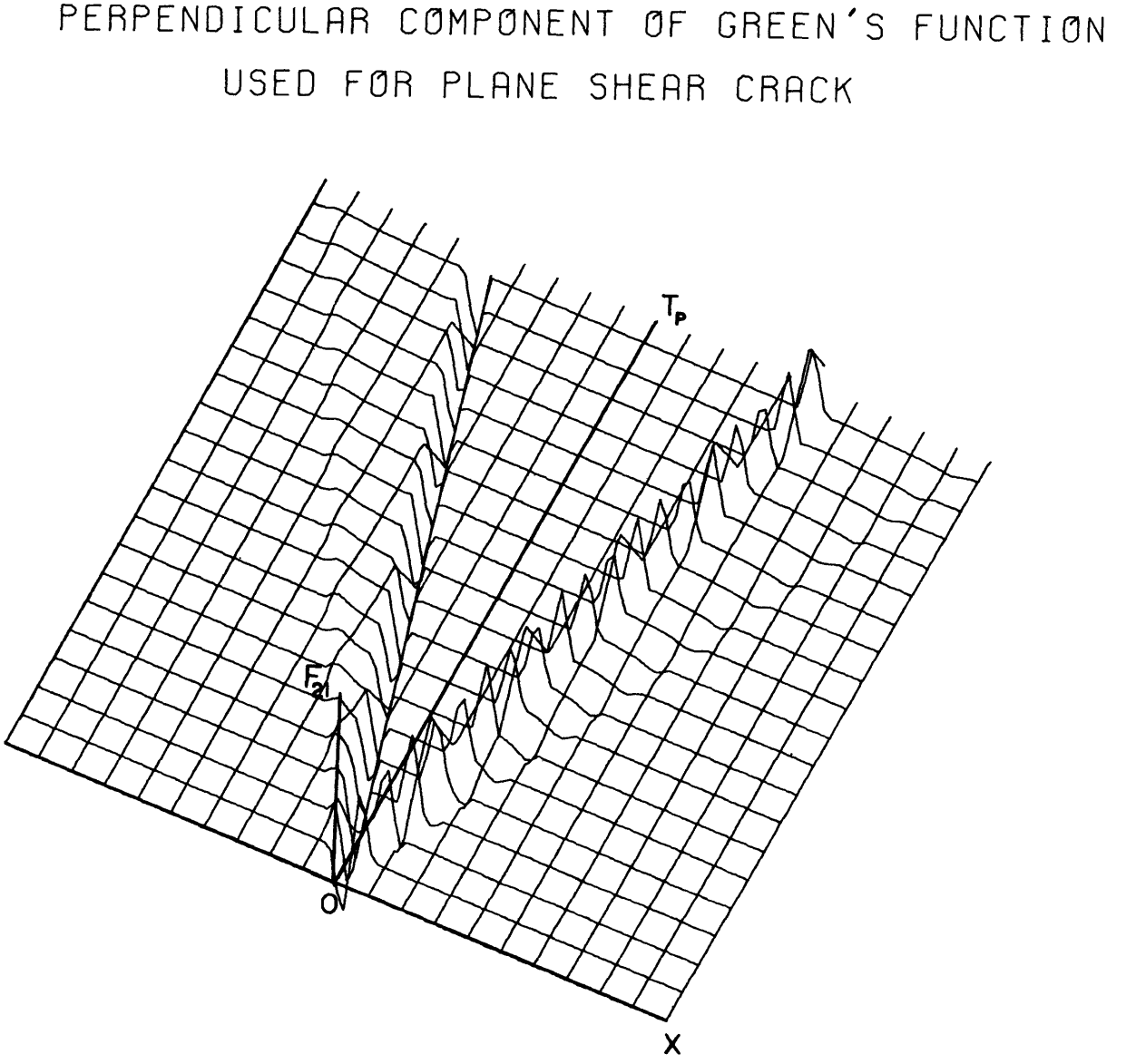

Figure 2.7. Composite plot showing the discretized kernel $F_{21}(X,Tp)$ giving the normal component of the Green's function for the in-plane problem. The P-wave and Rayleigh wave are clearly visible. $F_{21}(X,Tp)$ is antisymmetric about X = 0.

2.5 Comparison of numerical results for anti-plane crack with analytical result of Kostrov (1966)

We shall first compare our solution with the analytic solution given by Kostrov (1966) for the anti-plane crack to find the accuracy of our method. Kostrov gives the expression for displacements on the surface of the crack and stresses on the plane of the crack outside the broken region. The semi-infinite anti-plane crack which never stops will be considered as this is the only case for which the analytic solution of Kostrov is correct for an indefinitely long time interval. If the semi-infinite crack stops, then the wave reflected from the tip has to be taken into account. For a finite crack, the exact solutions found by Kostrov are correct only till the disturbances from one end of the crack reach the other end. After this, the multiple integrals that result from repeated wave diffractions cannot be obtained in closed form, even in simple cases.

We consider an infinite, elastic body which is initially under a homogeneous state of stress such that $\tau_{23} = \tau_o$. At $t = 0$, an instantaneous semi-infinite crack comes into existence, occupying the negative x_1-axis, the origin of the coordinate system being at the tip, and starts extending immediately in its own plane with a velocity equal

to half the shear-wave velocity. It is also assumed that the crack never stops but grows for all time.

On the crack surface, the value of the shear stress component τ_{23} will drop from the level of the prestress to some lower level, say τ_f, the dynamic frictional stress on the crack. As mentioned earlier, by the principle of superposition, we can take the initial stress to be zero and the final stress on the crack to be $(\tau_f-\tau_o)$. For complete stress release on the crack, $\tau_f=0$. We shall normalize all stresses by the stress drop $(\tau_o-\tau_f)$ so that all results presented from here on will be for a stress drop equal to unity, unless specifically stated otherwise. The wave-front generated by the fracture is shown in Fig. 2.8.

As explained in an earlier section, the problem of the crack in the infinite medium reduces to the half-space problem and we can use equation 2.9 to determine the displacement on the crack and the stresses on the plane of the crack outside the crack region.

The general expression for the displacement on the crack surface $x_2=0^+$ in terms of characteristic coordinates (ξ_1,η_1) can be written using equation (2.9), as

$$u_3(\xi_1,\eta_1) = \frac{1}{\pi\mu\sqrt{2}} \int_{K(\eta_1)}^{\xi_1} \frac{d\xi}{\sqrt{\xi_1-\xi}} \int_{-\xi}^{\eta_1} \frac{\tau_{23}(\xi,\eta)}{\sqrt{\eta_1-\eta}}\, d\eta \qquad (2.20)$$

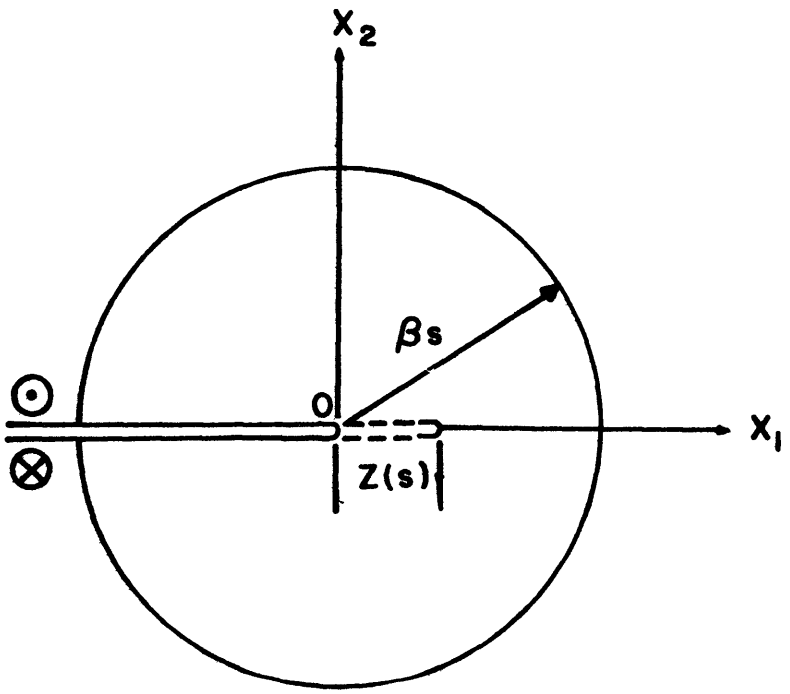

Figure 2.8. The wave-front generated by dynamic fracture for a semi-infinite antiplane shear crack. $x_1 = Z(s)$ gives the position of the crack-tip as a function of time.

where $\xi = \frac{\beta s - x_1}{\sqrt{2}}$, $\eta = \frac{\beta s + x_1}{\sqrt{2}}$, $\tau_{23}(\xi,\eta) \equiv \tau_{23}(x_1,s)$

and $K(\eta_1)$ is the solution of

$$\frac{\eta_1 - K(\eta_1)}{\sqrt{2}} = Z\left(\frac{\eta_1 + K(\eta_1)}{\sqrt{2}}\right)$$

where the position of the crack-tip as a function of time is given by $x_1 = Z(s)$. For the case when the crack-tip moves at the velocity $\beta/2$, $x_1 = \beta s/2$, whence $K(\eta_1) = \eta_1\left(\frac{2-\beta}{2+\beta}\right)$ Let us take $\mu = 1$ and $\rho = 1$ so that $\beta = 1$ and $K(\eta_1) = \eta_1/3$. As mentioned earlier, the stress drop is taken as unity,

$$\tau_{23}(\xi,\eta) = 1 \ ,$$

and we have:

$$u_3(\xi_1,\eta_1) = \frac{1}{\pi\mu\sqrt{2}} \int_{\eta_1/3}^{\xi_1} \frac{d\xi}{\sqrt{\xi_1 - \xi}} \int_{-\xi}^{\eta_1} \frac{d\eta}{\sqrt{\eta_1 - \eta}}$$

$$= -\frac{\sqrt{2}}{\pi\mu}\left[\sqrt{\frac{4\eta_1}{3}\left(\xi_1 - \frac{\eta_1}{3}\right)}\right. \qquad (2.21)$$

$$\left. + \left(\frac{\xi_1 + \eta_1}{2}\right)\left\{\frac{\pi}{2} + \sin^{-1}\frac{\xi_1 - 5\eta_1/3}{\xi_1 + \eta_1}\right\}\right]$$

From Kostrov (1966), the general expression for stress τ_{23} at any point (ξ,η) ahead of the crack on the plane of the crack is given by

$$\tau_{23}(\xi,\eta) = \frac{1}{\pi[\eta - N(\xi)]^{\frac{1}{2}}} \int_{-\xi}^{N(\xi)} \frac{\tau_{23}(\xi,u)\sqrt{N(\xi)-u}}{\eta-u}\, du \qquad (2.22)$$

where $N(\xi)$ is the solution of

$$\frac{N(\xi)-\xi}{\sqrt{2}} = Z\left(\frac{N(\xi)+\xi}{\sqrt{2}}\right)$$

The stress outside the crack on the plane of the crack is thus determined by the stress inside the crack. For the case when the crack-tip moves at half the shear wave velocity $x_1 = \beta s/2$ and $N(\xi) = 3\xi$, we have

$$\tau_{23}(\xi,\eta) = \frac{1}{\pi\sqrt{\eta-3\xi}} \int_{-\xi}^{3\xi} \frac{\tau_{23}(\xi,u)\sqrt{3\xi-u}}{\eta-u}\, du$$

$\tau_{23}(\xi,u)$ is the stress drop inside the crack, which we normalize to unity. If $\mu = 1$ and $\rho = 1$ so that $\beta = 1$,

$$\tau_{23}(\xi,\eta) = \frac{1}{\pi\sqrt{\eta-3\xi}}\left[4\sqrt{\xi} + 2\sqrt{\eta-3\xi}\,\tan^{-1}\frac{-2\sqrt{\xi}}{\sqrt{\eta-3\xi}}\right] \qquad (2.23)$$

If equation (2.23) is written in (x_1,s) coordinates, we have

$$\tau_{23}(x_1,s) = \frac{1}{\pi\sqrt{x_1 - Z(s_1)}} \int_{x_1-\beta s}^{Z(s_1)} \frac{\tau_{23}(v, s-x_1+v)\sqrt{Z(s_1)-v}}{x_1-v}\, dv$$

where s_1 is computed from $\beta s - x_1 = \beta s_1 - Z(s_1)$.
This can be written as

$$\tau_{23}(x_1,s) = \frac{\sqrt{1 - dZ/ds}}{\pi\sqrt{x_1 - Z(s)}} \int_{x_1-\beta s}^{Z(s)} \frac{\tau_{23}(v,\ s - Z(s) + v)}{\sqrt{Z(s) - v}}\, dv + O\left[\sqrt{x_1 - Z(s)}\right]$$

$$= \frac{k}{\sqrt{x_1 - Z(s)}} + O\left[\sqrt{x_1 - Z(s)}\right] \qquad (2.24)$$

where k is called the "stress-intensity factor".

The particle velocity behind the crack-tip can be obtained by differentiating equation (2.20) and using the relation

$$\frac{\partial u_3}{\partial s} = \frac{1}{\sqrt{2}}\left(\frac{\partial u_3}{\partial \xi} + \frac{\partial u_3}{\partial \eta}\right)$$

In $(x_1\text{-}s)$ coordinates, we can write

$$\frac{\partial u_3}{\partial s}(x_1, s) = -\frac{1}{\pi\mu}\,\frac{dz/ds}{\sqrt{1+dz/ds}}\,\frac{1}{\sqrt{z(s)-x_1}} \cdot \int_{x_1-\beta s}^{z(s)} \frac{\tau_{23}(v,\, s-z(s)+v)}{\sqrt{z(s)-v}}\,dv + O\left(\sqrt{z(s)-x_1}\right) = \frac{\dot{U}_3}{\sqrt{z(s)-x_1}} + O\left(\sqrt{z(s)-x_1}\right) \tag{2.25}$$

$\dot{U}_3$ is called the "velocity-intensity factor". The square-root singularity associated with the stress-intensity factor and the velocity-intensity factor commonly occurs at the tip of various types of cracks.

The problem of a semi-infinite crack extending at a constant velocity is a "self-similar" problem, since there is no characteristic length scale in the problem. Let us consider two points in the $(x_1\text{-}s)$ plane, given by say (x_1,s_1) and (x_2,s_2) such that $s_2 = (x_2/x_1)\, s_1$. Then,

$$u_3(x_2,s_2) = (x_2/x_1)\, u_3(x_1,s_1) \tag{2.26}$$

Thus, if we know the displacement at (x_1,s_1) we can find the displacement at (x_2,s_2) simply by multiplying by the factor x_2/x_1 without having to evaluate it from equation 2.22.

To compare our numerical solution with the analytical solution, we first evaluate equation (2.22) and plot the

displacement against $T_s = s\beta/d$. The numerical solution is determined using equations 2.16 and 2.18. We take $\Delta t = d/\beta \Delta Ts$ and $\Delta x = d\Delta X$, where Ts and X were defined in section 2.4. We solved the integral equation numerically for $\Delta t/\Delta x = .1, .2, .4, .5, .75, 1.0$. We expect some difference between the analytical and numerical solutions since the continuous motion of the crack-tip is approximated by discrete steps in the grid. For $\Delta t/\Delta x = .1$ and .2, the solution agrees almost exactly with the analytical solution for the first four or five time steps. (The agreement at the first point, however, will not be complete for any ratio of $\Delta t/\Delta x$ due to the uncertainty in the positions of the crack-tip within the discretization interval.) After the first few time-steps, the solution starts oscillating about the analytic solution, the oscillations becoming larger as X increases. For a given X, the amplitude of the oscillation is constant in time. The period of the oscillations are constant for all space and time.

For $\Delta t/\Delta x = .4, .5$, the numerical solution does not agree well with the analytical solution for the first four or five time-steps but afterwards, agrees very well, and has only minor oscillations about the analytic solution. $\Delta t/\Delta x = .5$ is found to have slightly smaller oscillations than $\Delta t/\Delta x = .4$. For $\Delta t/\Delta x = .75$ and 1.0, the numerical solution does not agree with the analytic one even after twenty time steps. Fig. 2.9 shows a comparison of the

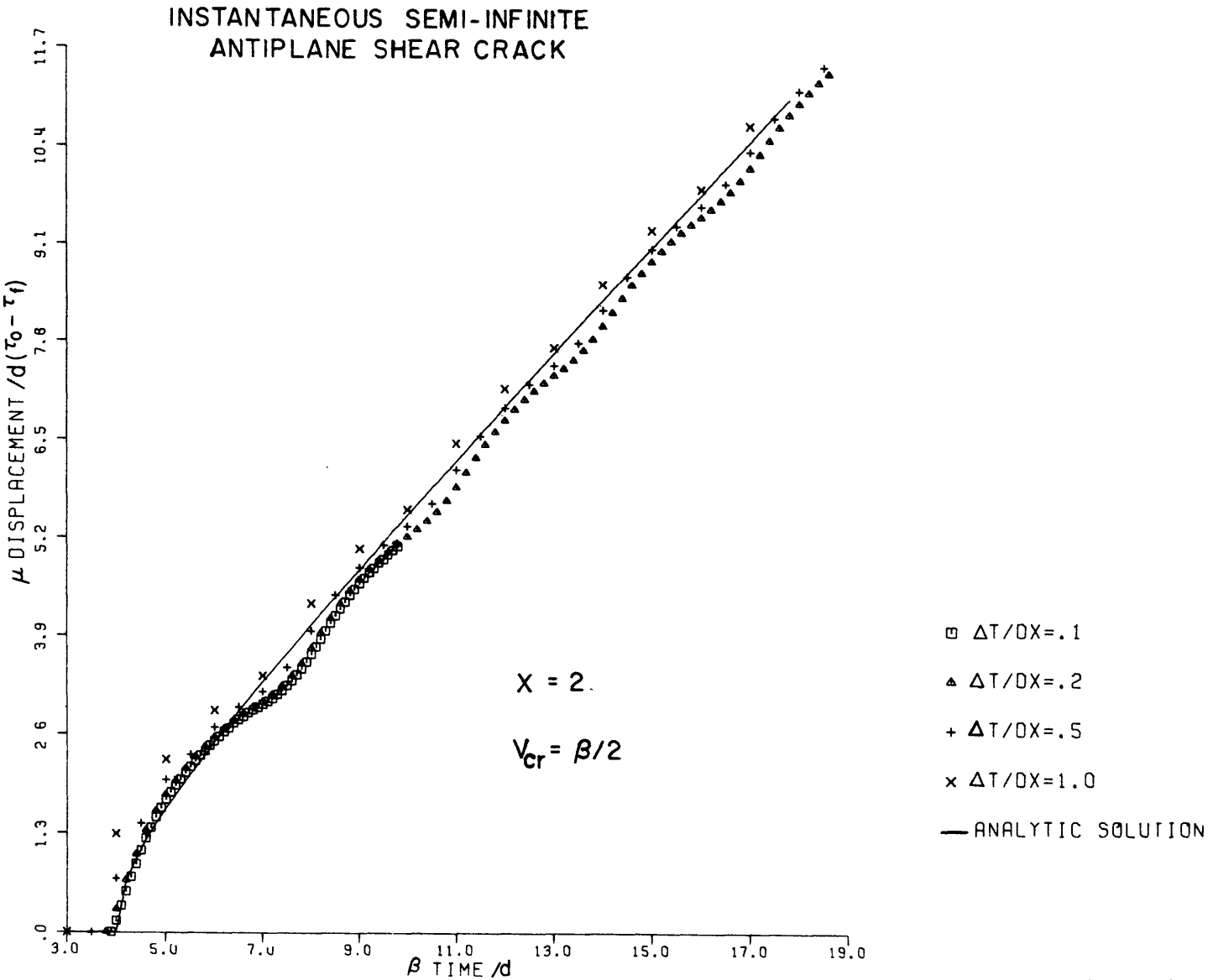

Figure 2.9. Comparison of numerical results for $\Delta T/\Delta X$ = .1, .2, .5 and 1.0 with the analytic solution at X (= x_1/d) = 2 for the semi-infinite instantaneous antiplane shear crack moving at half the shear-wave velocity. The best agreement with the numerical result is for $\Delta T/\Delta X$ = .5.

numerical results for various values of $\Delta t/\Delta x$, at a particular value of X, with the analytical solution.

Thus we see that for small $\Delta t/\Delta x$, the solution is poor in the later part, and for large $\Delta t/\Delta x$ it is poor in the early part. The optimum value for $\Delta t/\Delta x$ appears to be around .5.

The departure of the numerical solution from the analytical solution near the crack-tip can be reduced by going to smaller values of $\Delta t/\Delta x$ but then the amount of calculation and computer time involved will be increased.

Thus, we conclude that if we are interested in the fine details of motion near the crack-tip, we should use values of $\Delta t/\Delta x \leq .2$. If we are not interested in the motion near the crack-tip but want to obtain the motion at points in the interior of the crack, $\Delta t/\Delta x = .5$ is an optimum value.

We point out, in this respect, the work of Burridge (1969) who solves the same problem by a method essentially the same as our method, the only difference being in the method of discretizing the kernel in the integral equation. Burridge's result also shows that the solution near the tip does not agree well with the analytic solution of Kostrov, but the agreement seems to be good for any time later than a few steps after the crack-tip passage (Burridge chooses $\Delta t/\Delta x = 1.0$).

Fig. 2.10 shows the analytic and numerical solutions for the parallel component of the displacement on the plane $x_2 = 0^+$, plotted against time for various values of X. $\Delta t/\Delta x$ was chosen to be .5. The agreement between the two solutions is quite satisfactory.

The stresses obtained numerically are also compared against the analytical result (equation 2.23). Fig. 2.11 shows the analytical and numerical solution plotted against X for various values of Ts. The stress singularity at the tip is eliminated by our averaging scheme. Changing $\Delta t/\Delta x$ does not affect the stresses appreciably. After about 50 time steps, the stresses start showing minor oscillations, but the amplitude is negligibly small. To determine whether these oscillations are negligible or not, we solved the problem again, this time by smoothing the stresses when the oscillations start by taking three-point averages with the point where it oscillates being the center point of the averaging scheme. The oscillations are damped out but after 100 time steps, the corresponding displacements are the same, even in the second decimal place as the displacements when the oscillations in the stresses are not smoothed. So we conclude that the small oscillations in the stresses do not affect the displacement. The good agreement of our numerical result on stress near the tip with the analytic solution allows us to use the stress at the grid point immediately ahead of the crack tip in the fracture criterion, which will be discussed in the next chapter.

Figure 2.10. Comparison of analytical solution due to Kostrov (1966) with our numerical solution for a semi-infinite instantaneous antiplane shear crack extending at half the shear wave velocity.

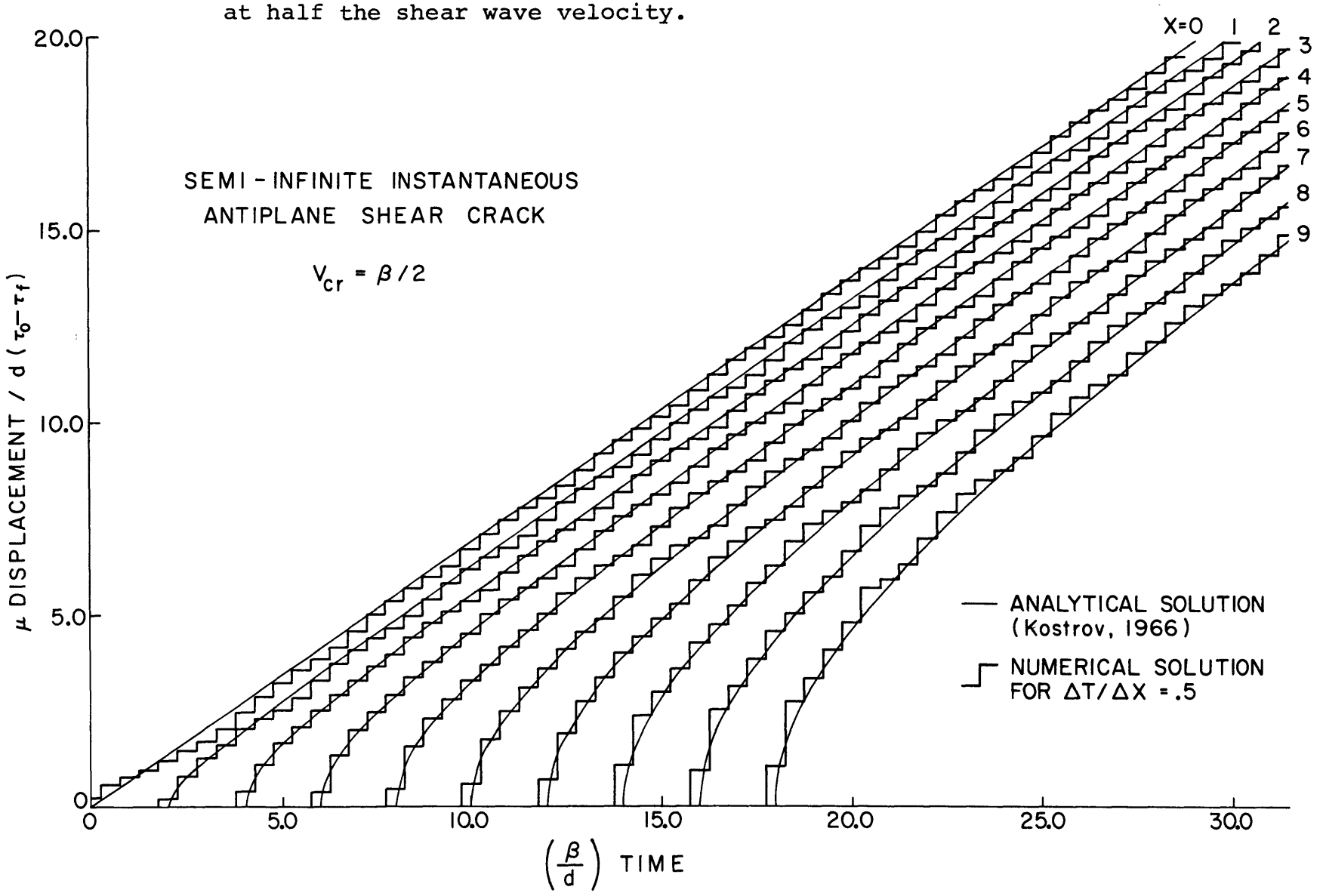

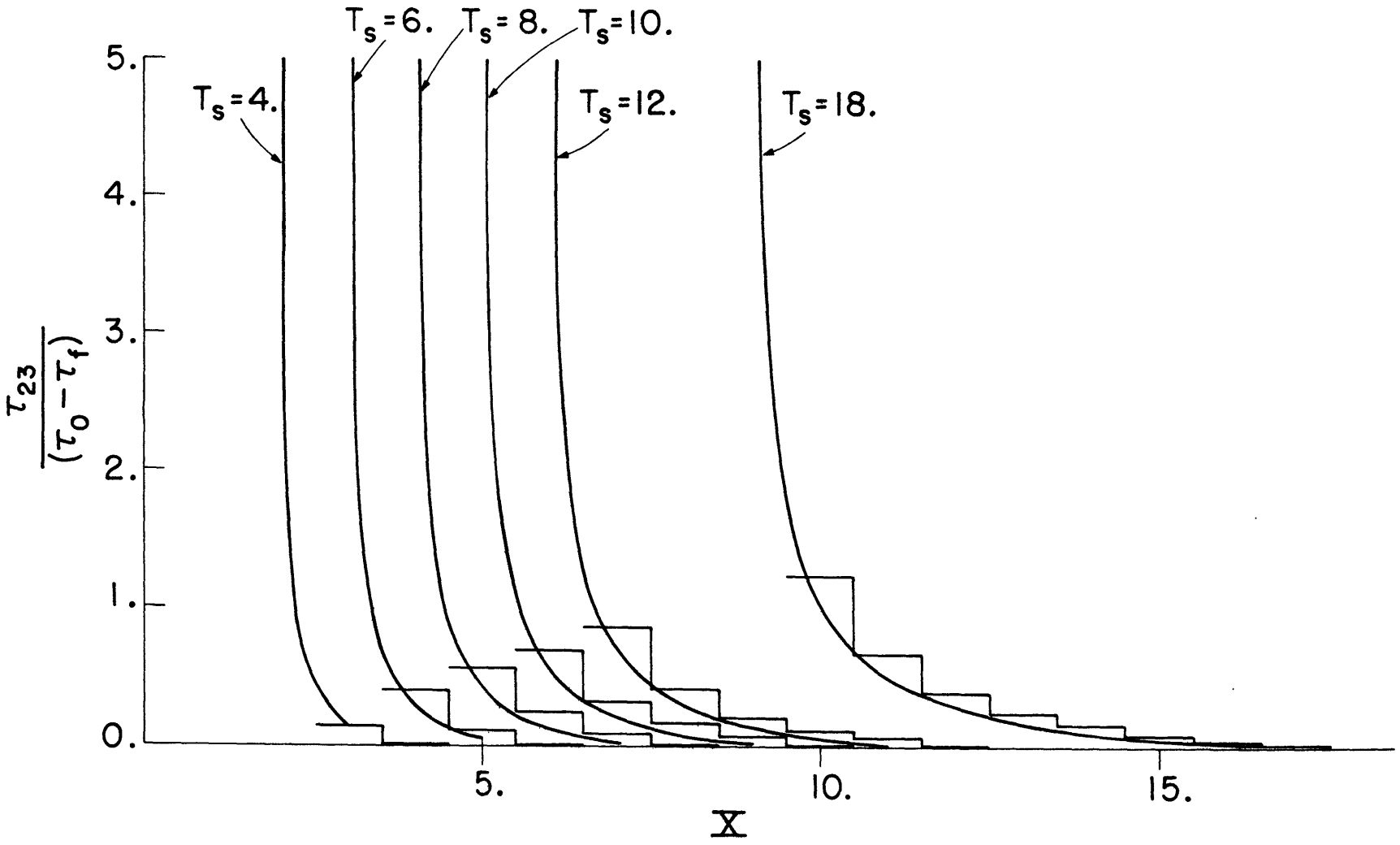

Figure 2.11. Comparison of stresses found by Kostrov (1966) with our numerical method for the same case as Figure 2.10, for $\Delta Ts/\Delta X$ = .5.

We also plot in Fig. 2.12 a comparison between the analytical and numerical results for the displacements when the crack-tip moves at the shear-wave velocity β, the case when $\Delta t/\Delta x = .5$. The agreement is found to be very good.

Figure 2.12. Same as Figure 2.10 but for the case when the crack-tip velocity is equal to the shear-wave velocity.

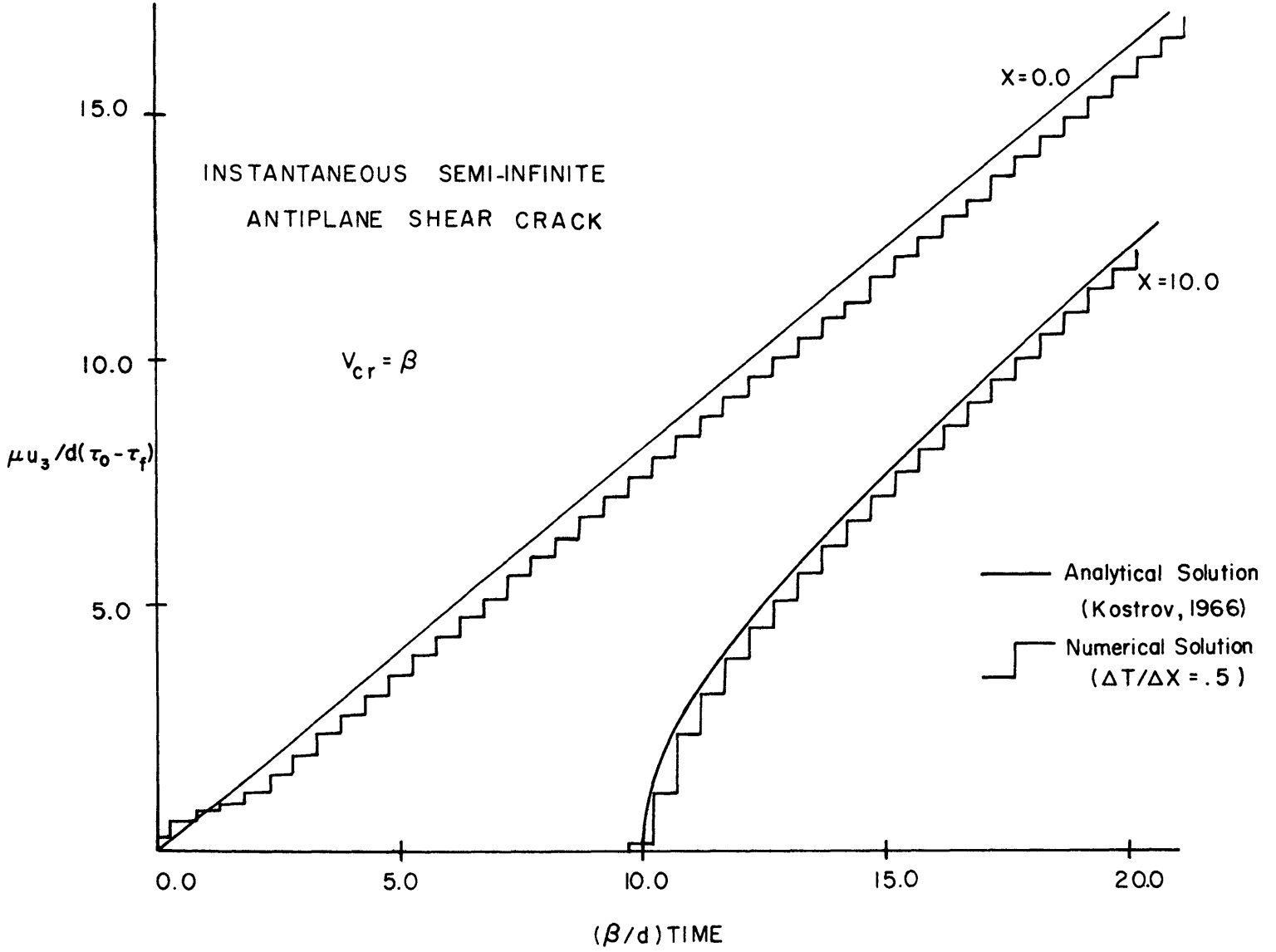

2.6 Comparison of our numerical results with existing numerical solutions of some in-plane crack problems

Since no analytic solution is available yet for a crack that extends at a constant velocity and stops, we compare our result with Madariaga's numerical solution for the case when the crack extends at half the P wave speed and stops. We shall make the crack stop to find the effect of the stopping phases on the displacement.

As in the anti-plane case, we consider an infinite, elastic body which is initially under a homogeneous state of stress whose only non-zero shear component is $\tau_{21} = \tau_o$, say, τ_o being a constant. At $t = 0$, a crack whose initial length is equal to one grid length in the space-dimension x_1 comes into existence and starts extending in both positive and negative x_1 directions at half the P wave speed. The origin of the coordinate system is taken at the center of the initial crack. The crack is stopped when it reaches a length equal to 41 times the grid-length in space. The wavefronts generated by the fracture, before it stops, is shown in Fig. 2.13.

The value of the shear stress component τ_{21} drops to some lower level, say τ_f, the dynamic frictional stress on crack from its constant initial value τ_o, on the crack surface. We shall take the stress-drop as the unit of stress. As shown before, the problem reduces to a half-

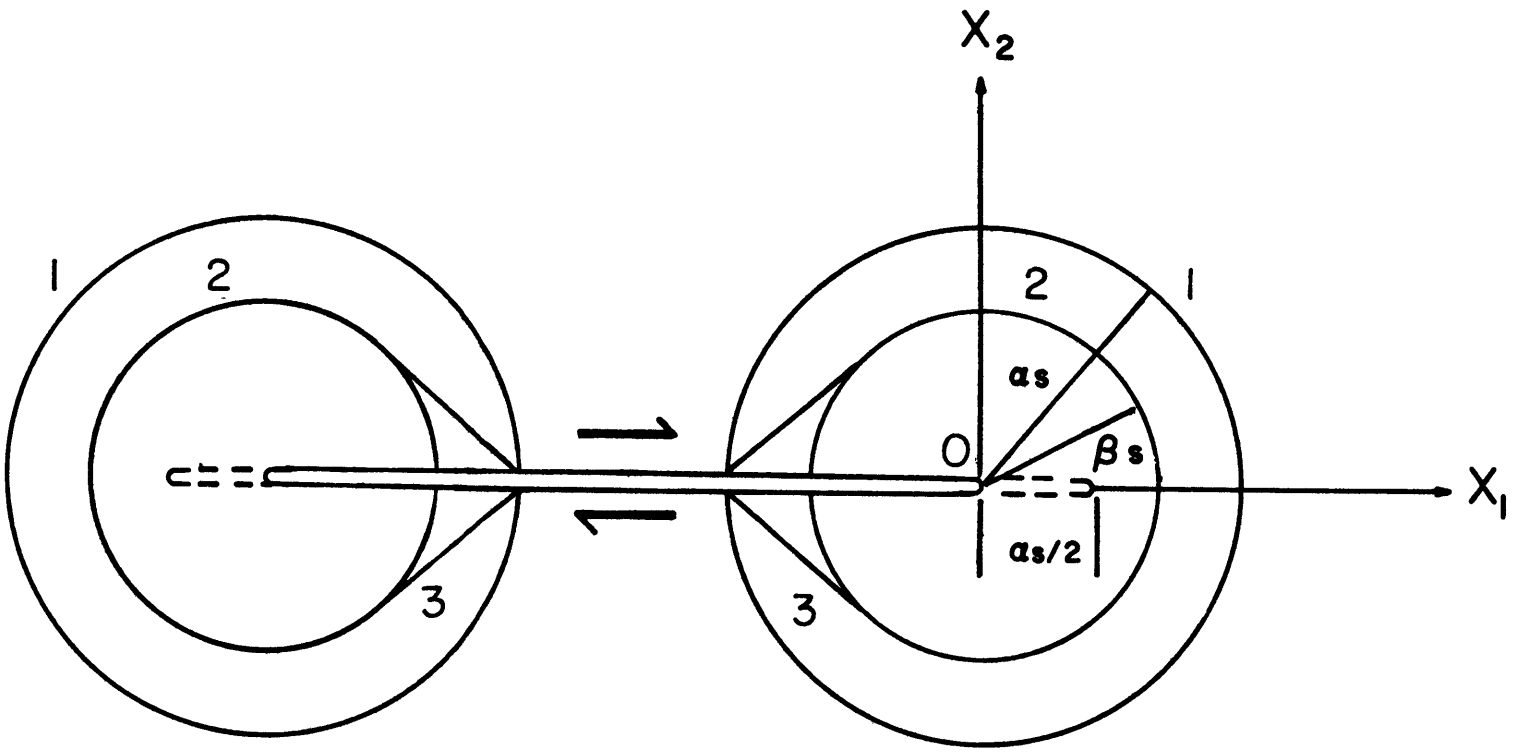

Figure 2.13. Wavefronts generated by dynamic fracture by a finite plane strain shear crack. The diffracted P, S and head-waves are shown by the numbers 1, 2 and 3.

space problem and we can use equation 2.13 and equation 2.19 to get the integral equation whose solution will give displacements on the crack as well as tractions on the plane of the crack outside the crack.

Madariaga (1976) directly discretizes the equation of motion by a leap-frog method on a staggered grid and determines the particle velocities inside the crack and stresses outside the crack. The displacements inside the crack are obtained by integrating the particle velocity. Madariaga does not allow a sudden jump in the stresses at the crack tip. Instead he introduces a smoothing of the stresses over the crack-tip from inside to outside of the crack. Because of this smoothing, his solution does not show the square-root rise of slip-function which is common to all the analytic solutions.

Fig. 2.14 shows a comparison of the numerical solution obtained by Madariaga for a crack extending bilaterally at half the P-wave velocity together with our solution for the parallel component of displacement for the same case. The displacements are plotted in Figure 2.14a at the $\wedge$ center of the fault in Figure 2.14b X=0.0 and $\wedge$ half-way between the center and the tip, X = .5, the final half-length of the crack being taken as unity. The result can be improved by increasing the number of grid points on the fault. In Fig. 2.14 we have taken $\Delta t = \frac{d}{\alpha}\Delta T_p = .025$ and $\Delta x = d\Delta X = .05$.

The stopping phases from tips are denoted by P_0 and S_0

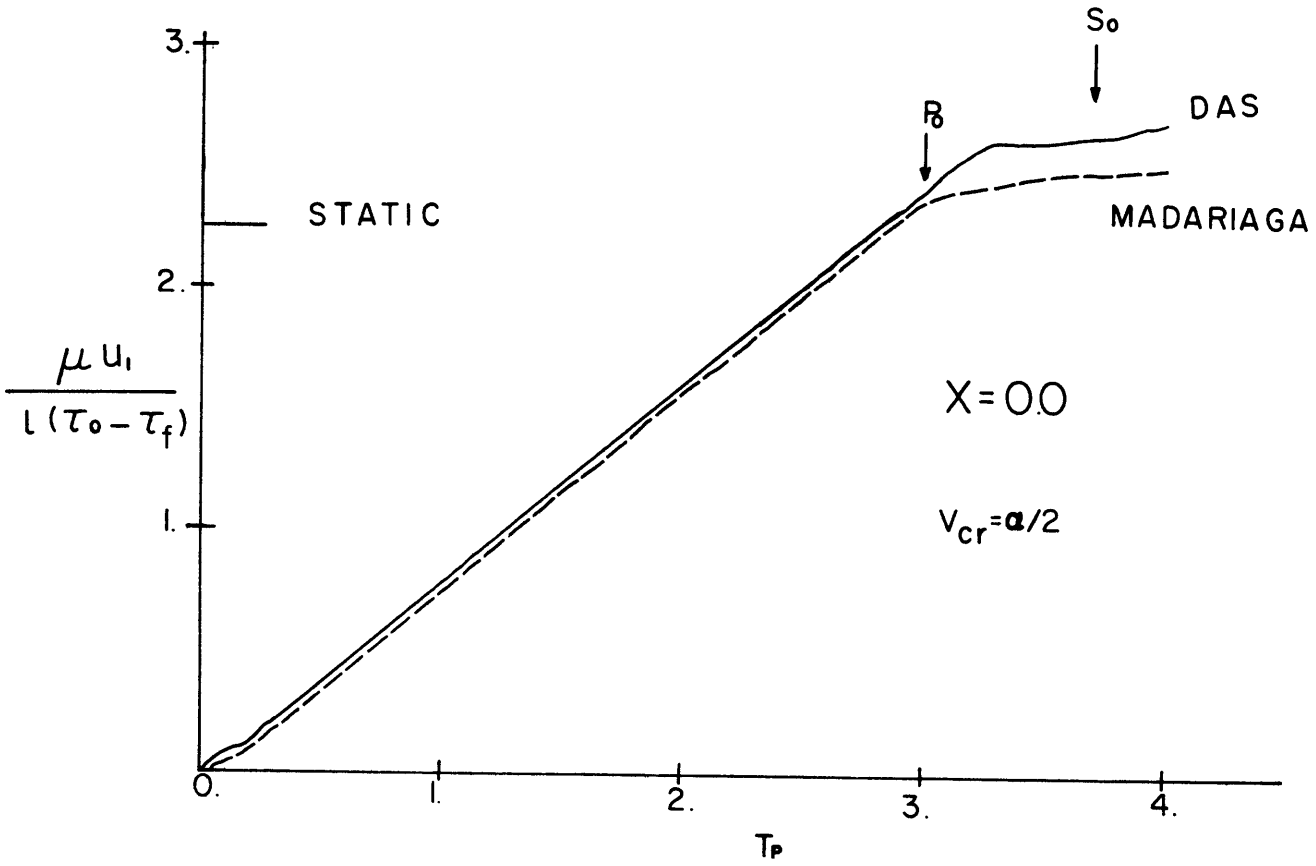

Figure 2.14. (a) Comparison of result obtained by Madariaga with that obtained using Hamano's method for a finite bilateral crack extending with velocity $\alpha/2$, and stopping when it reaches a half-length of unity. $\Delta Tp/\Delta X = .5$ in the case shown. The parallel displacements are plotted at the centre of the fault (X = 0). The static solution at the centre is shown. P_o, S_o denote the stopping phases.

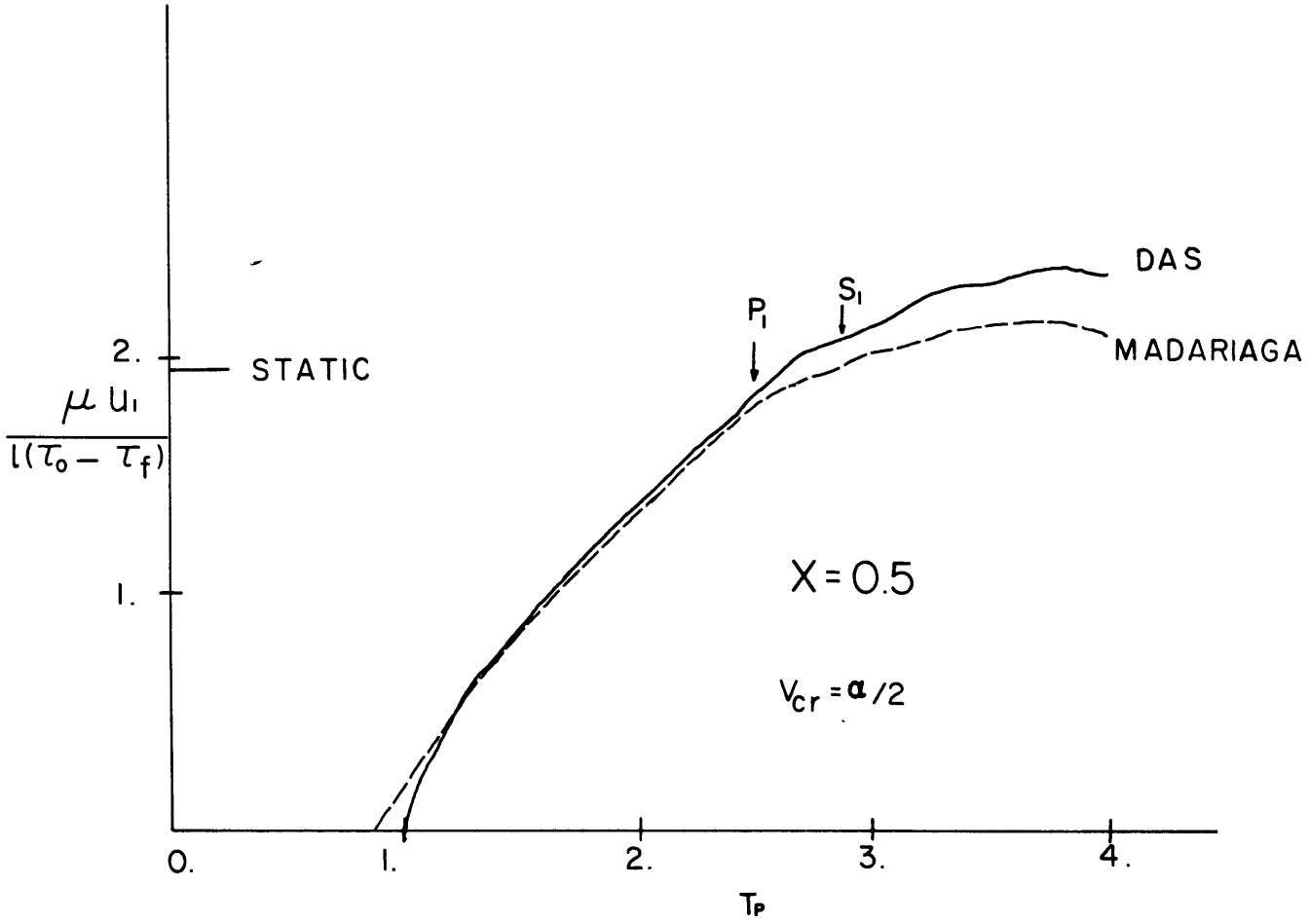

Figure 2.14. (b) Same as 2.14 (a) but the parallel displacements are plotted at the midpoint between the centre and the tip (X = .5). P_1, S_1 denote the stopping phases.

for X = 0.0 (here the stopping phases from both tips come in simultaneously) and for X = 0.5, the stopping phases from the nearer tips are denoted by P_1 and S_1 on Figure 2.14b. Our result agrees well with Madariaga's result till the P-stopping phase comes in, after which there is a difference of about 10% between the two results at Tp = 4.0 for X = 0.0 and of 15% at Tp = 4.0 for X = 0.5.

It is interesting to note in Fig. 2.14 that the crack does not stop as soon as the P stopping phases comes in but that there is a lag between the arrival of the P-stopping phase and the stoppage of slip on the crack. To quote from Madariaga, "it appears as if a 'healing' wave propagates inwards from the edge of the fault some time after the P and S stopping phases. The velocity of this healing wave appears to be variable but it is difficult to calculate due to numerical uncertainty in determining the healing time".

The static solution, for this case, is given by (Starr, 1928)

$$u_1(x_1) = \frac{9}{4}\sqrt{1-x_1^2} \quad , \quad -1 < x_1 < 1$$

$$= 0 \quad , \quad |x_1| > 1$$

At X = 0.0, the static solution is 2.25 and at X = 0.5, the static solution is 1.95. The static solutions are also shown in Fig. 2.14. The slip at the fault thus overshoots the static solution. The disagreement between Madariaga's

solution and ours at the first few points in time is due to the difference in smoothing.

Fig. 2.15 shows the component of displacement perpendicular to the fault plane found by the two methods, at X = 0.5 and X = 1.0. The corresponding static solution is given by Burridge (1969) as

$$u_2(x_1) = \frac{3}{4}\left(x_1 + \sqrt{x_1^2 - 1}\right) \qquad \text{for} \quad x_1 < -1$$

$$= \frac{3}{4} x_1 \qquad -1 < x_1 < 1$$

$$= \frac{3}{4}\left(x_1 - \sqrt{x_1^2 - 1}\right) \qquad 1 < x_1 .$$

Thus, the perpendicular component is not zero outside the crack but has some value in the whole plane of the crack, and is an odd function of x_1. There is a disagreement between Madariaga's result and our result in the early part of the perpendicular displacements. Near the arrival time of S waves from the nucleation point, we find a small but significant negative displacement but Madariaga does not. Richards' (1976) analytic solution, for a self-similar shear crack which does not stop, also shows this negative displacement, in favor of our solution.

Burridge (1969) also studied the same problem using the numerical method mentioned earlier. His results are quite similar to our results shown in Figs. 2.14 and 2.15. His solution is rougher than ours, because there are only

Figure 2.15. Same as Figure 2.14 but for the normal component of displacement, plotted at X = .5 and X = 1.0. P, S and C denote the arrival of the P and S waves from the first point of break and the passage of the rupture front.

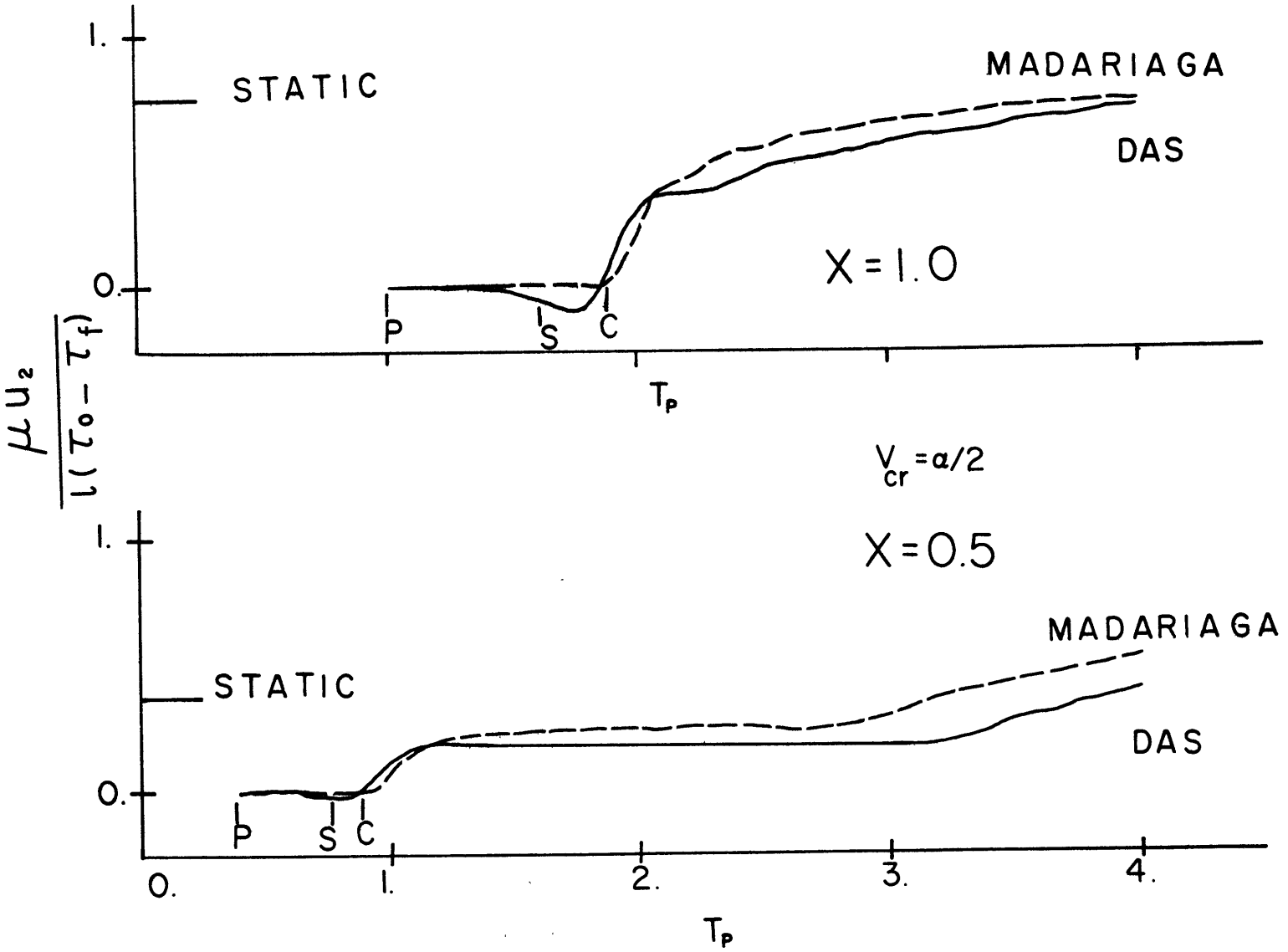

ten grid points over half the crack length, whereas in Madariaga's case and in our case we use twice as many grid points.

Figs. 2.16 and 2.17 show three-dimensional plots for the parallel and perpendicular components of displacement for the in-plane shear crack extending at half the P-wave velocity. They are again quite similar to the results obtained by Burridge (1969). Fig. 2.18 shows the comparison of our numerical solution with that of Madariaga for the parallel and perpendicular component of displacement when the crack-tip moves at the compressional wave velocity, α for the case when $\Delta t/\Delta x = .5$. The agreement between the two solutions is found to be very good.

In this chapter, we have shown that our numerical method gives results which agree well with existing analytical and numerical solutions. We have only considered the case of a crack-tip extending at a known constant velocity. In the next chapter, we shall show how we can find the motion of the crack-tip from the physical properties of the fault and the conditions of pre-existing stress on the basis of fracture criterion similar to the ones used by Griffith (1920), Irwin (1958), Barenblatt (1962) and Kostrov (1966).

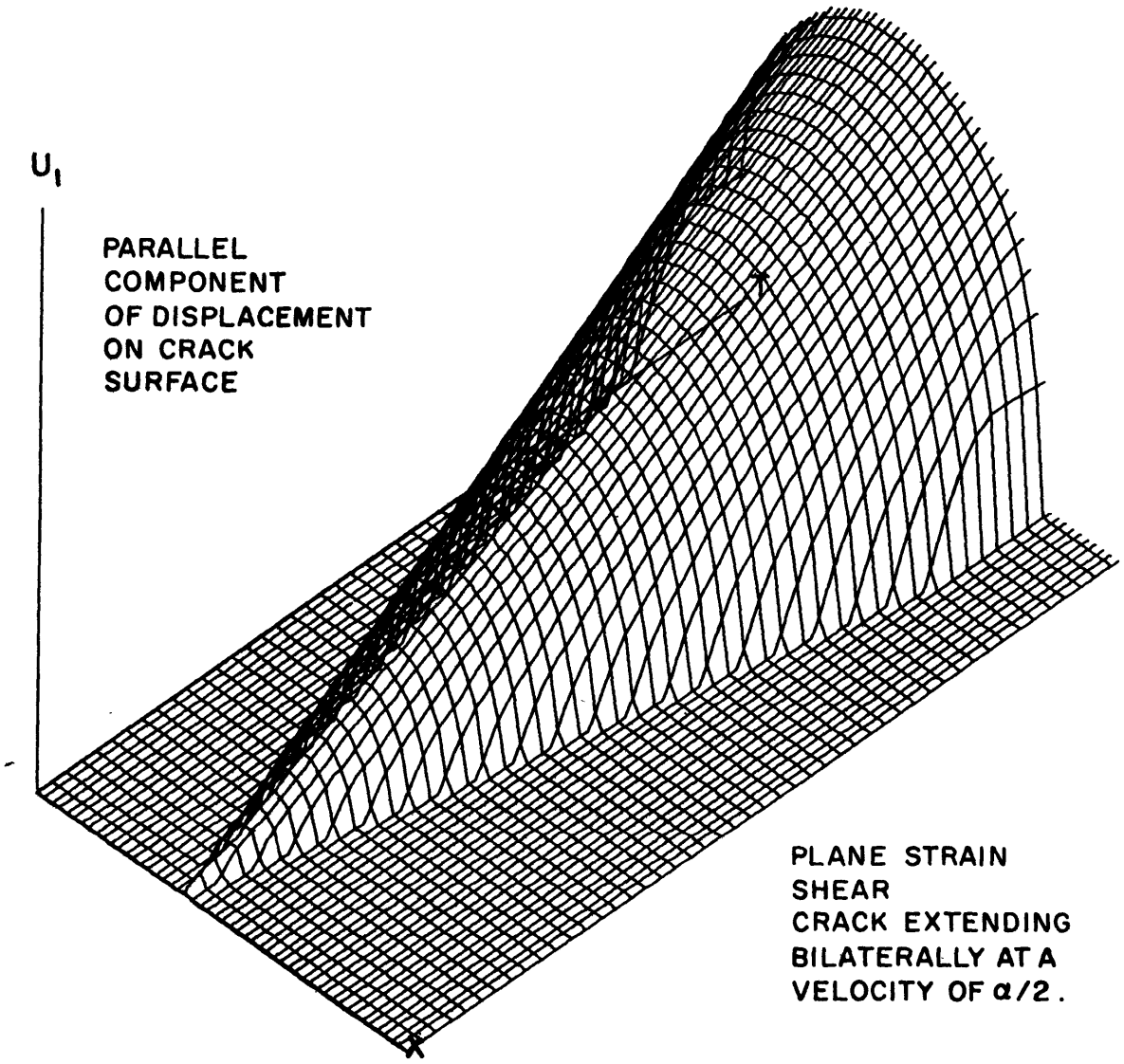

Figure 2.16. Composite plot showing parallel component of displacement on the crack surface for a bilateral crack extending at half the compressional wave velocity.

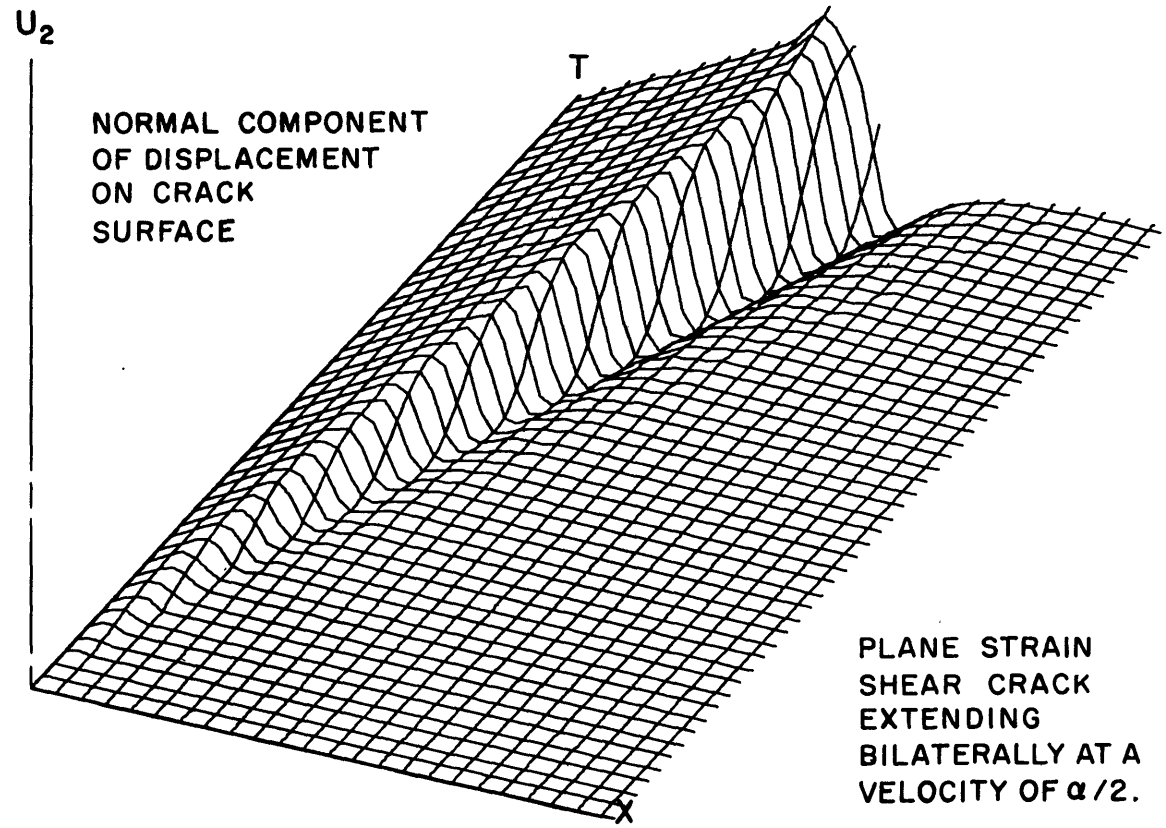

Figure 2.17. Same as Figure 2.16 for the normal component of displacement on the crack surface.

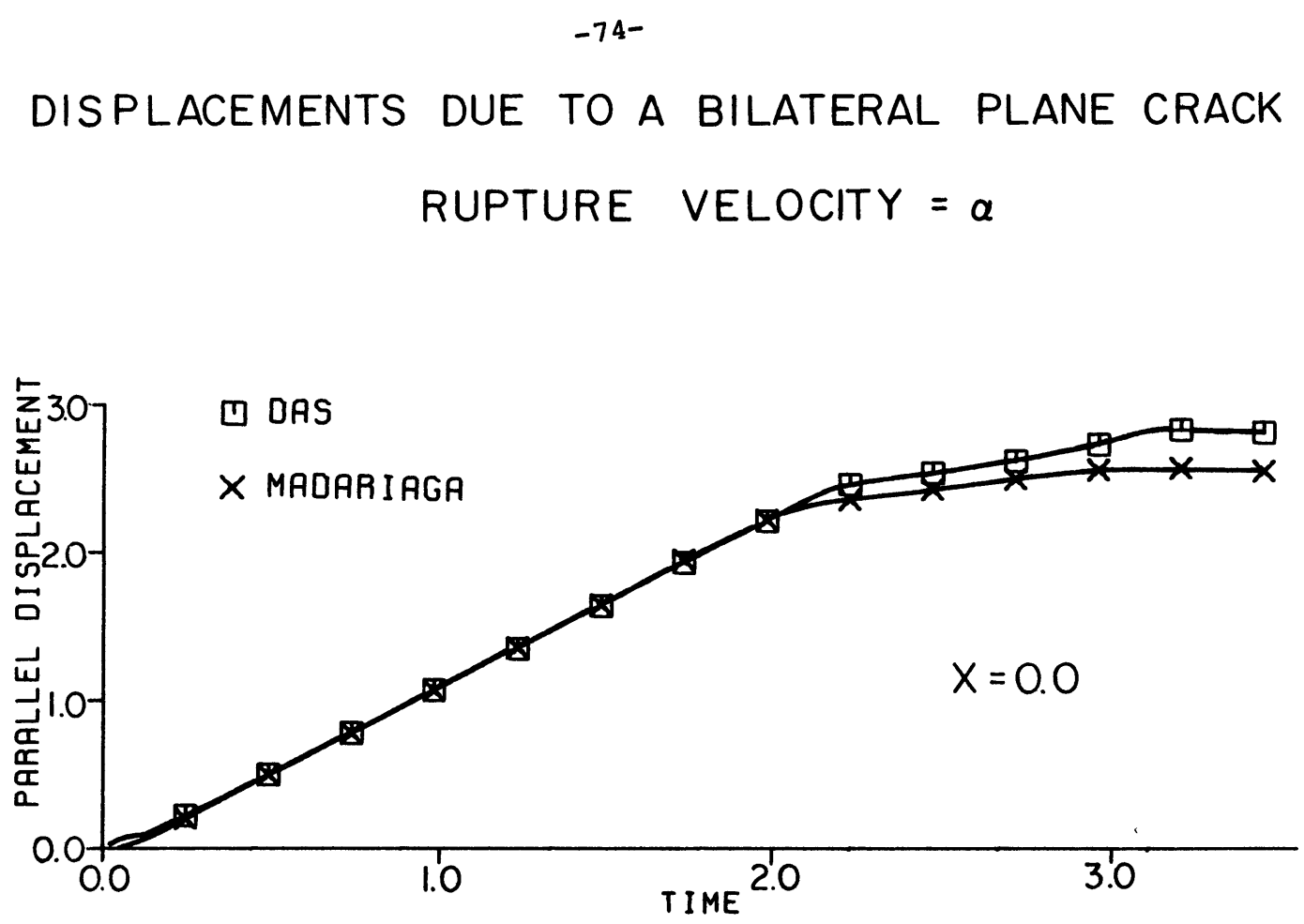

Figure 2.18. Same as Figures 2.14 and 2.15 but for case when crack tip moves at the velocity α.

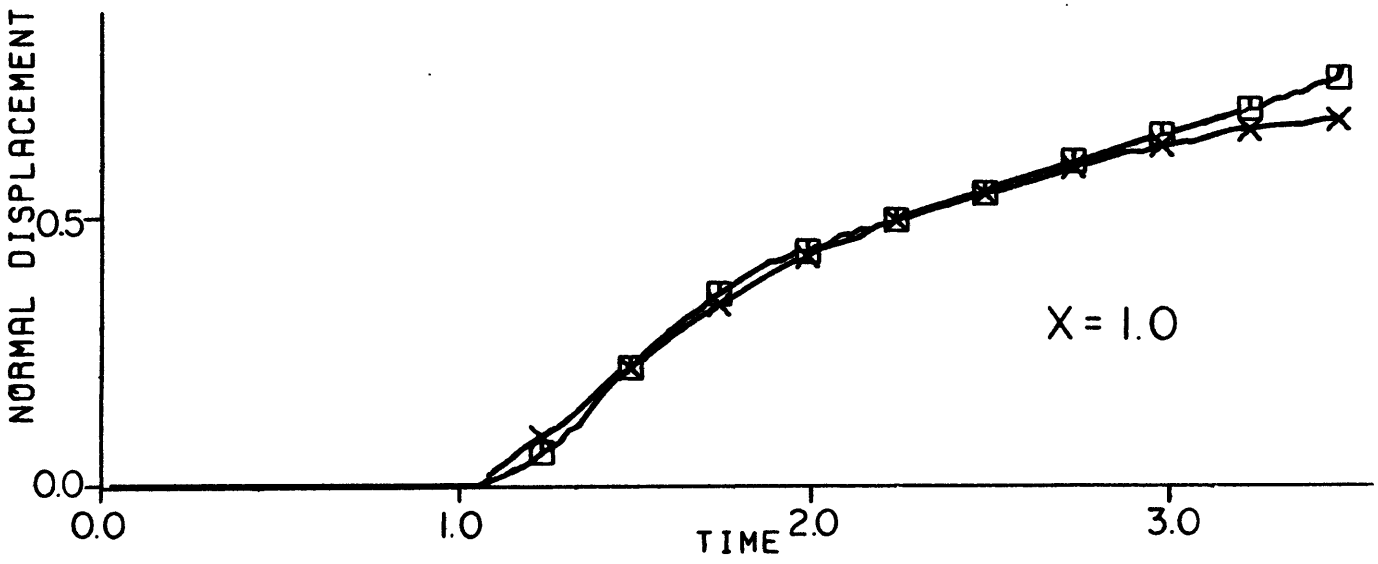

Chapter III

Fracture Criteria and Physical Parameters of a Shear Crack

In the previous chapter, the crack-tip position was known *a priori* as a function of time. In case the crack-tip position is not known, a fracture criterion is required to determine the rupture process. Kostrov (1966) has given an analytic solution for the position of crack-tip as a function of time for a semi-infinite instantaneous antiplane shear crack. We shall discuss his results and compare our numerical solution with his to find the relation between Hamano's fracture criterion and that of Irwin for the antiplane shear crack. For the in-plane shear crack, no analytical solution exists yet for the dynamic problem. Andrews (1976) has solved the problem of propagation of the in-plane shear crack by a finite difference technique for various values of the limiting rupture stress, and has shown that in certain cases, the velocity of the crack-tip goes from sub-Rayleigh to super-shear. We shall solve this problem by our method and compare our results with those of Andrews.

An "ideal" brittle body is defined to be one in which each element of the body can exist only in two states: either the element is continuous or it has been broken into two parts. No intermediate state exists and the material passes from the continuous state to the fractured state

at the edge of the crack.

A "non-ideal" brittle body is one in which an intermediate state exists between the broken and unbroken states, where the crack is not completely continuous or completely broken but is in a transitional state. This intermediate state is characterized by cohesive forces existing near the edges of the growing crack.

We next give a brief review of the mathematical theory of equilibrium cracks and discuss the fracture criteria of Griffith, Irwin and Barenblatt and Hamano.

Glossary of Symbols used in Chapter III

c = a constant $\simeq 2.0$ to 3.0

d_o = slip required for stress to drop [Andrews (1976)]

d_1 = width of end-zone in Barenblatt model

$g(\ell)$ = distribution of cohesive forces in end-zone

S = $(\tau_u - \tau_0)/(\tau_0 - \tau_f)$

t_c = time of onset of fracture

F = rate of work done in rupture process

$\vec{F}_D$ = frictional stress

G = $F/\dot{x}_1$ = energy release rate

K = modulus of cohesion

ℓ = distance from crack tip along crack surface $(0 < \ell < d_1)$ in Barenblatt model

L = instantaneous crack half-length

L_c = Griffith's critical crack half-length

W = work done by relaxing forces

γ = specific surface energy

μ_d = coefficient of dynamic friction

μ_s = coefficient of static friction

$\bar{\sigma}$ = average stress over grid

τ_0 = initial stress

τ_u = limiting rupture stress (or static friction stress)

τ_f = final stress (or dynamic friction stress)

§3.1 The mathematical theory of equilibrium cracks and discussion of fracture criteria.

Consider a crack of area S in a linearly elastic body subjected to a uniform state of stress τ_{ij}. Due to the applied stress field, there is a strain energy in the body. The crack surface is assumed to be stress-free. Let the area of the crack extend from S to S + δS, with the boundary condition that the new surface δS is also stress-free. The new stress-free surface δS is obtained by gradually relaxing to zero the stress on δS, or, equivalently, by gradually applying a traction with the same magnitude but opposite in sign to the one due to the initial stress on δS, while maintaining equilibrium. Due to the extension of the crack area from S to S + δS, the body loses strain energy it had accumulated from the application of the initial stress τ_{ij}. It is assumed that the body is held fixed at infinity. Let the displacement field before crack extension be u_i and after extension be $u_i + \delta u_i$ and let the stress field after crack extension be $\tau_{ij} + \delta\tau_{ij}$. Then the strain energy δW released in the extension δS is equal to the work required to close δS, and is given by

$$\delta W = \frac{1}{2} \int_{\delta S} n_j \, \tau_{ij} \, [\delta u_i] \, dS$$

where n_j is the normal to δS, $[\delta u_i]$ is the relative displacement of the crack surfaces and the integration is over the newly formed crack surface δS. For the extension δS to be possible, the strain energy lost by the body must at least be equal to the increase in surface energy $2\gamma\ \delta S$, where γ is the energy required to create unit area of crack surface or the "specific surface energy". Thus, crack extension requires that

$$\delta W \geq 2\gamma\ \delta S \qquad (3.1)$$

where γ is a material constant. This is Griffith's criterion for the static problem.

If the stress on the crack is released abruptly, then the problem becomes a dynamic one and we have to consider the kinetic energy of the system as well. Griffith's criterion can then be written as $\delta W - \delta K = 2\gamma\ \delta S$, where δK is the change in the kinetic energy of the body. Thermal effects are neglected. In the dynamic case as well, γ is a material constant characterising the rupture strength of the material. Brace and Walsh (1960) have measured γ experimentally in the laboratory for quartz and found it to be of the order of 10^3 ergs/cm^2 for tensile cracks. Griffith's criterion holds for an ideal, brittle body.

Irwin's fracture criterion

Griffith's criterion is a global criterion and is thus not convenient for practical applications. Irwin (1958) introduced a local criterion, that the crack extends when the stress intensity factor k at the tip of the crack exceeds a constant K/π. Irwin's criterion is equivalent to the Griffith criterion in the static case, in which the stress intensity factor and the energy flow per unit length of crack extension are uniquely related to each other.

The Barenblatt Crack Model and Fracture Criterion

Let us now try to understand what happens at the tips of the crack. If the distance between the two sides of the crack is greater than the radius of molecular attraction at all points, then the increase of surface energy due to crack extension will be given with sufficient accuracy by the product of the increment of surface area and the surface tension of the material. However, at the very ends of the crack the two faces remain very close together and large forces of atomic or molecular attraction exist across the two faces. In a sufficiently long crack, the error in strain-energy due to neglecting these molecular forces of attraction may be small, but for cracks of small length, the error may be significant.

Barenblatt (1959) represented these "attractions" or "cohesive forces" as intense force distributions acting at small zones at the crack tip. These cohesive forces pull the crack faces together. If the crack exists in an infinite body which is under a tensional load applied at infinity, a stress singularity is introduced at the tip which is tensile in nature (i.e. it tends to pull the two faces of the crack apart). If the cohesive forces are taken by themselves (i.e. no remote tension is applied), then they induce a stress singularity at the end which is compressive in nature (i.e. it tends to pull the two faces together). It is possible that the two stress singularities cancel one another and the final stress field has no singularity at the crack tip. Goodier (1958) says that this cancellation has to be <u>postulated</u> and is not subject to proof. It can be shown (Barenblatt, 1959) that as the result of the vanishing of the stress singularity, the two faces of the crack, after deformation, join smoothly in cusp form at the tips, as shown in Figure 3.1.

In Barenblatt's crack model, a transitional region exists between the broken and unbroken states of the crack, where the elements of the medium are neither continuous nor completely separate. The three postulates of his model are:

(i) The dimension d_1 of the transitional region is small

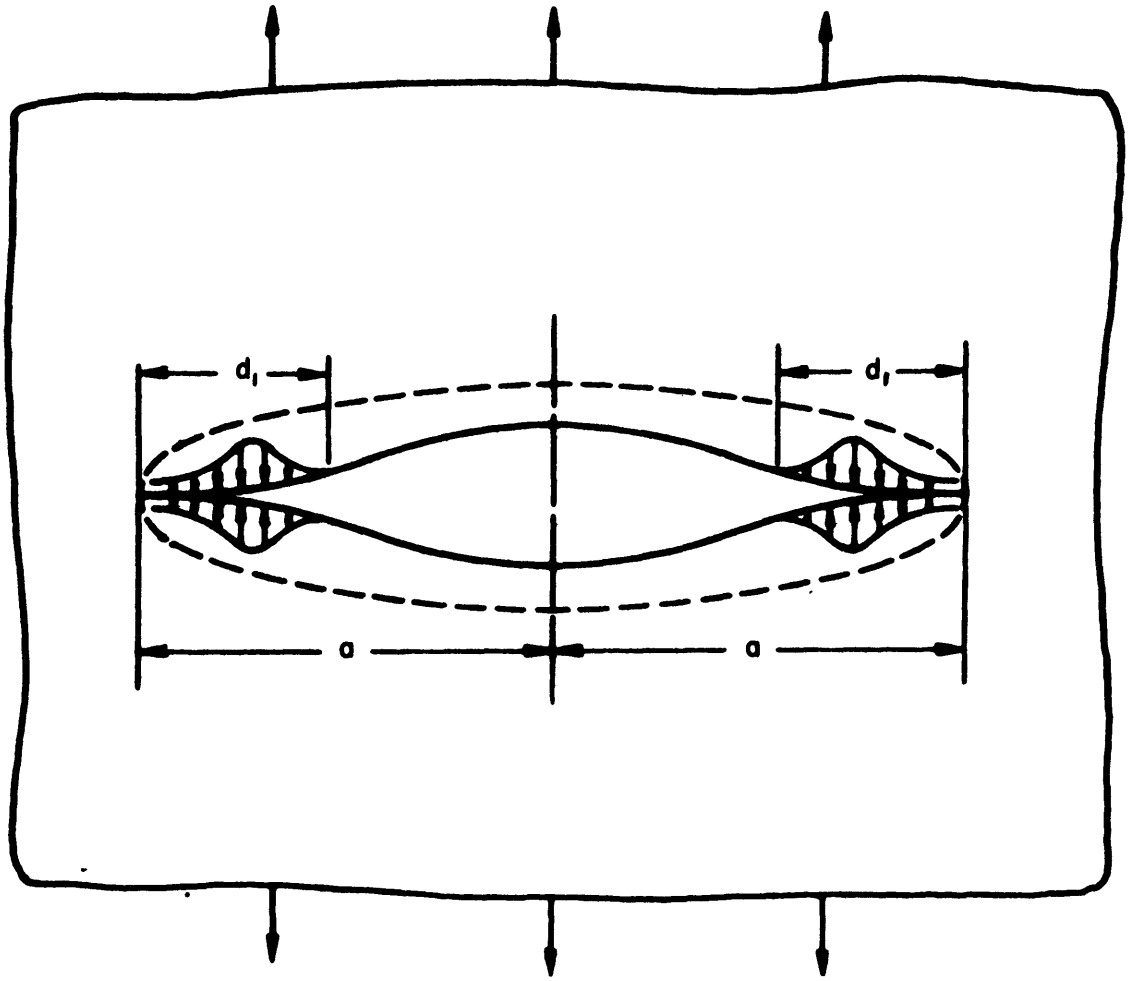

Figure 3.1 Schematic diagram showing the cohesive forces at crack tips in Barenblatt's theory, a is the crack-half-length, d_1 the length of the end-zones over which the cohesive forces act. The two faces of the crack join smoothly in cusp form at the tips of the crack. The dotted line shows the equilibrium shape of the crack, which is an ellipse.

in comparison with the size of the whole crack.

(ii) The distribution of the displacement in the transition region does not depend upon the acting load and for a given material under given conditions (temperature, composition and pressure of the surrounding atmosphere, etc.) is always the same.

According to this, the crack-tips in a given material under given conditions are always the same. During propagation of the crack, the transitional region moves over to another place but the distribution of the distortion remains the same. Since the cohesive forces attracting the two faces of the crack to one another depend only on the displacement distribution, the stresses due to the cohesive forces will be the same at the tip, as the tip moves.

(iii) The opposite sides of the crack are smoothly joined at the ends or, which amounts to the same thing, the stress at the end of a crack is finite.

Barenblatt derives his fracture criterion from the condition of boundedness of stress at the crack-tip, i.e. the requirement of cancellation of stress singularities at the tip. For finite stress at the tip, the cohesive forces must adjust themselves so that they reduce to zero the stress concentration factor k which the applied loads alone would produce. If k is too great, the cohesive forces

cannot cancel it and the crack will extend. This leads to the criterion

$$k = \int_0^{d_1} \frac{g(\ell)\, d\ell}{\sqrt{\ell}} = K/\pi \qquad (3.3)$$

where k is the stress-intensity factor calculated neglecting cohesive forces, ℓ is the distance from the crack-tip along the crack surface, $g(\ell)$ is the distribution of cohesive forces in the end zone, d_1 is the length of the end zone, and K is a constant. By the third assumption of Barenblatt, K is a material constant and is called the "cohesive modulus". It has the dimension of $[FL^{-3/2}] = [ML^{-1/2}T^{-2}]$, where L is the dimension of length, F the dimension of force, M the dimension of mass and T of time.

Barenblatt (1962), Goodier (1968) and Willis (1967) have shown that the critical load required for the extension of a crack in the static case using the Griffith and Barenblatt fracture criteria are the same. Goodier shows this by evaluating the work done at the tip, during an infinitesimal extension of the crack, by the forces near the tip. In the Barenblatt theory, since there is no stress singularity, there is no contribution to the work done at the tip from the "holding force" distribution (i.e. by the load on the body) on the crack extension and all work is done by the cohesive force distribution $g(\ell)$.

In Griffith's theory, all the work comes from the "holding force" distribution on the crack extension and results in a finite energy flow into the crack tip (Freund, 1972).

The form of the cohesive force as a function of distance between the faces of the crack is shown in Figure 3.2. The force of atomic attraction first increases in proportion to the separation between the two faces. But as the separation proceeds, the force rises to a maximum and then decreases towards zero as the two faces separate beyond the range of significant attraction. The exact form of this function is not known. Brace and Walsh (1960) have approximated it by a sine-function which is zero when the atoms on the two faces of the crack have their normal separation, then rises to a maximum f_{max}, which is of the order of Young's modulus, and is again zero at a distance equal to the atomic radius of these atoms.

It is thus seen that the fracture criteria of Griffith, Irwin or Barenblatt lead to the same result for the static case. Thus for the purpose of determining when a crack starts to propagate, it is immaterial which fracture criterion is used. However, if we want to determine the rupture process for a propagating crack, the result will depend on the fracture criterion used. The Barenblatt criterion offers a more realistic picture of the stresses near the crack-tip. In Griffith's theory γ is the material

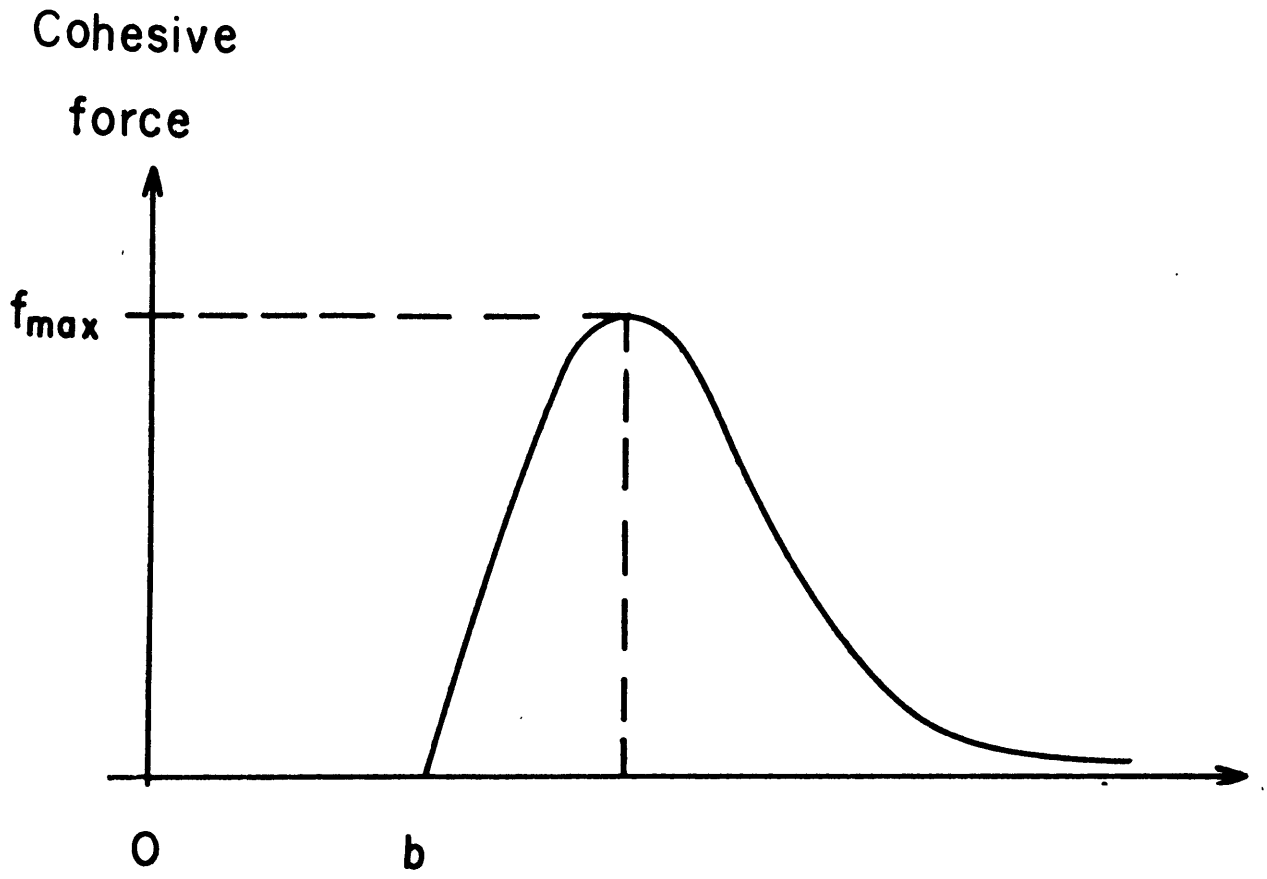

Figure 3.2 Form of the cohesive force as a function of the distance between the faces of the crack. At distances less than b there is no cohesive force i.e. b is the normal separation distance between the atoms.

constant and is independent of the crack-tip velocity $\dot{x}_1$. In the Irwin criterion, K is the material constant and during propagation the relation $k(\dot{x}_1) = \frac{K}{\pi}$ is satisfied, $k(\dot{x}_1)$ being the instantaneous stress-intensity factor for the dynamic problem and depends on $\dot{x}_1$ [Equation (2.24)], and the crack-tip position using the Irwin criterion will be different from that using Griffith's criterion. An example of this will be given in Section 3.3, for the antiplane shear crack and this will illustrate the difference between the fracture criteria.

The fracture criteria discussed above are not directly adaptable to numerical computation. Hamano (1974) introduced a fracture criterion suitable for numerical techniques. In this criterion, when the stress at a grid point outside the crack and nearest to the crack tip exceeds a certain critical value, the crack extends by one grid point. This stress may be considered as an average of an analytic solution over the grid length d immediately ahead of the crack-tip (Fig. 3.3). Since the analytic solution for the stress τ is approximated near the crack-tip by

$$\tau = \tau_f + \frac{k}{\sqrt{x_1}},$$

where x_1 is the distance from the tip, the stress at the grid point obtained by the numerical method can be obtained as

Figure 3.3 Figure showing the form of the stress near the crack-tip as a function of the distance from the tip. The analytic solution shows the square-root singularity at the tip. The discrete solution is step-like and is approximately equal to the averaged value of the analytical solution over a grid.

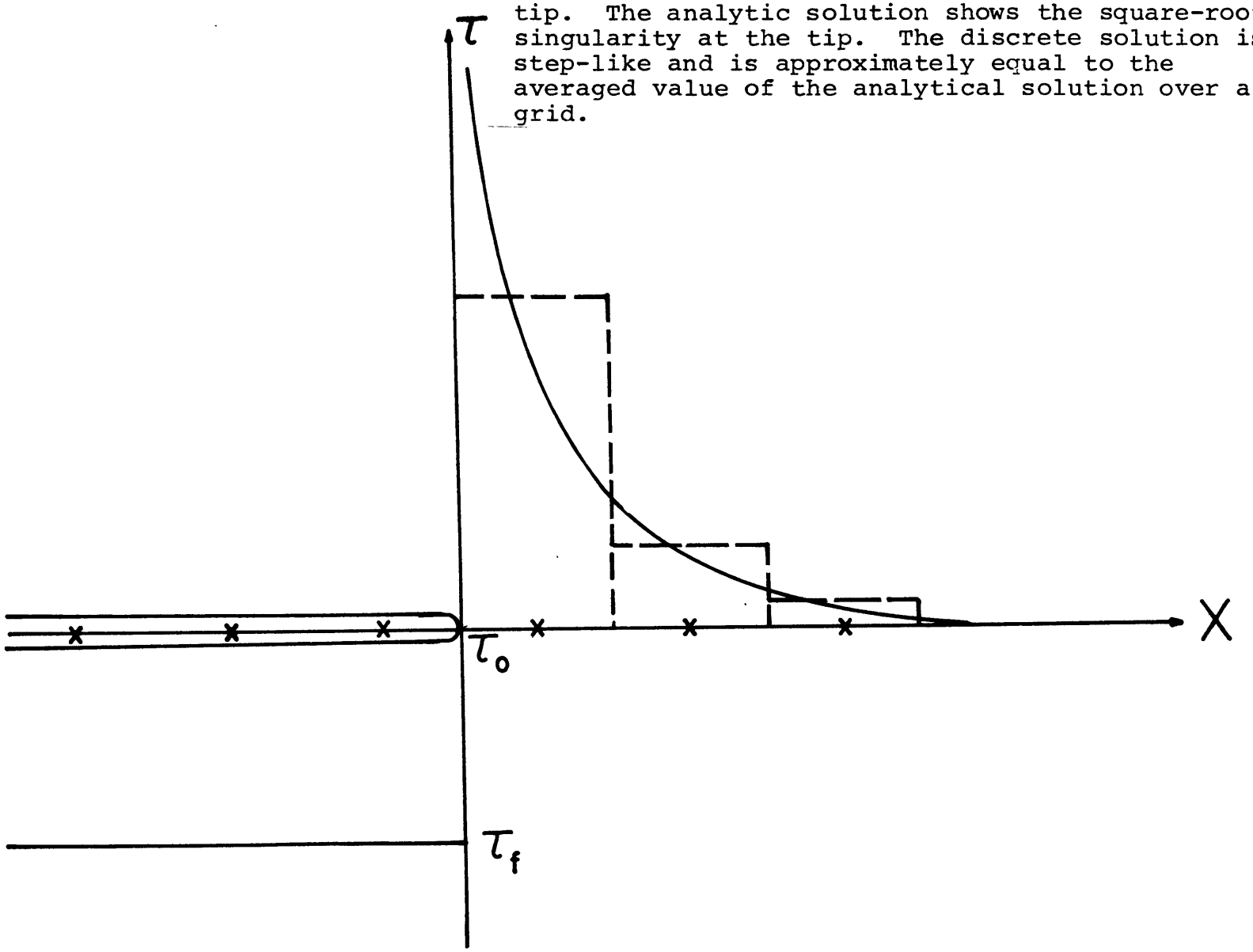

$$\bar{\tau} \doteqdot \tau_f + \frac{1}{d} \int_0^d \frac{k}{\sqrt{x_1}} \, dx_1$$

$$= \tau_f + 2k/\sqrt{d} \qquad (3.4)$$

Equations (28), (31), (34) and (37) of Ida and Aki (1972) show that the stress singularity term refers to τ_f, the stress inside the crack rather than to τ_o, the initial stress.

Then, we find the stress intensity factor k is related to $\bar{\tau}$ by

$$k \doteqdot \frac{(\bar{\tau} - \tau_f) \sqrt{d}}{2}$$

In other words, Hamano's criterion that $\bar{\tau}$ must exceed a certain critical stress τ_u is approximately equivalent to Irwin's criterion that the stress intensity factor k must exceed k_c. k_c and τ_u are related by

$$k_c \doteqdot \frac{(\tau_u - \tau_f) \sqrt{d}}{2}$$

We shall introduce a factor c to relate k_c and τ_u exactly as

$$k_c = \frac{(\tau_u - \tau_f) \sqrt{d}}{c} \, . \qquad (3.5)$$

We expect c to be about 2. Thus, Hamano's criterion is an approximate form of Irwin's criterion.

§3.2 Friction on the crack surface.

In our previous discussion, a point on the fault-plane was broken according to some fracture criterion and the final stress inside the broken region was put equal to the dynamic frictional stress, but the frictional arrest of the slip motion was not considered. Inside the ruptured region, the slip is resisted by the dynamic friction between the two sides of the crack. If μ_d is the coefficient of dynamic friction, which is assumed to be a constant and $[\dot{u}_1]$ is the relative velocity across the crack plane $x_2 = 0$, then the frictional stress $\vec{F}_D^+$ on the upper side of the fault (i.e. $x_2^+ = 0$ plane) is

$$\vec{F}_D^+ = -\mu_d \, \tau_{22}^{initial} \, \mathrm{sgn}[\dot{u}_1] \text{ when } [\dot{u}_1] \neq 0 \qquad (3.6)$$

where $\tau_{22}^{initial}$ is the normal component of initial stress on the body. This is Coulomb's law of friction. τ_{22} remains constant throughout the rupture process in the case of a plane fault in an infinite, homogeneous medium (Richards, 1976) so that $\vec{F}_D$ is time-independent. The stress on the lower side of the fault is opposite in sign to $\vec{F}_D^+$. The negative sign in equation (3.6) indicates that friction resists slip. We may assume that the slip at any

point on the fault is arrested when the slip velocity reaches a certain value, which we may call the "critical velocity". If we take the critical velocity to be zero, we would get the case analogous to the "stick-slip" of rock mechanics. In this case, the motion is stopped when the slip velocity tends to reverse sign, i.e. when the slip has reached its maximum value. There is thus no overshoot in displacement but there will be an overshoot in the stress inside the crack at the time of arrest and the final stress on the crack will be lower than the dynamic frictional stress. If the critical velocity is taken to be large and negative, then there will be no frictional arrest of sliding and there will be an overshoot in the displacement. The slip at a point will stop, in this case, only after the waves reflected from the crack-tip(s) become negligible. If the critical velocity is positive, the slip will stop before it reaches its maximum value. Once a point is stopped, it will not slip until the stress exceeds the static friction stress.

Burridge (1973) has considered the case of in-plane self-similar shear cracks with friction but lacking cohesion, i.e. the stress intensity factor $k = 0$. He assumes that initially the two crack faces are not welded together but merely pressed together and that the static limiting friction is high enough to prevent slippage on the crack plane.

Thus, in addition to equation (3.6), he has the condition

$$|\vec{F}_D^+| \leq -\mu_s \tau_{22}^{\text{initial}} \text{ when } [\dot{u}_1] = 0 \qquad (3.7)$$

where μ_s is the coefficient of static friction. Burridge has shown that when a zone of slip, governed by a Coulomb law of friction, spreads, only certain rupture speeds are possible. Such a crack cannot propagate at speeds except at the Rayleigh wave speed, at which the stress intensity factor vanishes. Burridge showed that even at the Rayleigh velocity, the stress ahead of the crack at the S-wave front may exceed the static friction and cause the fault to slip. If $\frac{\tau_u - \tau_0}{\tau_0 - \tau_f} > 1.63$, where τ_u is the static friction stress, the crack can run at the Rayleigh velocity. If the static limiting friction is sufficiently low, the crack may propagate at the P-wave velocity.

Burridge and Halliday (1971) have considered cohesionless antiplane shear cracks having friction. The fracture criterion is that a rupture will propagate when the stress at the tip overcomes the static frictional stress. The assumption of lack of cohesion implies that the stress-intensity factor $k = 0$. They find that for such a crack to decelerate and stop, the stress-drop must change sign. If a negative stress drop cannot exist, then the crack will propagate with the shear-wave velocity and will never stop.

It may be well to point out here the basic difference

between Hamano's criterion and that of Burridge and Halliday. Burridge and Halliday do not have a stress-singularity at the crack-tip while Hamano does have the stress concentration at the tip, which is only smoothed. Thus Hamano's criterion is for cracks having cohesion and is different from the criterion used by Burridge (1973) and Burridge and Halliday (1971).

§3.3 Determination of relation between Hamano's and Irwin's fracture criterion.

Kostrov (1966) analytically determined the rupture process for a semi-infinite instantaneous antiplane shear crack in an infinite medium by using Griffith's fracture criterion, i.e. assuming γ is a material constant. Following a method similar to Kostrov's, we can find the rupture process for Irwin's fracture criterion, i.e. assuming the stress-intensity factor K is the material constant. Then, the constant c defined by equation (3.5) can be determined by comparing the fracture process as found by Hamano's method and as found by Irwin's criterion.

Following Atkinson and Eshelby (1968) we define G, the "energy release rate" as the amount of energy which "leaves" the material by way of the tip, calculated per unit length of the crack tip advance. The rate of work done in the rupture process is given by

$$F = -\frac{\pi}{2} k[\dot{U}_j^+ - \dot{U}_j^-] \tag{3.8}$$

where k is the stress-intensity factor and $\dot{U}_j^{\pm}$ are the velocity-intensity factor on $x_2^{\pm} = 0$. This equation is derived in Appendix I. k and $\dot{U}_j^{\pm}$ were given in equations (2.24) and (2.25) for the semi-infinite antiplane shear crack. Substituting these relations in equation (3.8) we

get

$$\frac{F}{\dot{x}_1} = G(x_1,\dot{x}_1) = \frac{\pi k^2}{\mu\sqrt{1 - \dot{x}_1^2/\beta^2}} \tag{3.9}$$

where

$$k = \frac{\sqrt{1 - \dot{x}_1/\beta}}{\pi} \int_{x_1-\beta s}^{x_1} \frac{f(v)\ dv}{\sqrt{x_1 - v}} \tag{3.10}$$

$\tau = f(x_1)$ is the stress inside the crack and thus a known quantity in equation (3.10). $\dot{x}_1$ is the instantaneous crack-tip velocity. If all the work done is spent in increasing the surface energy of the newly formed crack surface, then

$$G(x_1,\dot{x}_1) = 2\gamma \tag{3.11}$$

where γ is the specific surface energy of the body. This is the equation of motion of the crack-tip. $G(x_1,\dot{x}_1)$ does not depend on the acceleration of the tip so that if we regard the tip as a "particle" it has no inertia. [The sudden jump at the tip from a zero velocity to a finite velocity is allowable because of this property that the tip has no inertia!!] However, Husseini et al. (1975) showed that the tip can extend into a region where no stress exists (cf. Chapter 4).

Using equations (3.9) and (3.11) we get a non-linear differential equation for the crack-tip motion. This

equation is, in general, not easy to solve analytically. For two very special cases, Kostrov (1966) has found the analytic solution, one of which we discuss next, and the other in Section 3.4.

Kostrov (1966) studied the case of an infinite, elastic body, initially under a homogeneous state of stress $\tau_{23} = \tau_0$, say. At time $t = 0$, a semi-infinite crack instantaneously appears and the stress on the crack surface is taken to be completely released. The geometry of the crack is shown in Figure 2.2. As in section 2.5, we can take the initial stress to be zero and the final stress on the crack to be τ_0 (since there is complete stress release, $\tau_f = 0$). Then $f(x_1) = \tau_0$. If we normalize all stresses by τ_0, we can take $f(x_1) = 1$. The stress intensity factor is given by equation (3.10) as

$$k(\dot{x}_1) = \frac{\sqrt{1 - \dot{x}_1/\beta}}{\pi} \int_{x_1 - \beta s}^{x_1} \frac{dv}{\sqrt{x_1 - v}}$$

$$= \frac{2\sqrt{1 - \dot{x}_1/\beta}}{\pi} \sqrt{\beta s} \qquad (3.12)$$

Kostrov uses the fracture criterion that fracture occurs when the stress-intensity factor found without regard to the cohesive forces is equal to the modulus of cohesion K divided by π, K being a function of $\dot{x}_1$ only. From equation (3.9) and this condition we get

$$\frac{K(\dot{x}_1)}{\pi} \equiv k(\dot{x}_1) = \sqrt{\frac{\mu G}{\pi}\sqrt{1 - \dot{x}_1^2/\beta^2}}$$

so that

$$K(\dot{x}_1) = \sqrt{\pi\mu\, G\sqrt{1 - \dot{x}_1^2/\beta^2}} \tag{3.13}$$

and thus

$$K(0) = \sqrt{\pi\mu G}\ .$$

The crack remains stationary as long as $k(0) < \frac{K(0)}{\pi}$. The time t_c of onset of fracture is given by the condition $k(0) = \frac{K(0)}{\pi}$, and using equation (3.12) this leads to

$$t_c = \frac{K^2(0)}{4\beta} \tag{3.14}$$

We can also find an equation for the position of the crack-tip as a function of time, using the criterion that during propagation $k(\dot{x}_1) = \frac{K(\dot{x}_1)}{\pi}$. [Here $K(\dot{x}_1)$ is <u>not</u> a material constant.] This gives the differential equation

$$\frac{K(\dot{x}_1)}{\pi} = \frac{2}{\pi}\sqrt{1 - \dot{x}_1/\beta}\ \sqrt{\beta s} \tag{3.15}$$

If $K(\dot{x}_1)$ is bounded, then from the above equation $\dot{x}_1 \to \beta$ for $t \to \infty$. Thus, the velocity of the tip tends to the shear wave velocity for large t and once the crack starts propagating it never stops. For purely brittle fracture, we can take $G = 2\gamma$, and using $k(\dot{x}_1) = K(\dot{x}_1)/\pi$, and the equations (3.12) and (3.13) we find the position of the crack-tip as a function of time as

$$x_1 = \beta s + \beta\left(\frac{\pi}{2} - 1 - 2 \tan^{-1} \frac{s}{t_c}\right) t_c \qquad (3.16)$$

Thus, Kostrov used the condition $k(\dot{x}_1) = \frac{K(\dot{x}_1)}{\pi}$ and assumed γ to be the material constant to determine equation (3.16).

Let us solve the same problem analytically using Irwin's fracture criterion. For the moving crack, Irwin's criterion can be written as $k(\dot{x}_1) = \frac{K(0)}{\pi}$, where K is now the material constant, and is its value for zero rupture velocity. Then, from equations (3.12) and (3.13) we get

$$2\sqrt{1 - \frac{\dot{x}_1}{\beta}}\ \sqrt{\beta s} = \frac{K(0)}{\pi}$$

The time of onset of fracture t_c is the same as given by equation (3.14). Then, the above equation can be written as

$$s = \frac{t_c}{(1 - \dot{x}_1/\beta)} ,$$

which can be solved to give the crack-tip position x_1 as a function of time s, as

$$x_1 = \beta(s - t_c) - \beta t_c \log s/t_c \qquad (3.17)$$

Let us now solve the same problem once again, this time numerically using Hamano's criterion and determine the rupture process required. We assume that a point breaks when the stress at that point reaches a limiting rupture

stress τ_u, say. If the final state of stress of the system is not zero but has some value τ_f, then the fracture criterion is that a point breaks when the stress jump $(\tau_u - \tau_f)$ exceeds a certain limit. Let us define the dimensionless quantity

$$S = \frac{\tau_u - \tau_0}{\tau_0 - \tau_f} \tag{3.18}$$

where τ_0 is the initial stress on the crack. Then

$$(1 + S) = \frac{\tau_u - \tau_f}{\tau_0 - \tau_f}$$

is the stress jump normalized to the stress drop $(\tau_0 - \tau_f)$, and from (3.5),

$$1 + S = \frac{ck_c}{(\tau_0 - \tau_f)\sqrt{d}} \tag{3.19}$$

is the fracture criterion. The sign of τ_f is opposite to that of τ_0 and τ_u, since the stress inside the crack is of opposite sign to the stress outside the crack. Kostrov took $\tau_f = 0$. In Figure 3.4, we plot the position x_1 of the crack-tip as a function of time t as found using Hamano's criterion for various values of S. These are given by step-like lines. We also plot on the same figure, the curve given by equation (3.17), i.e. using Irwin's criterion, for various values of t_c. These are given by the continuous lines. The value of t_c for which the analytic curve fits

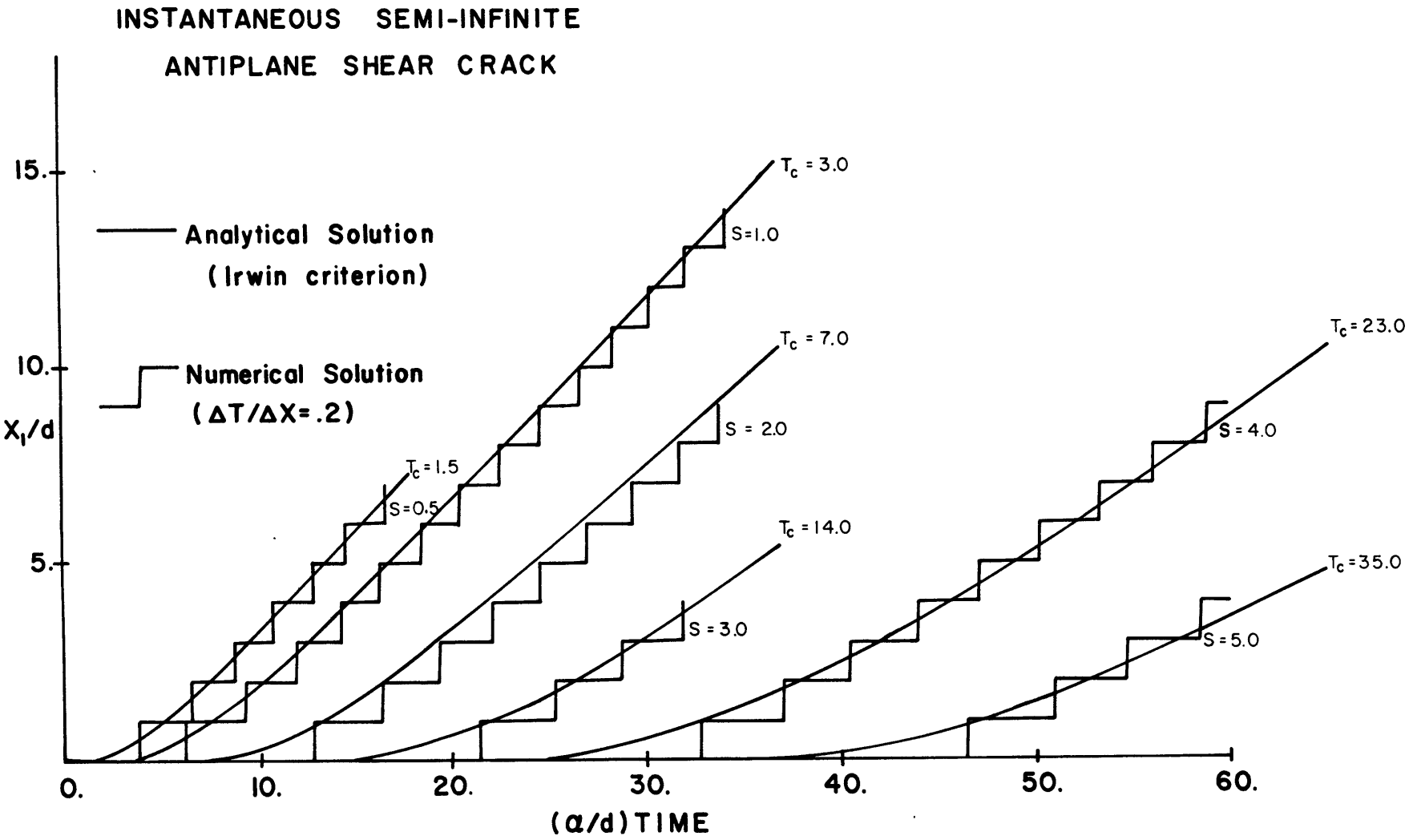

Figure 3.4 Position of crack-tip (x_1/d) as a function of time ($\alpha t/d$) for various values of S using Hamano's criterion are given by step-like lines. Equation (3.16) is plotted for various values of $\alpha t_c/d$.

the numerical solution the best is taken as corresponding to the S of the numerical solution. Table I shows the values of $\alpha t_c/d = T_c$ for various values of S. Now using the relation

$$1 + S = \frac{ck}{(\tau_0 - \tau_f)\ d}$$

and finding k(0) from equation (3.12), and remembering that equation (3.12) was normalized by the factor $(\tau_0 - \tau_f)$, we get

$$c = (1 + S)\ \frac{\pi}{2} \sqrt{\frac{\alpha/\beta}{T_c}}$$

from which the values of c shown in Table I for different values of S are obtained. As we can see, c lies between 2.4 and 2.0 and approaches 2.0 as S increases, i.e. as the critical stress for rupture becomes greater. Note also the difference between the crack-tip locus determined by Kostrov using Griffith's criterion (equation (3.16)) and that by using Irwin's criterion (equation (3.17)). For the same t_c, the curve for Griffith's criterion lies above the curve for Irwin's criterion, i.e. the Griffith crack moves faster than the Irwin crack.

Table I

S	$\alpha t_c/d = T_c$	c
0	0	∞
.5	1.5	2.53
1	3.0	2.39
2	7.0	2.34
3	14.0	2.21
4	23.0	2.16
5	35.0	2.10

§3.4 Semi-infinite instantaneous antiplane shear crack with concentrated loading.

Kostrov (1966) also studied the case of a semi-infinite antiplane shear crack in an infinite medium, with a concentrated loading applied at a point behind the crack-tip and analytically determined the crack-tip motion using Griffith's criterion. We shall solve the same problem analytically using Irwin's fracture criterion and we shall also solve it numerically by Hamano's method and compare the results.

The geometry of the crack is the same as in Figure 2.2, but now a concentrated load $\tau_{23} = p^o\delta(x_1 + x_1^o)$ is applied at the point $x_1 = -x_1^o$ at time $s = 0$, so that the crack surface is stress-free except at the point $x_1 = -x_1^o$. The stress-intensity factor, which was defined by equation (2.24), is

$$k(x_1) = \frac{\sqrt{1 - \dot{x}_1/\beta}}{\pi} p^o \int_{x_1-\beta s}^{x_1} \frac{\delta(v + x_1^o)}{\sqrt{x_1 - v}}\, dv$$

$$= \frac{p^o}{\pi} \frac{\sqrt{1 - \dot{x}_1/\beta}}{\sqrt{x_1 + x_1^o}} H(\beta s - x_1^o) \qquad (3.20)$$

where $H(\ \ )$ is the Heavyside unit step-function, so that k is zero for $\beta s < x_1^o$, i.e. until the disturbance due to the suddenly applied load reaches the crack-tip, i.e. $x_1 = 0$ for

$\beta s < x_1^o$.

At time $s = x_1^o/\beta$,

$$k = \frac{p^0}{\pi\sqrt{x_1^o}} \sqrt{1 - \dot{x}\ (0)} \leq \frac{p^o}{\pi\sqrt{x_1^o}}$$

We shall extend the Irwin's fracture criterion to the dynamic case by assuming that

$$k(\dot{x}_1) = \frac{K(0)}{\pi}$$

The crack will propagate if the condition

$$\frac{p^o}{\sqrt{x_1^o}} > K(0)$$

is satisfied, and the crack-tip motion is determined by the differential equation

$$\frac{p^o}{\pi} \quad \frac{1 - \dot{x}_1/\beta}{x_1 + x_1^o} = \frac{K(0)}{\pi} \tag{3.21}$$

The crack-tip will stop when $\dot{x}_1 = 0$. Let the position at which the crack-tip stops be x_m. Then, from equation (3.21)

$$\frac{p^{02}}{K^2(0)} = x_m + x_1^o$$

or

$$x_m = \frac{p^{o2}}{K^2(0)} - x_1^o \tag{3.22}$$

Substituting (3.22) into (3.21) we get

$$\frac{1 - \dot{x}_1/\beta}{x_1 + x_1^o} = \frac{1}{x_m + x_1^o} \tag{3.23}$$

as the differential equation giving the crack-tip motion in terms of x_m. Equation (3.21) gave the crack-tip motion in terms of K(0). It would seem possible to use the relation

$$1 + S = \frac{cK(0)}{\sqrt{d}\ (\tau_0 - \tau_f)}$$

and solve (3.21) for various values of S, and we would not have needed to know x_m to find the crack-tip position. However, we only know the values of the constant c for the values of S shown in Table I, and so we shall not follow this approach. Instead, we solve (3.23) under the condition that $x_1 = 0$ when $s = x_1^o$, and obtain the position of the crack tip as a function of time for the Irwin criterion as

$$\beta t = x_1^o + (x_m + x_1^o)\ \log \frac{x_m}{x_m - x_1}$$

or

$$\alpha t = \sqrt{3}\ [x_1^o + (x_m + x_1^o)\ \log \frac{x_m}{x_m - x_1}], \qquad (3.24)$$

$$x_1^o \leq \beta s$$

Let us now solve the same problem using our numerical method. We take $\frac{x_1^o}{d} = 2$ for our example, where d = grid length in the x_1-direction. We shall normalize all lengths by d, all times by α/d and all stress by p^o. Then, the condition that crack propagation will occur is

$$\frac{1}{\sqrt{2/d}} > K(0)$$

Here

$$S = \frac{\tau_u - p^o}{p^o},$$

so that

$$1 + S = \frac{\tau_u}{p^o} = \tau_u$$

when $p^o = 1$.

$$1 + S = \frac{cK(0)}{\sqrt{d}}$$

by equation (3.19) which gives the condition for crack propagation as $S \tilde{<} .4$ for $c \simeq 2.0$ and as $S \tilde{<} 1.9$ for $c \simeq 4.0$. By our numerical method, we find by trial that the crack propagates only for the values $S \leq .3$ and does not propagate for $S \geq .4$. This numerical result is consistent with the necessary condition for crack propagation for values of $c \geq 2.0$. [For $c = 1.5$, the condition is $S < .07$.] In Table I, we noted that the smaller the value of S, the larger the value of c, with the extreme value that when $S = 0.0$, $c \to \infty$. So it is likely that c is much larger than 2.0 for S values of .1, .2 and .3. To find the position of the crack-tip as a function of time for S = .1, .2 and .3 we have to evaluate equation (3.24) but we need to know the value of $\frac{x_1}{d} = \frac{x_m}{d}$ at which the crack stops to do this. We find x_m/d from our numerical method. For $S = .2$ and $S = .3$, $x_m/d = 5$ and $x_m/d = 1$ respectively.

For S = .1, it is rather difficult to determine the exact stopping point of the crack, since for small values of S, the usually small oscillations in the stresses outside the crack become significant. However, as an approximate value of x_m/d we take that value of x_1/d at which the crack speed is the lowest as the value of x_m/d and find that for S = .1, x_m/d = 21. Figure 3.5 shows the analytical solutions for Irwin's criterion for crack-tip position as a function of time [equation (3.24)] for x_m/d = 1, 5, and 21. The numerical solutions for S = .1, .2 and .3 are also plotted on the same figure. Even for S = .1, the agreement is good, surprisingly so, since we are dealing with very small values of S, and x_m/d was only an approximate value for this case. Using the values of x_m/d we obtained from our numerical solution, we find the values of c for S = .1, .2 and .3 (Table II). The values of c are quite consistent with the values obtained in Table 1.

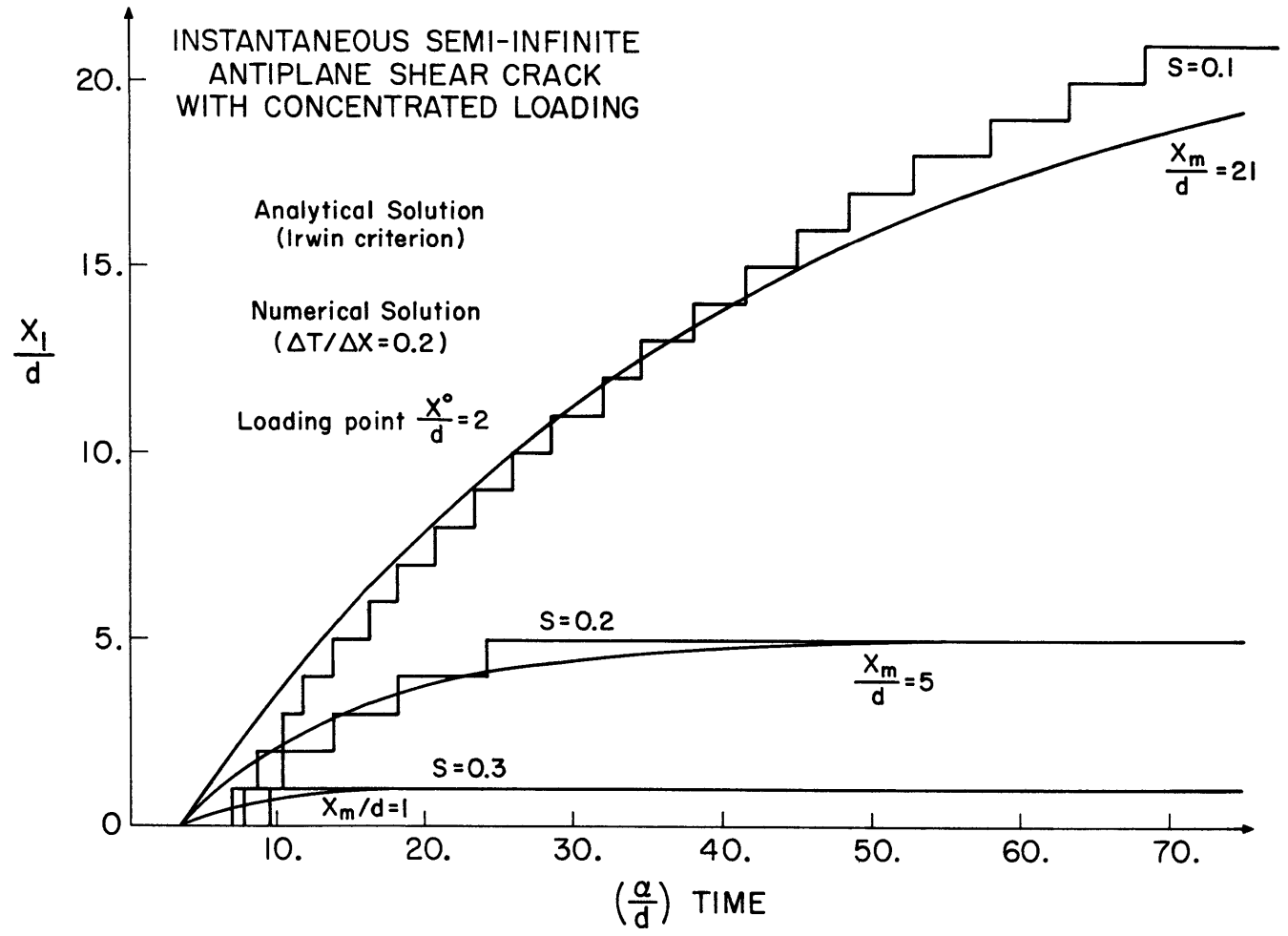

Figure 3.5 Same as figure 3.4 but for the case of concentrated loading at the point $X_1^\circ/d = 2$, behind the crack tip. The continuous line is given by equation (3.24).

Table II

S	x_m/d	c
.1	21	5.3
.2	5	3.2
.3	1	2.3

§3.5 Comparison of our numerical solution for in-plane shear crack with results of Andrews (1975).

In this case no analytical solution similar to the one obtained by Kostrov (1966) for the anti-plane shear crack exists yet. Kostrov (1975) has analytically determined the expression for the stress-intensity factor for the semi-infinite and the finite in-plane shear crack for the case when the crack-tip velocity is lower than the Rayleigh wave velocity. Fossum and Freund (1975) derived similar expressions to determine the crack-tip velocity in some special cases. However, the amount and complications of the calculations involved are prohibitive and do not make this a feasible approach to the problem.

Andrews (1976) has found a numerical solution for an in-plane shear crack that starts from a finite length, propagates bilaterally according to the Ida-Griffith fracture criterion, accelerates to some terminal velocity and continues to propagate at this velocity for ever. The initial half-length L_c is taken as the Griffith critical half-length and is the minimum half-length required for the crack to start propagating quasi-statically, i.e. without the generation of waves. Andrews uses a finite difference method to solve the problem. He assumed, following Ida (1972), that the traction τ across the fault

plane is related to the slip Δu by the following relations:

$$\tau(\Delta u) = \tau_u - (\tau_u - \tau_f)\ \Delta u/d_o, \quad \Delta u < d_o$$

$$\tau(\Delta u) = \tau_f \qquad\qquad , \quad \Delta u > d_o$$

where, τ_u and τ_f have the same meaning as in Section 3.3, and d_o is the slip required for the stress to drop to τ_f. The inelastic work done at the rupture front in excess of the work done against the stress τ_f is identified as the specific surface energy γ and given by

$$\gamma = \frac{1}{4}\ (\tau_u - \tau_f)\ d_o$$

The boundary conditions on the fault are

(i) When the fault is not slipping,

$$|\tau_0 + \tau_{21}| \leq \tau(\Delta u), \text{ if } \frac{\partial \Delta u}{\partial t} = 0.$$

(ii) During slip,

$$\tau_0 + \tau_{21} = \tau(\Delta u) \cdot \text{sign}(\frac{\partial \Delta u}{\partial t}), \text{ if } \frac{\partial \Delta u}{\partial t} \neq 0.$$

These conditions are the same as those given by equations (3.6) and (3.7). With these boundary conditions, Andrews studied the symmetric propagation of a plane shear crack, starting from initial half-length L_c. Andrews has given his results in terms of the two dimensionless quantities L_c/L and S, where L is the instantaneous crack half-length

and S was defined by equation (3.17). He studies the rupture velocity in the parameter space of L_c/L and S (Fig. 3.6). He finds that if S is greater than about 1.63 (in agreement with Burridge (1973)), the rupture velocity is always less than the Rayleigh wave velocity, and the rupture velocity approaches the Rayleigh wave velocity as L increases, i.e. the ratio L_c/L decreases. For values of S less than 1.63, the crack starts with a sub-Rayleigh velocity but as the crack length increases, the velocity changes from sub-Rayleigh to super-shear and finally approaches the P-wave velocity. Fig. 3.6 shows this transitional region where the velocity changes from sub-Rayleigh to super-shear.

We shall now solve the same problem as Andrews by our numerical method. To find the starting crack-length, we need to know L_c for different values of S. From the work of Starr (1928), the stress-intensity factor k is related to the crack-half-length by the relation,

$$k = (\tau_0 - \tau_f) \sqrt{L/2}$$

The critical stress-intensity factor and the critical crack length are thus related by the formula $k_c = (\tau_0 - \tau_f)\sqrt{L_c/2}$, where "critical" means the value at the start of rupture propagation. Also, from equation (3.19) we have

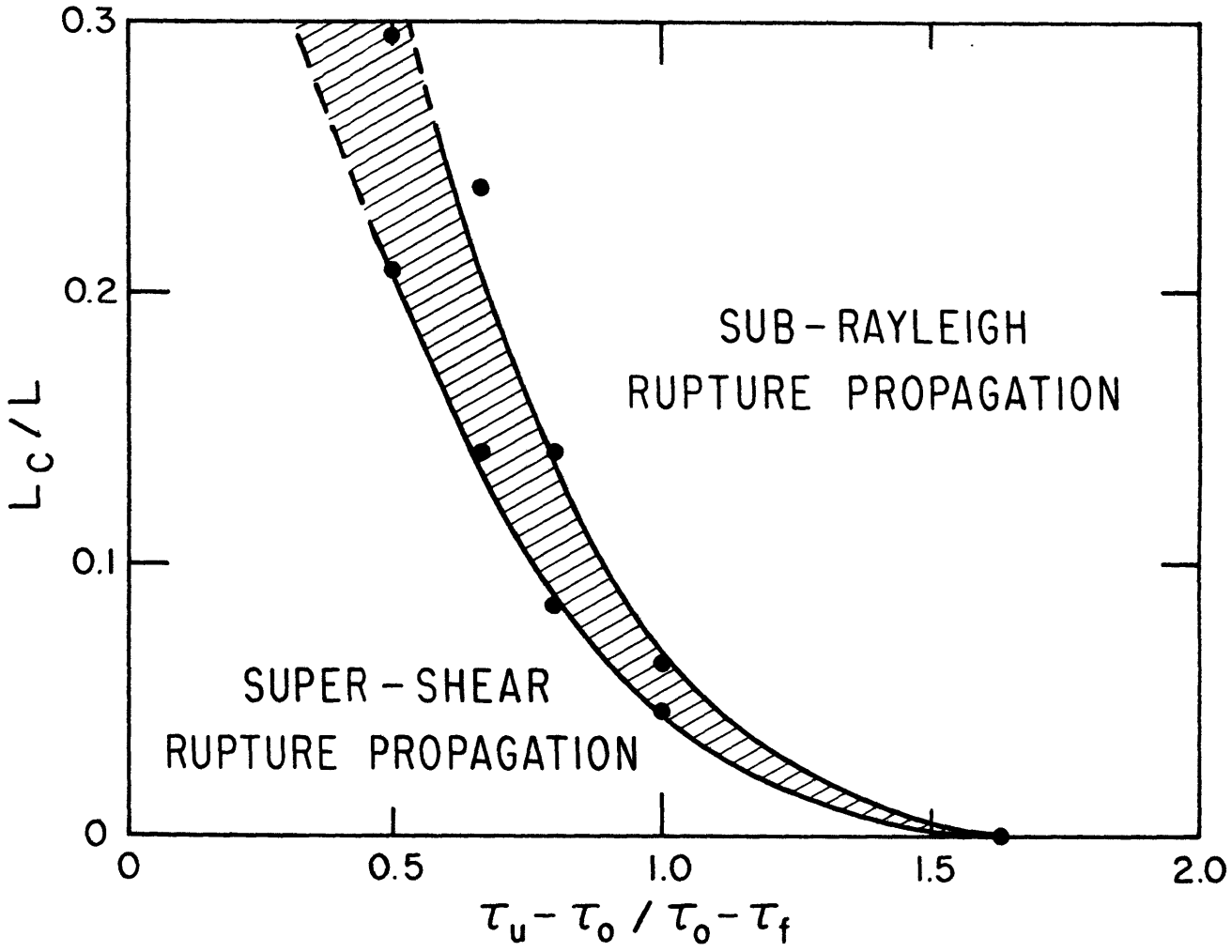

Figure 3.6 Andrews (1976) plot of rupture velocity domains in the parameter space of L_C/L and S. Shaded region is the region of transition from sub-Rayleigh to super-shear velocities.

$$1 + S = \frac{ck_c}{(\tau_0 - \tau_f)\sqrt{d}} \tag{3.25}$$

Thus, we get the relation between S and L_c, as

$$\frac{L_c}{d} = \frac{2(1 + S)^2}{c} \tag{3.26}$$

Table III shows the values of $2L_c/d$ for various values of S. We use these values of L_c as the initial half-length and solve the problem for various S. Fig. 3.7 shows our results in a plot similar to Andrews. Qualitatively, we find the same result as Andrews. However, the zone of transition is not exactly the same. Remembering that Andrews says that his values of L_c/L may be in error by a factor of two and that he uses Griffith's criterion and we use Irwin's criterion, we conclude that our results are in qualitative agreement with his results. In any case, both Irwin-Barenblatt fracture criterion and Ida-Griffith criterion lead to the surprising result that, for $S < 1.63$, the rupture velocity of in-plane shear crack grows to the P-velocity as the crack length increases. This result is unexpected. Previous works on in-plane shear crack propagation, usually under the assumption of sub-shear velocity propagation, indicated that the propagation velocity could not exceed Rayleigh velocity. In-plane tension crack, on the other hand, does not exceed Rayleigh wave velocity because of the nature of Green's function for that problem (Hamano, 1974).

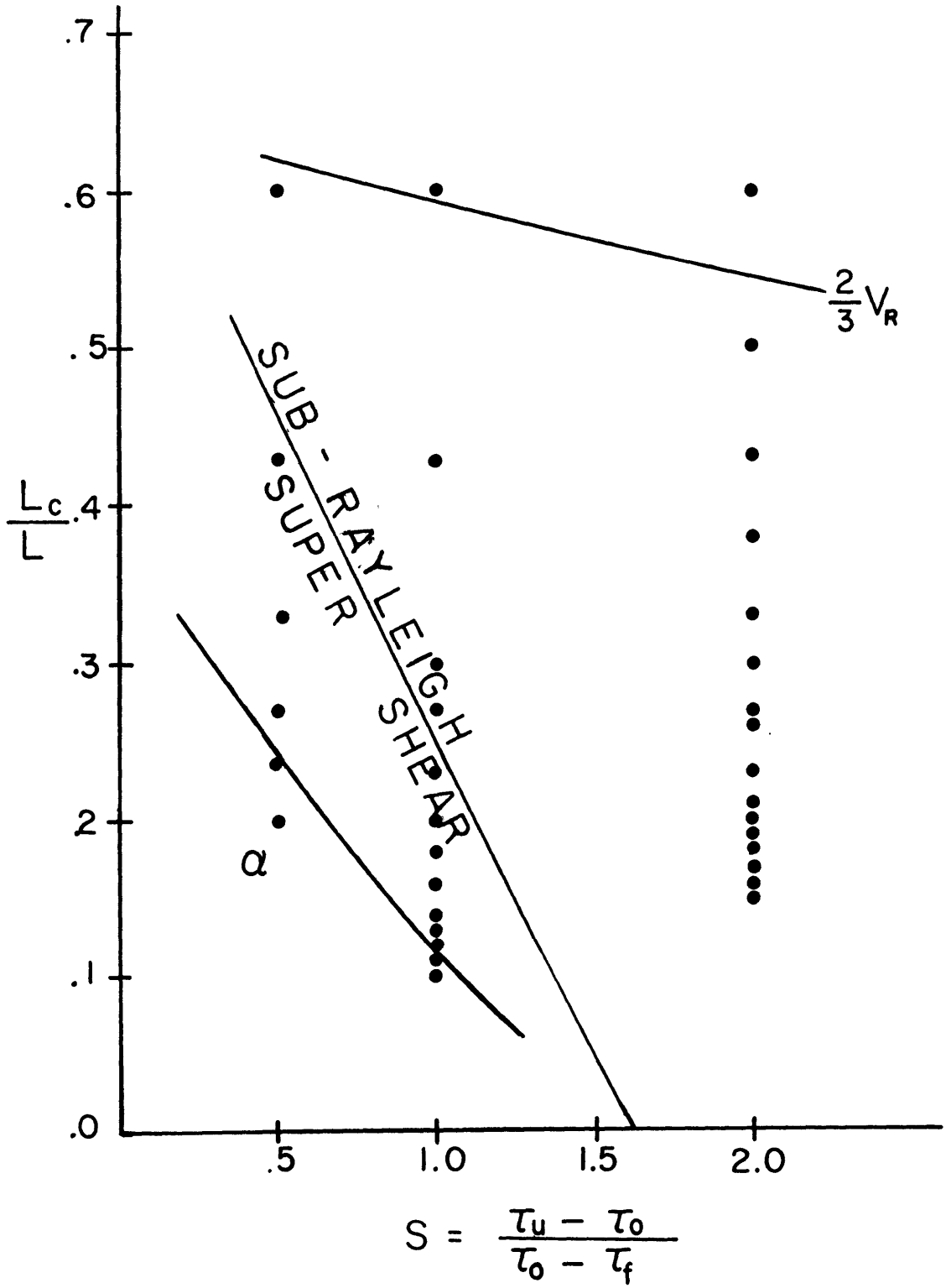

Figure 3.7 Contour plot showing the crack-tip velocity for different values of the parameters L_c/L and S for an in-plane shear crack, starting from one initial Griffith's critical length of L_c.

Table III

S	c	$2L_c/d$
0	∞	0.0
.5	2.53	1.41
1	2.39	2.80
2	2.34	6.57
3	2.21	13.11
4	2.16	21.41
5	2.10	32.65

3.6 Estimation of γ, the specific surface energy

Ida (1973) estimated γ to be of the order of 10^{10} ergs/cm^2 for earthquakes, from the observed maximum seismic motion due to an earthquake. Takeuchi and Kikuchi (1973) independently proposed a similar value from a rough estimate of time needed for the rupture velocity to approach the terminal velocity. Let us try to estimate γ for earthquakes from our foregoing results.

We saw in the previous section (section 3.6) that for the in-plane shear crack if $S = \frac{\tau_u - \tau_o}{\tau_o - \tau_f}$ is less than 1.63, the crack speed can exceed the shear wave speed and may reach the compressional wave speed. A review of the literature reveals that for most earthquakes studied so far, the rupture velocity is less than the shear wave velocity (Tsai and Patton, (1972), Eaton (1967), Kanamori (1970a, 1970b, 1971, 1972), Takeuchi and Kikuchi (1973), Wu and Kanamori (1972), Niazy (1975), Aki (1968), Filson and McEvilly (1967), Tsai and Aki (1968), Abe (1974a, 1974b) and others). A single example (Fukao, 1970) was found where the rupture velocity was not only higher than the shear wave velocity but also higher than the P-wave velocity. This is essentially the case of simultaneous rupture over the fault surface. We must note that in the studies mentioned above, the rupture velocities determined from seismograms are an <u>average</u> of rupture velocities over the entire length of the fault. Our results of the previous section show that for constant

S, the fault starts with a low velocity and accelerates to the terminal velocity, the terminal velocity depending on the value of S. Thus, the average velocity reported for earthquakes may be lower than the true terminal velocity. However, the smaller S is, the quicker the terminal velocity is reached. Therefore, we expect that rupture velocity close to P wave velocity would be reported for most earthquakes if S is very small. Since we don't observe that, S cannot be much smaller than 1.6. Probably, S is of the order of 1.

From equation (3.19), we have the relation between the parameter S and the critical stress intensity factor k_c as

$$1 + S = \frac{c\, k_c}{\tau_\infty \sqrt{d}}$$

where τ_∞ is the applied stress at ∞. On the other hand, for in-plane shear crack, γ and k_c are related by

$$\gamma = \frac{\pi k_c^2}{4\mu} \quad \frac{\lambda+2\mu}{\lambda+\mu} \qquad 2(1-\nu)$$

λ, μ being Lame parameters (c.f. Andrews, (1976)).

For $\lambda = \mu$, this gives $\gamma = \frac{3\pi}{8\mu} k_c^2$

Using the above equations, we find the relation between γ and S as

$$1 + S = \frac{c\sqrt{8\mu\gamma}}{\tau_\infty \sqrt{d}\sqrt{3\pi}} \qquad \ldots \qquad (3.27)$$

Let us assume some typical values of μ, τ_∞, and d appropriate for an earthquake:

$$\mu \sim 3 \times 10^{11} \text{ dynes/cm}^2$$
$$\tau_\infty \sim 10^8 \text{ dynes/cm}^2$$
$$d \sim 10^5 \text{ cm, (d being the grid length in our numerical method)}$$

If we use $c \sim 2$ and $\gamma \sim 10^3$ ergs/cm^2, then from equation (3.27) we find that

$$1 + S \sim 10^{-3}$$

or $$S \sim -.999$$

This result is unacceptable because S cannot be negative by definition. c becomes large as S approaches zero (Table II) keeping S positive. In any case, γ cannot be of the order of 10^3 ergs/cm^2 if S for an earthquake is of the order of 1. For the condition $S \sim 1$ to be satisfied, γ must be 10^9 ergs/cm^2. This value corresponds to the grid interval of 1 km which may be appropriate for a fault that is 10 kilometers long. For a fault that is 100 kilometers long, the corresponding d would be about 10 km. For $S \sim 1$, this gives $\gamma \sim 10^{10}$ ergs/cm^2. For a fault 1000 kilometers long, d = 100 km and $S \sim 1$ leads to $\gamma \sim 10^{11}$ ergs/cm^2. Thus, the fact that the average rupture speeds for major earthquakes are less than the shear wave speed implies that the apparent γ for large earthquakes is

of the order of 10^{10} ergs/cm^2 in agreement with the estimates of Ida (1973) and Takeuchi and Kikuchi (1973).

Laboratory experiments of Brace and Walsh (1962) in quartz give the value of γ to be of the order of 10^3 ergs/cm^2. The cause of this discrepancy between laboratory samples and large earthquakes was attributed by Andrews (1975) and by Brace (personal communication) to the fact that in the case of an earthquake, instead of a single fracture surface, a large number of small cracks are created in the fault gouge. The total surface area of these cracks may be several orders of magnitude larger than the main fracture surface and the resulting value of γ would be much larger than that in the laboratory where there is only one single fracture surface. Andrews (1975) also suggested another reason to account for this discrepancy. When the crack length becomes large, the region around the tip with stress above a critical value increases and the work spent in plastic deformation around the tip becomes large. These reasons give the probable explanation for the discrepancy between laboratory results and the results based on maximum rupture velocity determined for earthquakes.

CHAPTER IV

Application to the Study of Earthquake Source Mechanisms

In this chapter, we shall apply our method developed in earlier chapters to the problem of earthquake source mechanism. We shall study, for example, the displacement field for unilateral in-plane shear crack propagation for various distribution of the parameter S along the fault, where S, defined by equation (3.18) is a measure of the strength on the fault plane. S is related approximately to the critical stress-intensity factor by equation (3.19) and to the specific surface energy (for the static case) by equation (3.27). We shall simulate an obstacle to rupture propagation by a box-car distribution of S (Hamano, 1974) and study how the presence of one or more obstacles on the fault-plane affect the near- and far-field displacements and their spectra. We shall also study the effect of initial stress distribution on crack propagation. We are especially interested in how a crack stops for various distributions of S and initial stress.

4.1 Unilateral propagation of in-plane shear crack and comparison with experimental results of Archuleta and Brune (1975)

We shall first present some theoretical results for unilateral propagation at a fixed velocity and then consider the case of unilateral propagation for a uniform distribution of S to compare with Archuleta and Brune's

experiment on a crack propagation in foam rubber.

Hanson et al. (1974) first solved the two-dimensional problem of unilateral crack propagation which propagates at a constant velocity of .4 times the compressional wave-velocity and then stops. The initial crack-length is taken as L/7, L being the final crack-length. Hanson et al. have used a finite-difference technique to solve the problem. We shall solve the problem for a slightly different rupture velocity.

We take the initial crack length to be L/21, where L is the final crack length. The geometry of the crack and the direction of the initial applied stress is as shown in Figure 2.3 except that the crack now only occupies the positive part of the x_1-axis, with the fixed tip at $x_1 = 0$. The right tip moves with a constant velocity of $\alpha/2$ in the x_1-direction. The trajectory of the crack tip for the general case of non-uniform sub-shear rupture velocity is shown in Figure 4.1. The symmetry that existed in the bilateral case, about the $x_1 = 0$ axis, no longer exists in the present problem. Thus the stresses and the normal component of displacement in the regions S_1, S_2 and S_3 have to be separately calculated. S_1 is the crack region, S_2 is the region outside the crack to the right of the moving tip and S_3 is the region outside the crack to the left of the fixed tip. As the crack starts propagating, the waves generated by the moving tip are reflected from the fixed tip almost immediately. As a

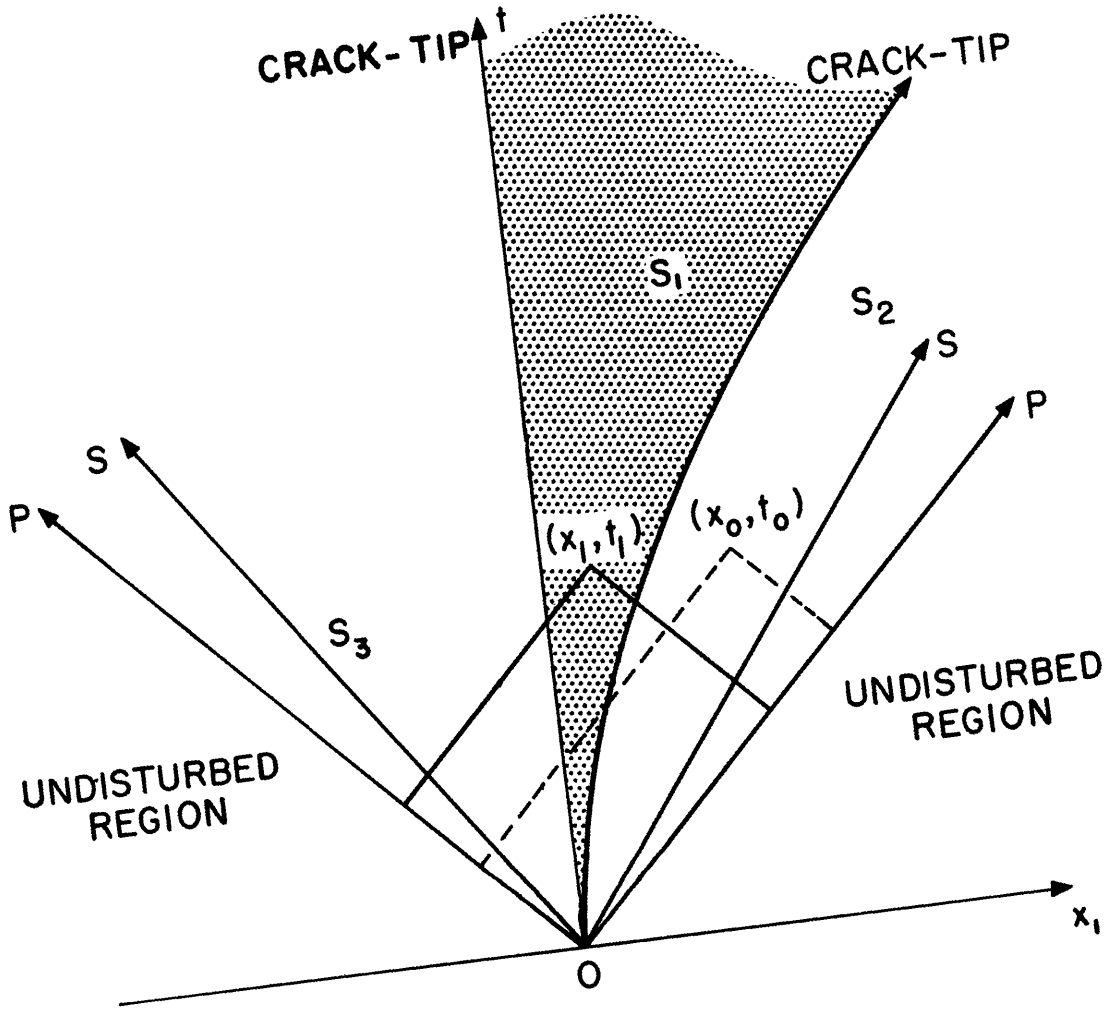

Figure 4.1 Trajectory of the crack-tip in the $(x_1\text{-}t)$ plane for the unilateral in-plane shear crack propagation. S_1 is the crack region, S_2 and S_3 are the regions to the right and left of the moving and fixed tips respectively.

result of this, the displacement-time history on the crack surface due to an unilaterally propagating fault is much more complicated than that due to a bilaterally propagating fault.

Using the method described in Chapter 2, we solve the integral equation (2.16) with the initial and boundary conditions given by equation (2.4) and (2.6) respectively. The grid ratio $\alpha\Delta t/\Delta x_1$ is taken as .5 and $\alpha = \sqrt{3}\beta$. All displacements are normalized by the quantity $L(\tau_o - \tau_f)/\mu$, where μ is the modulus of rigidity, L is the crack-length and $(\tau_o - \tau_f)$ is the stress-drop. (For the bilateral case discussed in Section 2.6, we used the crack half-length in the normalizing factor instead of the total crack length as in the unilateral case, in keeping with the usual convention found in the literature). In Figure 4.2 we show the parallel and normal components of displacements at four different points along the fault for the half-space $x_2 \geq 0$. The four points are denoted by X = .025, .52, .9, .975 where $X = x_1/L$. The point X = .025 is located very close to the fixed tip, the point X = .52 about half-way between the fixed tip and the final position of the moving tip and the point X = .975 is very close to the final position of the moving tip. We see that at X=.025, the parallel component motion is very small and the normal component displacement shows a negative sign, (negative indicates displacement in the negative x_2-direction, cf. Figure 2.3). The maximum value of the parallel component is reached at

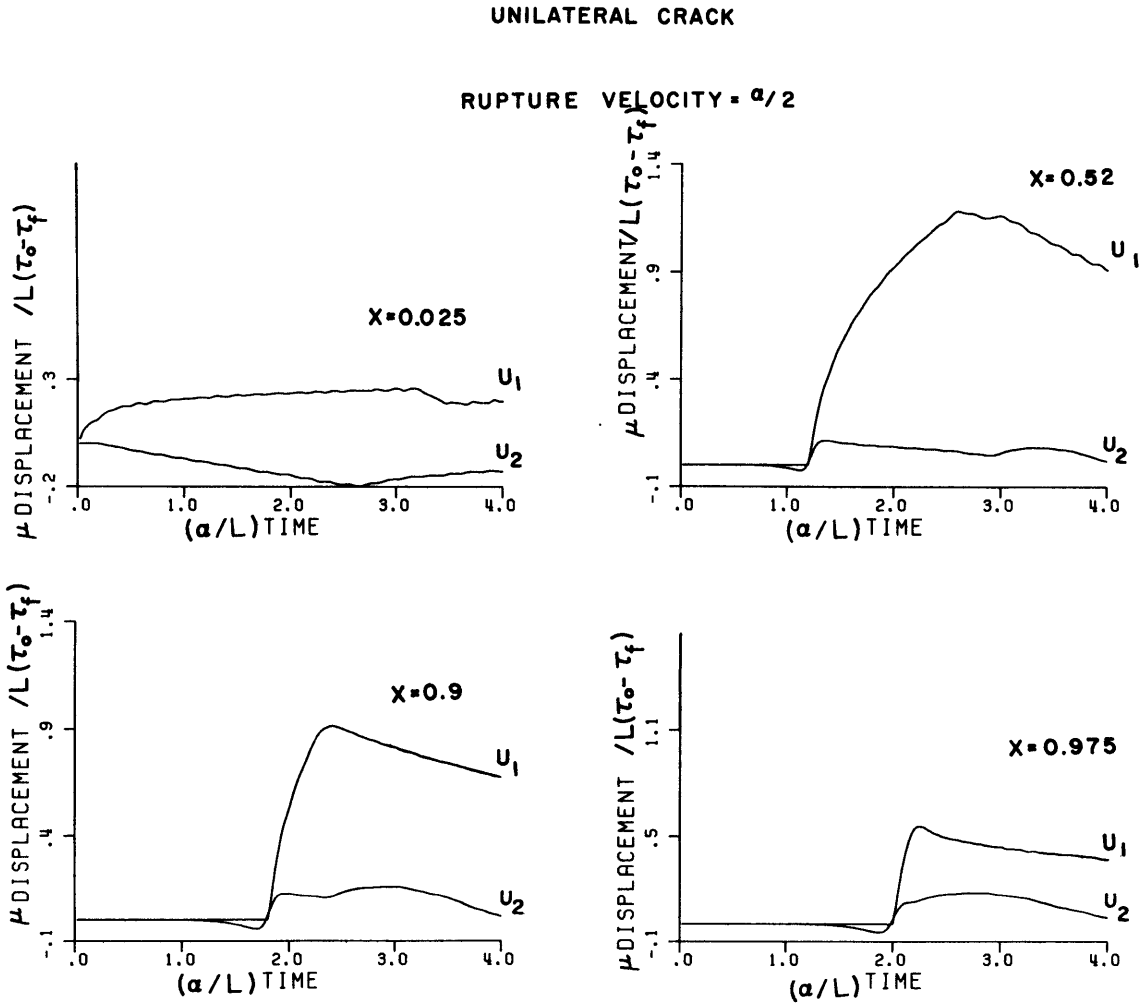

Figure 4.2.

Normalized parallel (u_1) and normal (u_2) components of displacements at four points along the crack surface for unilateral crack of rupture velocity $\alpha/2$.

X = .52 at a time given by 2.65 (α/L). The phase generated at the stopping of the moving tip reaches this point at time 2.52 (α/L) so that the maximum value of the parallel component is reached just after the P stopping phase reaches this point. The corresponding normal component is very small. The normal component starts movement with the initial P arrival, and has a negative sign until the rupture front passes, after which it changes sign and becomes positive. At X = .9, the parallel component is smaller than at X = .52 and again is non-zero before the rupture front passes after which it changes sign, the maximum negative displacement being larger than at X = .52. At X = .975, both components of displacement are small and the absolute value of the maximum negative displacement is larger than at X = .9. For the case we have plotted, frictional arrest of sliding was not implemented and the displacements were allowed to decrease from their maximum value resulting in an overshoot (i.e. the final displacement is not the maximum displacement). On the other hand, if the static friction arrests the fault slip when the crack velocity reverses sign, the displacements would remain at the maximum value it reached. In that case, the stress on the crack-plane will be of opposite sign to the initial stress and the stress drop (the initial minus the final stress) on the crack would be greater than that in the static case (cf. Section 3.2).

To demonstrate the difference in nature between unilateral and bilateral crack propagation, we compare the parallel components of displacement for the half-space $x_2 \geq 0$ for the two

cases in Figure 4.3 and the normal component of displacement for the two cases in Figure 4.4, when the crack-tip is constrained to move at half the P-wave velocity. We shall implement frictional arrest of sliding and stop the slip when it reaches its maximum value. The displacements are normalized by the factor $L(\tau_o - \tau_f)/\mu$ where L is the crack half-length for both the unilateral and bilateral case. (These two figures are the only figures in which we shall deviate from our usual convention of using the total crack length in the normalizing factor for the unilateral case). The normalized displacements are plotted as a function of x_1/L, the normalized distance from the origin, along the crack plane, at time intervals given by $\Delta T_p = .5$, where $T_p = \alpha t/L$. The time required for a P-wave to travel the crack half-length L is taken as the unit of time. Thus, the line labeled as 2 corresponds to the time when P wave travel the full length of the crack. The normal component displacement for the bilateral crack is plotted with the same normalization in distance and time. Since the displacement for the bilateral crack are symmetrical about the origin, 0, we plot one side of it.

The normal component displacement for the unilateral

Figure 4.3. Comparison of the parallel component of motion on the crack surface as a function of the distance from the point of crack initiation, O, for unilateral and bilateral in-plane shear crack with rupture velocity $\alpha/2$.

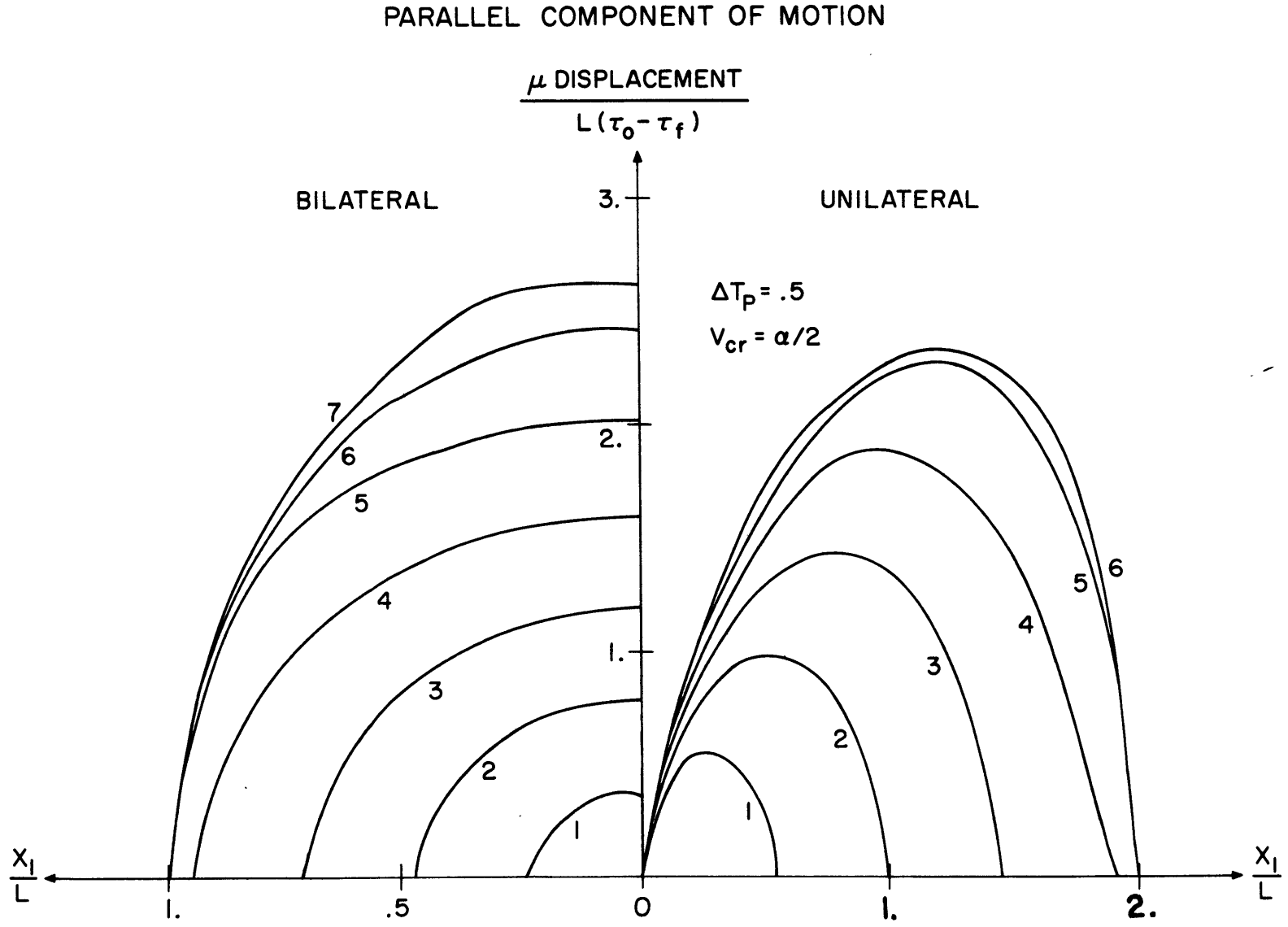

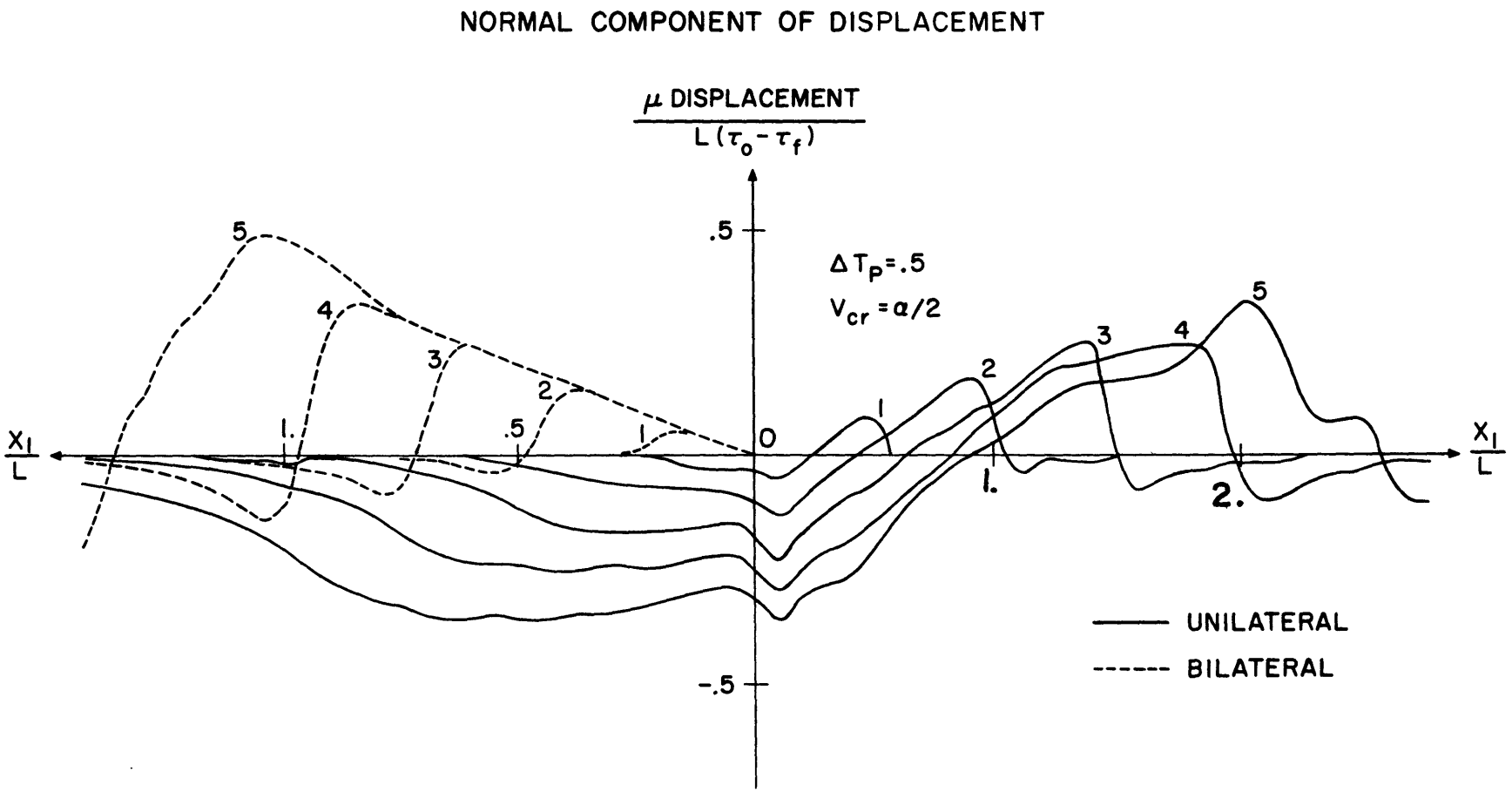

Figure 4.4 Same as Figure 4.3 but for the normal component of motion.

case in Figure 4.4 has been plotted for $-3<x_1/L<3$. (The scale in Figure 4.4, for the unilateral case, is given by the numbers below the x_1/L axis and the scale for the bilateral case is given by the numbers above the x_1/L axis). Our results confirm the conclusion of Hanson et al. (1974) that the dynamic displacement field for unilateral crack propagation is quite different from that for bilateral crack propagation.

We now describe the experiment of Archuleta and Brune (1975) who made a study of the velocity and displacement field due to a "stick-slip" event in foam rubber ("stick-slip" means here that the slip stops when the particle velocity reverses sign). They simulate a pre-existing strike-slip fault which intersects the free surface by making a semi-circular cut of radius 80 mm in the center of one of the square sides of a .76 x .76 x .38 m^3 block of foam rubber. Figures 4.5a and 4.5b show respectively the side and top view of the block with the cut in it. By gluing 3/4 inch plywood to opposite sides of the foam rubber, uniform normal and shear stress as shown in Figure 4.5b can be applied to the block using the machine described by Brune (1973). The block size is such that the dynamic processes at the fault surface terminate before the reflections from the sides of the blocks return to the fault surface. To create a stick-slip event, the normal stress is first fixed at some constant value, and then

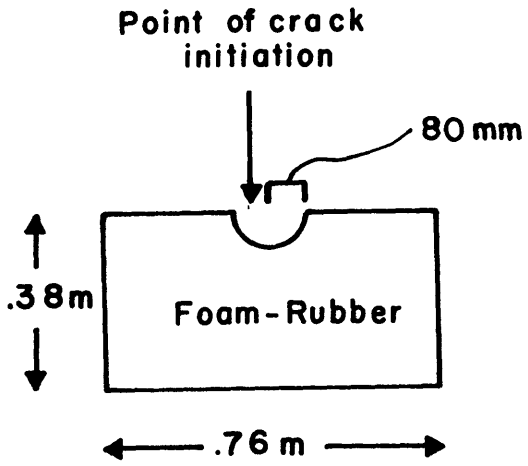

SIDE-VIEW
(Centre Section)

Figure 4.5a. Schematic representation of experimental set-up of Archuleta and Brune's (1976) experiment, showing side view of foam rubber block with cut in center.

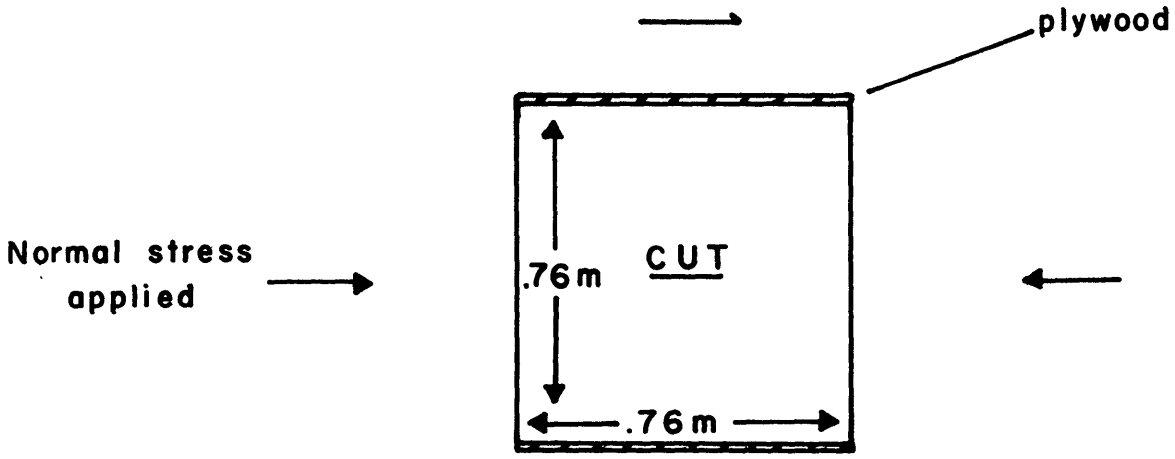

TOP - VIEW

Figure 4.5b. Same as 4.5a but top-view of foam rubber block and cut.

the shear stress is applied by displacing the two plywoods glued to the foam rubber in opposite directions. The shear tractions on the sides of the fault are increased until a stick-slip event occurs. Beads are planted on the surface of the foam rubber on the two sides of the cut and a wire grid is placed about 10 mm above the surface of the foam rubber as a reference grid against which the displacement of the beads may be measured. A fast camera films the surface of the foam rubber as the stick-slip event occurs. By measuring the displacement of the beads on enlarged frames of the film, the displacement-time history of the stick-slip event is found.

It was found that the propagation had been essentially unilateral, initiating 30 mm from the left end, as shown in Figure 4.5a. The rupture velocity was found to be between $.6\beta$ and $.7\beta$. Archuleta and Brune have plotted the parallel component of displacement at the center and the normal component of displacement at the tips of the fault. The final static value of the parallel component motion is .6 mm at the center of the crack. The final normal component displacements are .25 mm and .18 mm at the left and right tips respectively. The average value of the static parallel displacement was .48 mm. Comparing this with the analytical expression (Eshelby, 1957) for the average static displacement, the stress drop is found to be $.016\mu$.

Let us now solve the spontaneous propagating crack

problem for the unilateral, in-plane shear crack to compare with Archuleta and Brune's experiment described above. Instead of giving the crack-tip velocity a priori, the velocity is determined from a cohesive force distribution on the crack plane. The parameter S defined by equation (3.18) is taken to be uniform along the crack plane and the crack is stopped when the tip reaches the twenty-first grid point by making S very large beyond this point. Frictional arrest of sliding is not implemented. In Figure 4.6 we plot the parallel and normal components of displacement versus time at four points along the fault on the fault-plane, for the case when S = .25 for the half-space $x_2 \geq 0$. The normalized position of the points along the fault are given by $X = x_1/L = .025$, .52, .9, .975, L being the crack length. The crack-tip velocity was found to be slightly lower than the P-wave velocity. The time at which the crack reached its final length is about 1.25 times the time required for a P-wave to traverse the full crack length once. The general features of the displacement are the same as for the case of unilateral propagation at a constant velocity of $\alpha/2$. But, interestingly, the normal component of displacement is zero till the rupture front passes, a result different from the case of propagation at the fixed velocity of $\alpha/2$. After the passage of the rupture, the normal component reaches a somewhat higher amplitude than the case of fixed rupture velocity at $\alpha/2$.

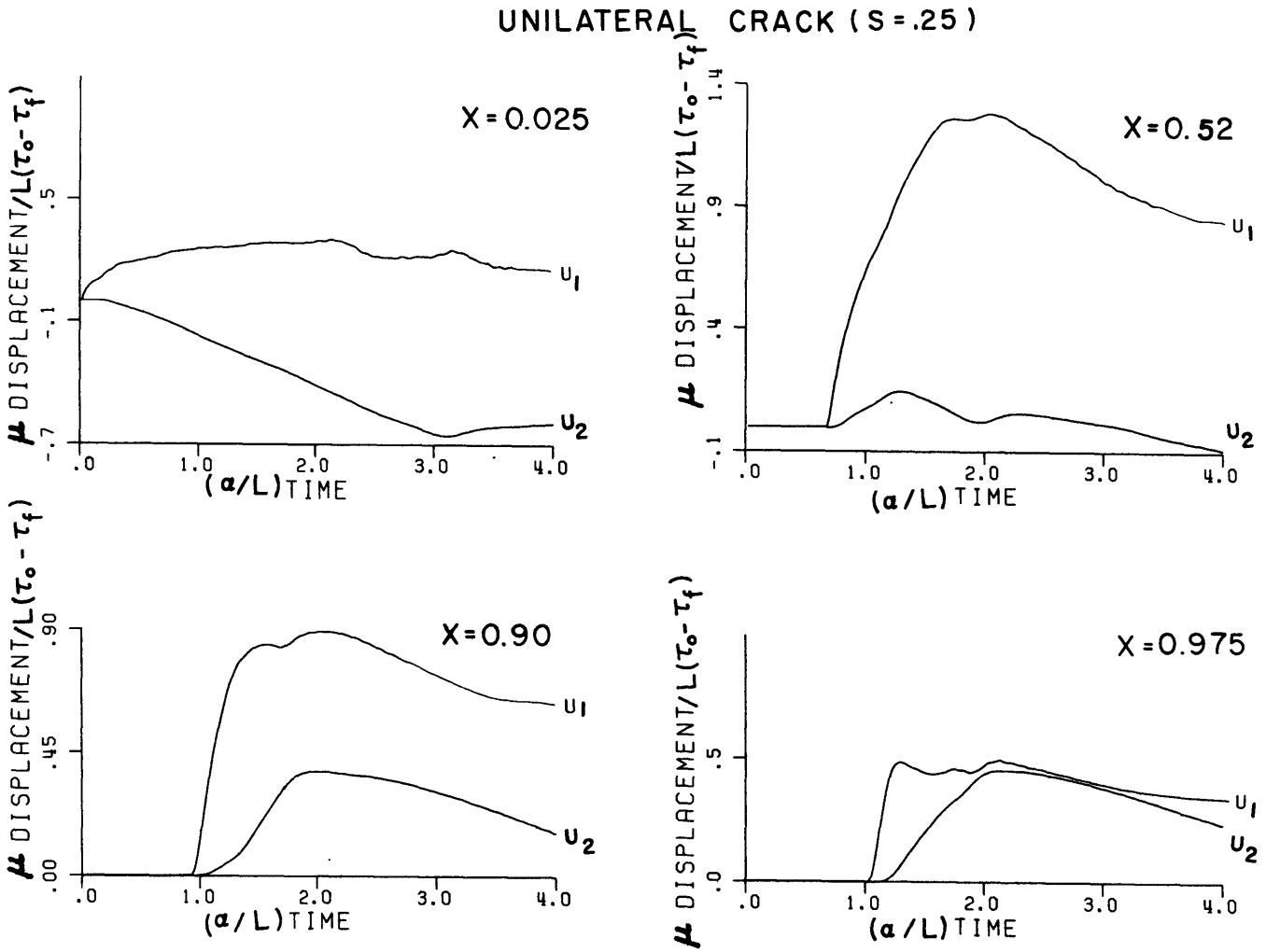

Figure 4.6. Normalized parallel and normal components of motion at four points along the crack surface, for spontaneous crack propagation.

The reason for the absence of motion before the arrival of the rupture front in the spontaneous case is simply that in this case, the P-wave from the first point of break and the rupture front arrive nearly simultaneously at every point along the fault-plane. (Reference to Figures 2.15 and Figure 2.18 shows that a similar conclusion holds for the case of bilateral crack propagation as well.) For the case of unilateral rupture propagation at the constant velocity of $\alpha/4$ (not plotted) we find that the normal component of displacement at a point is initially negative but changes sign when the S-wave (or Rayleigh wave, since these two waves are not easily distinguishable as their velocities are very close to one another) from the first point of break arrives at that point. In this case just after the passage of the S- (or Rayleigh) wave, the normal component reaches its final value. The reason for the normal component of motion being negative initially for rupture velocities less than α can be found by examining the discretized Green's function $F_{21}(X, T_p)$ for the normal component given by equations (2.12) and (2.15) and shown in Figure 2.7. The initial motion is negative till the S-wave or Rayleigh wave comes in when it changes sign and becomes positive. Richards (1976) found a similar result for an elliptical self-similar shear crack which grows at a speed less than β and never stops.

The properties of unilateral crack propagation are the following:

(i) The parallel component of displacement always has the same sign (positive, referred to Figure 2.3 for $x_2 \geq 0$), the maximum displacement at any instant occurring near the instantaneous center of the crack.

(ii) The rising part of parallel displacement at a point is steeper the closer the point is to the final position of the moving tip i.e. the rise time at X = .975 is shorter and at X = .025 is very gradual.

(iii) For constant rupture velocity of $\alpha/2$, the normal component of motion at a point is non-zero soon after the P-wave from the first point of break arrives at the point and changes sign from negative to positive as the rupture front passes the point. For a constant rupture velocity of $\alpha/4$, this reversal takes place when the S-wave or Rayleigh wave from the first point of break arrives at the point. For the case of spontaneous rupture propagation for low values of $S = (\tau_u - \tau_o)(\tau_o - \tau_f)$ on the fault, for which rupture propagation velocity become close to α, there is naturally no distortion ahead of the tip, as exists for a case of rupture propagation at constant velocity of less than α.

(iv) The normal component motion is very complicated due to the fact that the crack rotates about its instantaneous center which moves as the crack propagates.

We had some difficulties in reproducing a spontaneous crack propagation which agrees completely with experimental results of Archuleta and Brune. In their experiment, they found that the rupture velocity was about .6β to .7β and was uniform almost from the beginning.

From our previous results on the relation between the rupture velocity and the parameter S, this implies a large value of $S = \frac{\tau_u - \tau_0}{\tau_c - \tau_f}$, where τ_u in this case is the static friction holding the two faces of the precut crack together. Then, we found for a large uniform S distribution unilateral propagation of in-plane shear crack requires a long time before the rupture velocity reaches the terminal velocity. A slow acceleration of rupture is not consistent with Archuleta and Brune's experimentally observed crack-tip history. To reproduce a case in which the terminal velocity is reached very quickly, we needed small S and then the terminal velocity will be the P-wave velocity. We may be able to reconcile these contradictions by assuming a particular non-uniform distribution of S. Instead of trying to find such an S distribution, however, we decided to use a small uniform value of S, in view of the similarity in displacements between the case of spontaneous propagation with small S(0.25) (Figure 4.6) and the case of rupture propagation at the velocity $\alpha/2$, (Figure 4.2) which is very close to the observed terminal velocity of Archuleta and Brune. Thus, so far as the displacements are concerned, our conclusions in this section will not be affected by our

choice of small S.

There is another difference between their experiment and our computation. The problems set up in their experiment are three-dimensional and concerned with the crack intersecting the free surface. In our problem, we have considered a two-dimensional crack in an infinite medium. We shall show below that it is meaningful to compare the ratio of the maximum (which is the final displacement for "stick-slip" event) parallel and normal displacement, in spite of the difference in the problem solved by us and the experiment of Archuleta and Brune. The general broad features of the two solutions, e.g. the form of the parallel and normal components of displacement as a function of time, are found to be quite similar.

As supporting evidence, we compare below the static solutions for a two-dimensional plane shear crack (Starr, 1928) and a three-dimensional circular shear crack in an infinite medium (Eshelby, 1957) to show their similarity. Let u_1 and u_2 be the displacement components at the crack along x_1 and x_2 axes (cf. Figure 2.1) for the two-dimensional in-plane shear crack of length 2 . For the circular shear crack of radius , let u_1 and u_2 be the displacements at the crack along the direction of applied shear stress and normal to the plane of the crack respectively.

Three-dimensional circular shear crack of radius ℓ

$$u_1 = \frac{12}{7\pi} \frac{\Delta\tau}{\mu} \sqrt{\ell^2 - x_1^2}$$

$$= .55 \frac{\Delta\tau}{\mu} \sqrt{\ell^2 - x_1^2}$$

$$u_2 = \frac{x_1}{7} \frac{\Delta\tau}{\mu}$$

$$= .14 \frac{\Delta\tau}{\mu} x_1$$

$\Delta\tau$ = stress drop

Two-dimensional plane shear crack of length 2ℓ

$$u_1 = \frac{3}{4} \frac{\Delta\tau}{\mu} \sqrt{\ell^2 - x_1^2}$$

$$= .75 \frac{\Delta\tau}{\mu} \sqrt{\ell^2 - x_1^2}$$

$$u_2 = \frac{x_1}{4} \frac{\Delta\tau}{\mu}$$

$$= .25 \frac{\Delta\tau}{\mu} x_1$$

This shows that the static displacements inside the crack for a 2-D plane crack and a 3-D circular crack differ only by a constant factor and u_1/u_2 = 3 and 4 respectively for the two cases. This justifies comparing our theoretical results for two-dimensional crack with the experiments of Archuleta and Brune. The ratio of the maximum parallel displacement to the maximum normal displacement is about 3:1 in our theoretical result as well as in the form rubber experiments.

A most interesting result is that the normal component motion in both our theoretical result and in Archuleta and Brune's experiment / does not exhibit an impulse-like displacement form such as observed at Station #2 for the Parkfield earthquake of 1966 and explained in terms of a propagating step-like slip dislocation. For example, if we consider a step-function slip in a propagating in-plane shear dislocation (Boore, Aki and Todd (1971)) or Eshelby (1949)), the normal component shows an impulsive, symmetric form with a logarithmic singularity log (x_1-vt) at the rupture front, $x_1 = vt$, v being the velocity of rupture propagation. This discrepancy is probably due to the fact that for the Parkfield earthquake the fault was long and thin. The slip may have been quickly terminated by reflections from the bottom of the fault and the slip function was more like a step-function than the square-root (of distance from tip) dependence for a crack.

4.2 Study of the Effect of Obstacles On the Fault-plane on the Near-Field and Far-Field Displacements

We shall study the effect of obstacles (high strength region in the fault plane) on rupture propagation and their effect on far-field seismograms. Our method of finding the displacements and slip velocities for a spontaneous propagation as a function of the strength parameter S defined by equation (3.18), is particularly suited to such a study.

We consider a two-dimensional fault in an infinite medium which is homogeneous and linearly elastic everywhere off the crack plane and the fault extends only in its own plane. We shall simulate obstacles by regions where the parameter S is large. Such representation of obstacles by regions where S is large was first done by Hamano (1974). Let us first study the bilateral propagation of an antiplane shear crack with initial length L/10 and final length 2L. We shall consider the following four cases.

Case SH-O

Smooth propagation without obstacles

Case SH-1

One obstacle at center of each half of the fault plane, which never break.

Case SH-2

Two obstacles on each half of fault-plane which never break.

Case SH-3

Two obstacles on each half of fault-plane which break after a while, spontaneously.

Figures 4.7 and 4.8 show the position of the obstacles on one half of the fault-plane. We have plotted the value of the critical normalized stress jump (1 + S) across the crack-tip (strength parameter, see section 3.3) assigned to the fault plane as a function of distance from the center, for the above four cases. (1 + S) is only plotted for half the fault because of symmetry. The parallel displacements on the crack are computed by solving the integral equation (2.16) under the initial and boundary conditions, given by equations (2.4) and (2.6) respectively. We consider the case where the slip on the crack stops when the slip velocity reverses sign. These displacements are also shown in Figure 4.7 and 4.8. The displacements are normalized by $L(\tau_o - \tau_f)/\mu$ and are plotted against normalized distance x_1/L along the crack where L is the half crack-length. The displacements are plotted also for half the crack, because of symmetry. The slip velocity on the crack is found by numerical differentiation of the parallel displacement on the crack using a three-point central difference formula. In Figure 4.9 we show a comparison of the normalized slip velocities at the three points along the fault given by $x_1/L = 0.0, .55, .95$ for the case SH-O, as determined by us with those determined by the method of Madariaga (1975) in which velocities are determined directly from his finite difference scheme. The slip velocities are normalized to $\beta(\tau_o - \tau_f)/\mu$, β being the shear wave velocity. Since numerical differentiation is a "roughing" operation, it introduces oscillations in our slip velocities. They oscillate about

Figure 4.7. Strength distribution on crack plane and corresponding displacements on the crack for the cases SH-0 and SH-1.

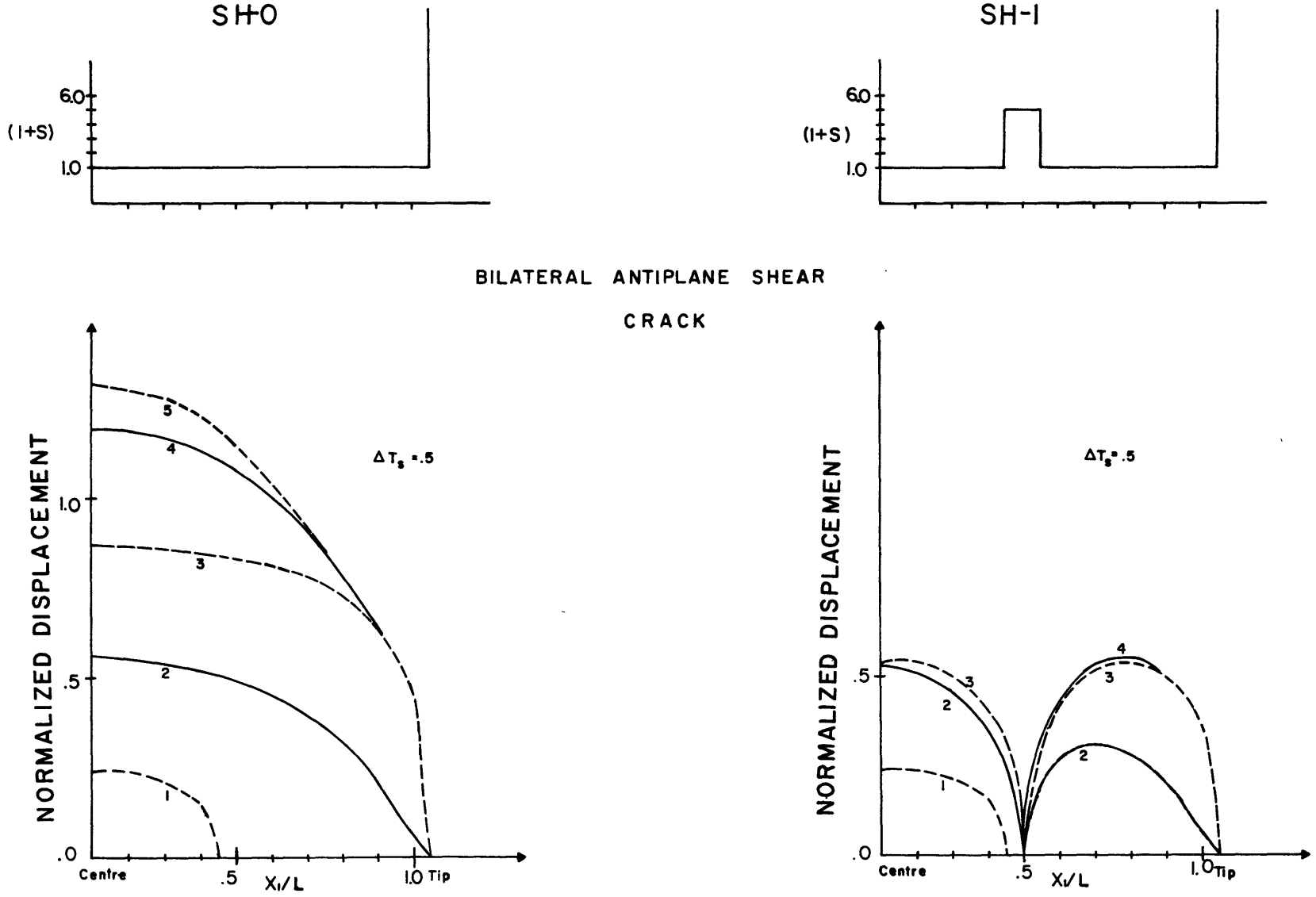

Figure 4.8 Same as Figure 4.7 but for cases SH-2 and SH-3.

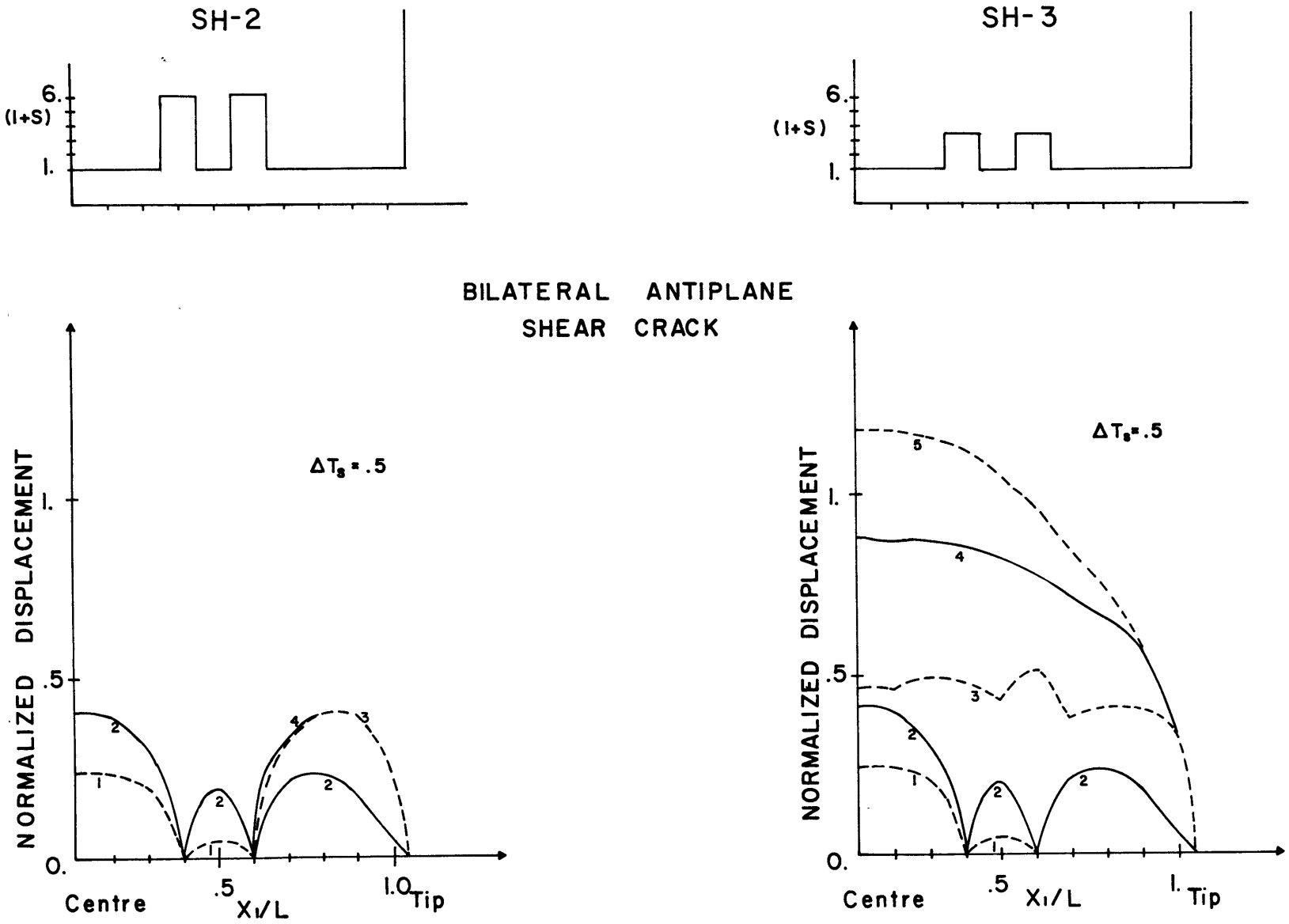

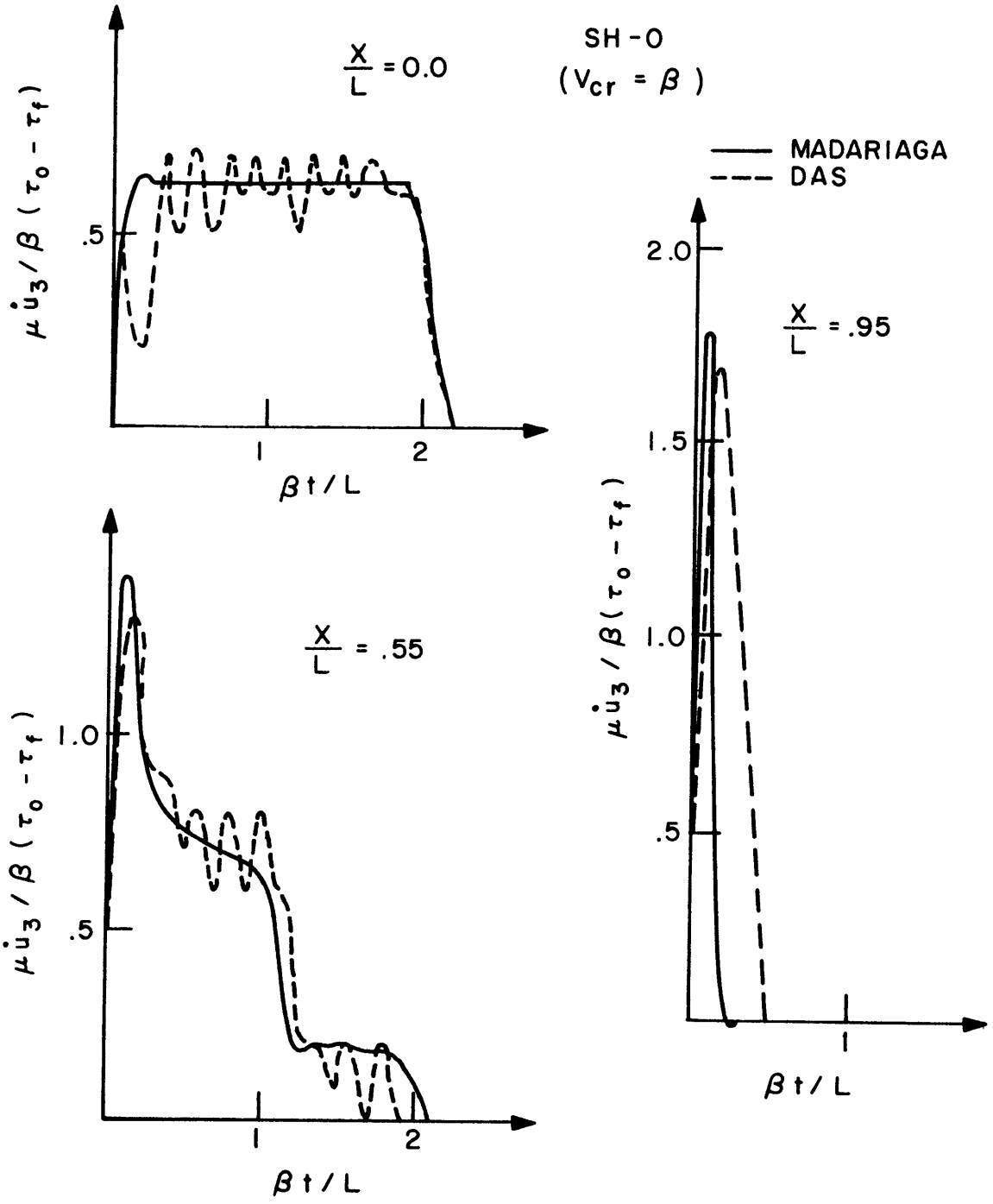

Figure 4.9. Comparison of particle velocities on the crack plane determined by us with those of Madariaga for case SH-O, at three points along the crack.

Madariaga's solution. From Figure 4.9 we see that there are about 5 cycles per unit of normalized time $\beta t/L$, in the oscillations. Since L is ten times the grid-length, the oscillations in the slip velocities affect wave-lengths of about two times the grid length. Since our numerical method of solving the integral equation (2.16) is accurate only down to wave-lengths of about five grid lengths, the numerical oscillations in the slip velocities will not affect the wavelengths where we consider the solution to be accurate.

We shall use these slip velocities on the crack to determine far-field wave-forms and spectra. Before we do this, let us examine the condition under which the use of our two-dimensional fault model to study the far-field is justified. For a circular crack, the form of the slip function (Madariaga, 1975) is very similar to that for a two-dimensional crack (Figure 2.14) and, as we showed in Section 4.1, the final static values differ only by a constant factor. Thus, for this case, the two-dimensional model will give reasonable results. For a long, thin crack, the application of the two-dimensional model is more restrictive. Aki (1968) shows that the width of the fault H is not important to the total motion if the following inequality between the width H, the frequency f and the distance of the observation point from the fault R is satisfied: $\sqrt{f/cR}\ 2H/\pi >> 1$, where c is the velocity of the waves concerned. This can be written as $\lambda R/H^2 << 2/\pi$,

where λ is the wavelength of the wave concerned ($\lambda = c/f$). This inequality will be satisfied for very small R, i.e. if the observation point is on or very close to the fault. Thus we are justified in using the slip velocities on the fault obtained from two-dimensional calculation to determine far-field displacements and spectra in three-dimension.

The far-field waveforms can be computed from the slip velocity on the crack by the relation (Haskell, 1964), (neglecting the radiation pattern and distance dependence)

$$u(\vec{r}, t) = \int_{S_1} \Delta\dot{u}\left(\vec{\xi}, t - |\vec{r}|/c\right) d\Sigma_\xi \quad \ldots\ldots (4.1)$$

where $\vec{\xi}$ is the location vector of a point on the fault , $\vec{r}$ is the location vector pointing from $\vec{\xi}$ to an observation point, and S_1 is the fault plane. We define θ as the angle between the x_2-axis and $\vec{r}$ i.e. the direction to the receiver. $\Delta\dot{u}(\vec{\xi},t)$ is the slip velocity at $\vec{\xi}$ at time t, and c is the velocity of the wave observed at far-field. It is possible, in theory, to obtain the far-field pulse shapes by numerical integration of equation (4.1). However, this is not a practical method because of the singularities involved in $\Delta\dot{u}$.

A more convenient method is to introduce the double Fourier transform of $\Delta\dot{u}(\vec{\xi},t)$ with respect to $\vec{\xi}$ and t as

$$B(\vec{k}, \omega) = \int_{-\infty}^{\infty}\int \Delta\dot{u}\left(\vec{\xi}, t\right) e^{-i\omega t + i\vec{k}\xi} \, dt \, d\xi$$

where $\vec{k}$ is the wave-number and ω is the angular frequency. If $\vec{\xi} = (\xi, 0, 0)$,

$$B(k,\omega) = \int_{-\infty}^{\infty}\int \Delta u(\xi, t)\, e^{-i\omega t + ik\xi}\, dt\, d\xi \tag{4.2}$$

where k is the wave-number component in the x_1-direction. Using a far-field approximation on $|\vec{r}|$ in (4.1) we find, following Aki (1967), that,

$$u(\theta,t) = \int_{-\infty}^{\infty} B(\omega \sin\theta/c,\ \omega)\ e^{i\omega t}\, d\omega \tag{4.3}$$

which gives the far-field wave form for different θ. We use the fast Fourier transform technique to get $B(k,\omega)$ and $u(\theta,t)$.

Figures 4.10, 4.11, 4.12 and 4.13 show contour plots of the amplitude spectrum $\mu B(k,\omega)/\beta(\tau_o - \tau_f)$ in the k-ω space for the four cases under study. The contours are plotted at a unit interval in amplitude spectrum. The far-field S-waves are determined by the region of k-ω space in which $k \leq \omega/\beta$. This is because only waves with phase velocity $\omega/|k|$ (along the plane S_1) greater than the medium velocity β can radiate into the medium. Waves with smaller phase velocity than β are inhomogeneous S waves (i.e. having imaginary x_2-component wave number) trapped near the fault. The far-field spectrum at angle θ is proportional to $B(k,\omega)$ along the line $k = \omega \sin\theta/\beta$.

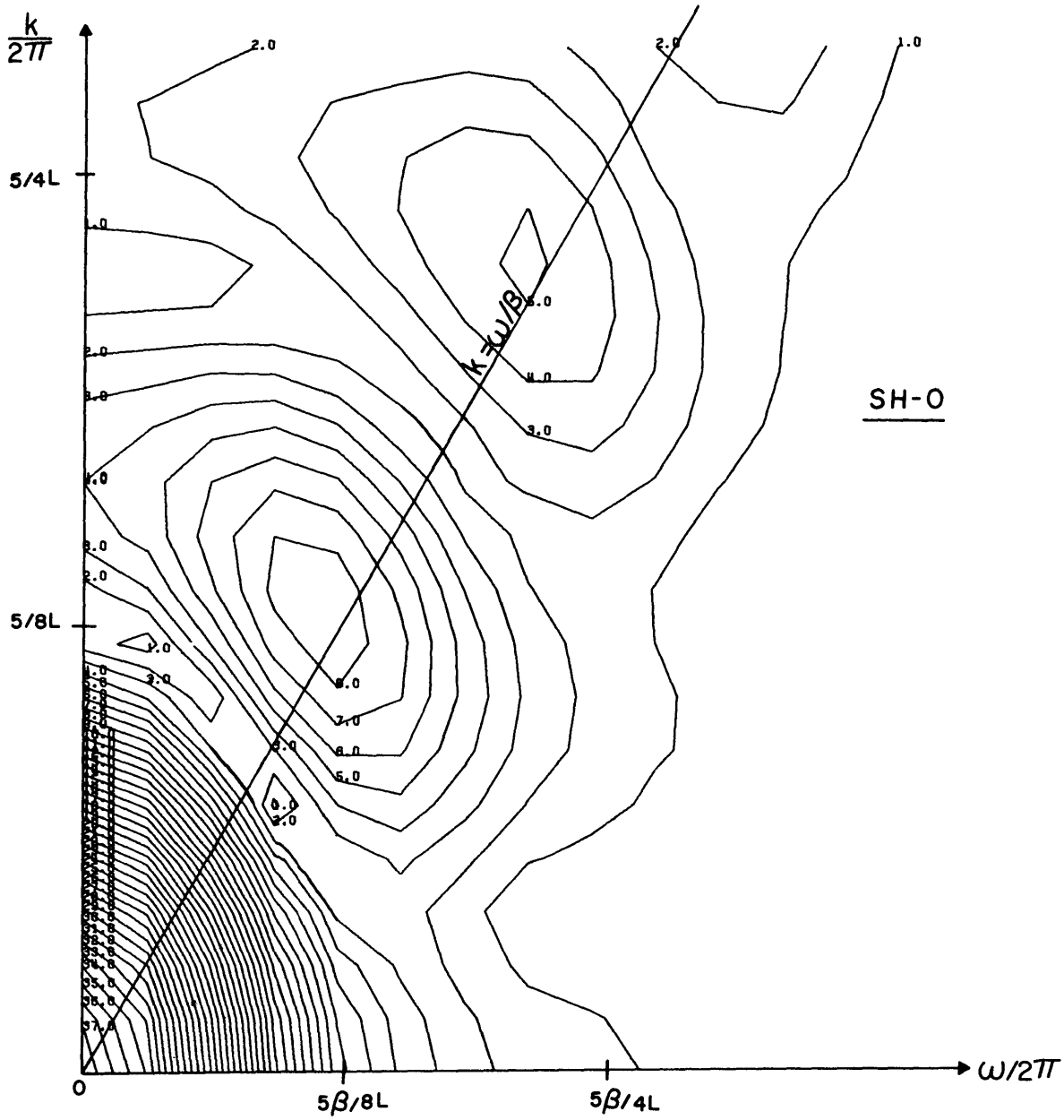

Figure 4.10. Amplitude spectrum $\mu\ B(k,\omega)/\beta(\tau_o - \tau_f)$ in k-ω space for case SH-O.

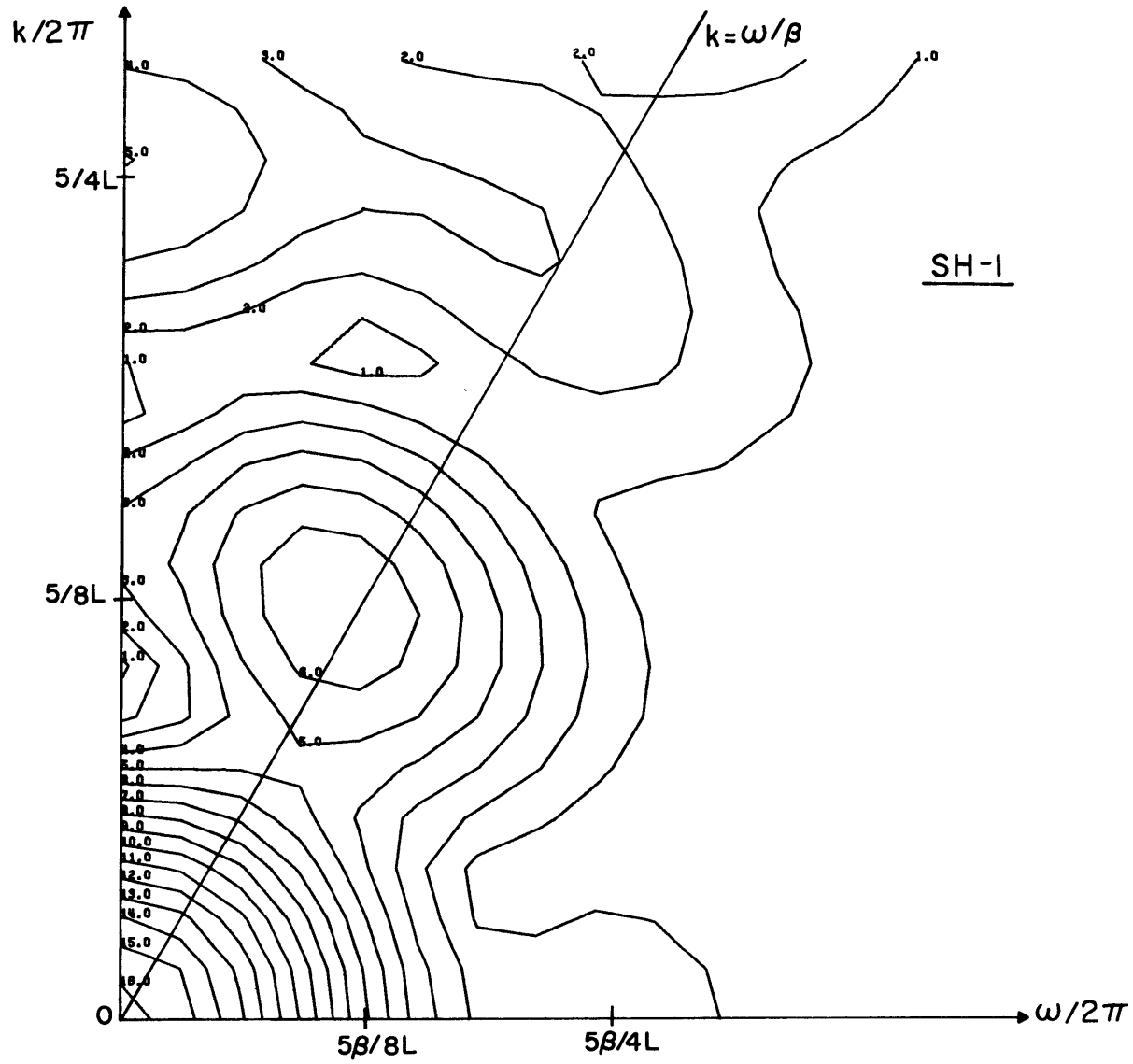

Figure 4.11. Same as Figure 4.10 but for case SH-1.

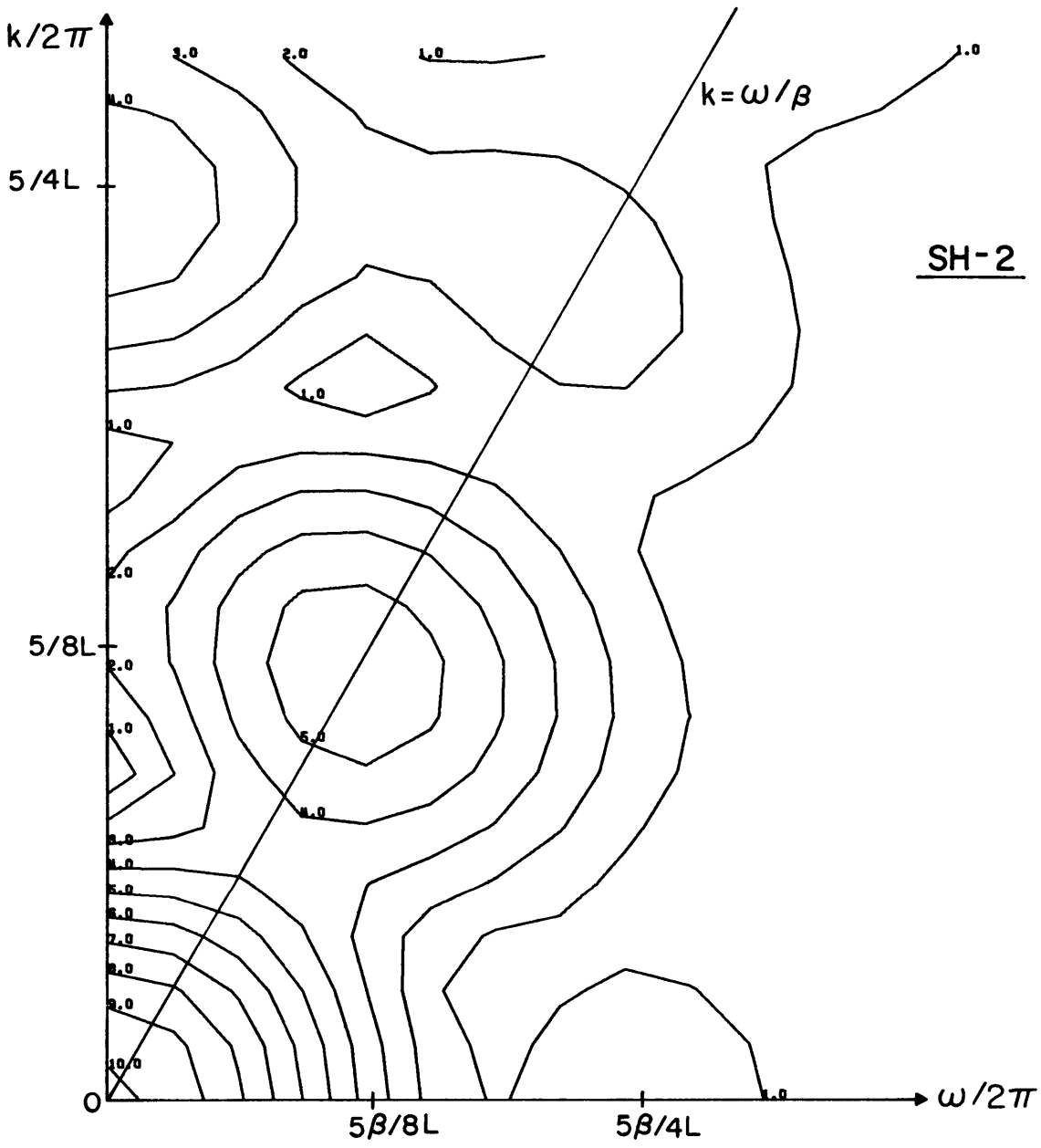

Figure 4.12. Same as Figure 4.10 but for case SH-2.

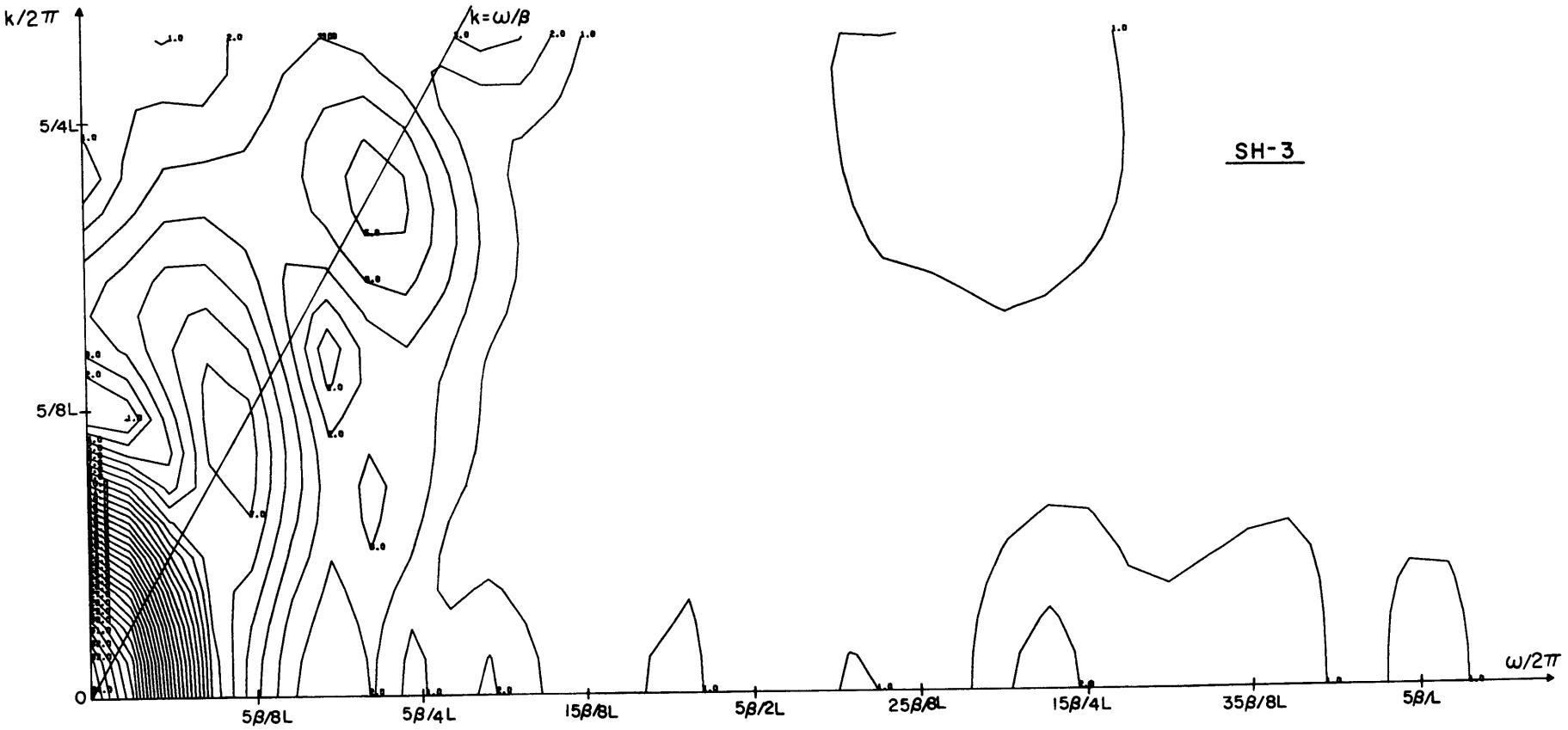

Figure 4.13. Same as Figure 4.10 but for case SH-3.

Thus, this diagram gives far-field spectra for S waves for all directions at a glance.

The logarithm of normalized amplitude spectrum against the logarithm of frequency is plotted on the right side of Figures 4.14, 4.15, 4.16 and 4.17 for θ = 0°, 14.5°, 30° and 90° for the four cases SH-O, SH-1, SH-2 and SH-3. The normalizing factor for the amplitude spectrum is the value of te spectrum at ω = o, k = o. Since we are considering the case in which the slip never reverses direction, u(r,t) will have the same sign for all t. The maximum value of spectrum is at ω = o, k = o, and the normalized spectrum is always less than unity. In Figs. 4.14 through 4.17, each spectra is shifted by one decade in amplitude relative to the one above it for the purpose of clarity. In figures showing the cases SH-1, SH-2 and SH-3, we have indicated by dotted lines the corresponding spectra for SH-O for comparison. The lines of slope ω^{-2} and ω^{-3} are also shown in the figures. We have plotted the spectra up to the frequency given by $\omega L/\beta$ = 10.0. For L = 10d, where d is the grid length in numerical solution of the integral equation (2.16), this corresponds to a grid length of $2\pi d \approx 6d$. This is longer than our earlier estimate of the limiting wave length 5d above which the error in numerical calculation may be neglected. Let us now look at the corner frequency, defined as the frequency of intersection of the low and high frequency asymptote in the spectrum drawn in the log-log plot.

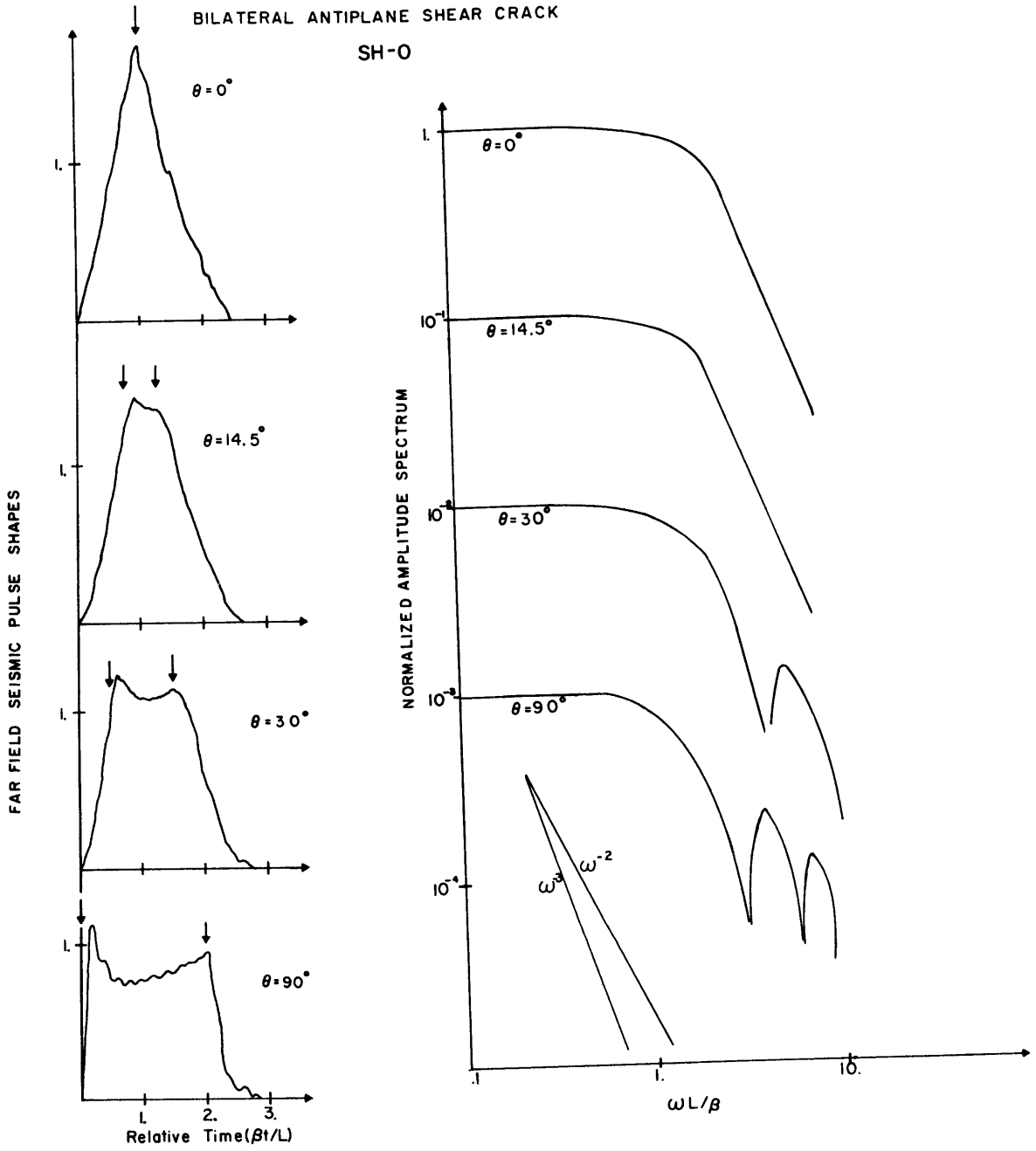

Figure 4.14. Far-field displacements and spectra at different azimuths for case SH-O.

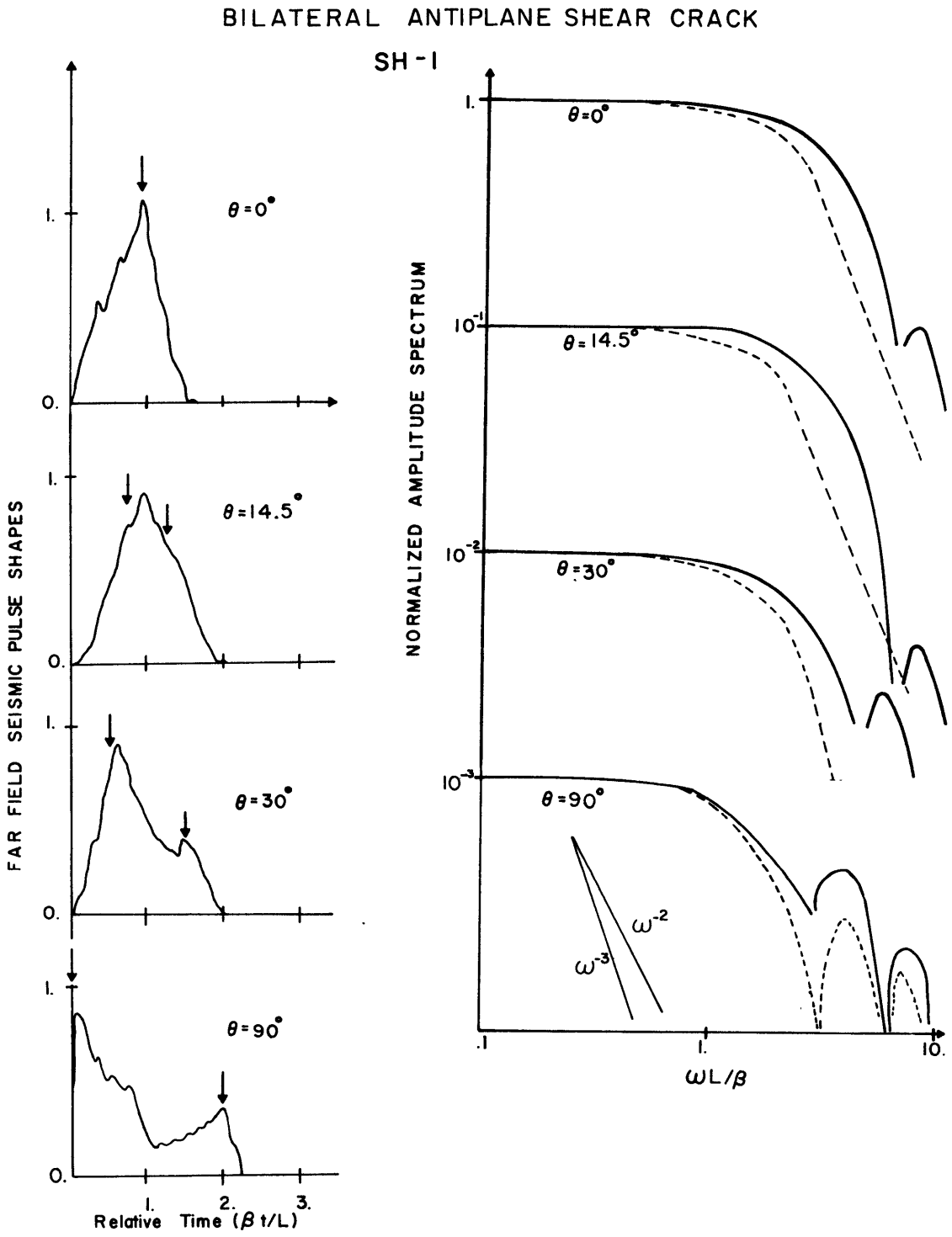

Figure 4.15. Same as Figure 4.14 but for case SH-1.

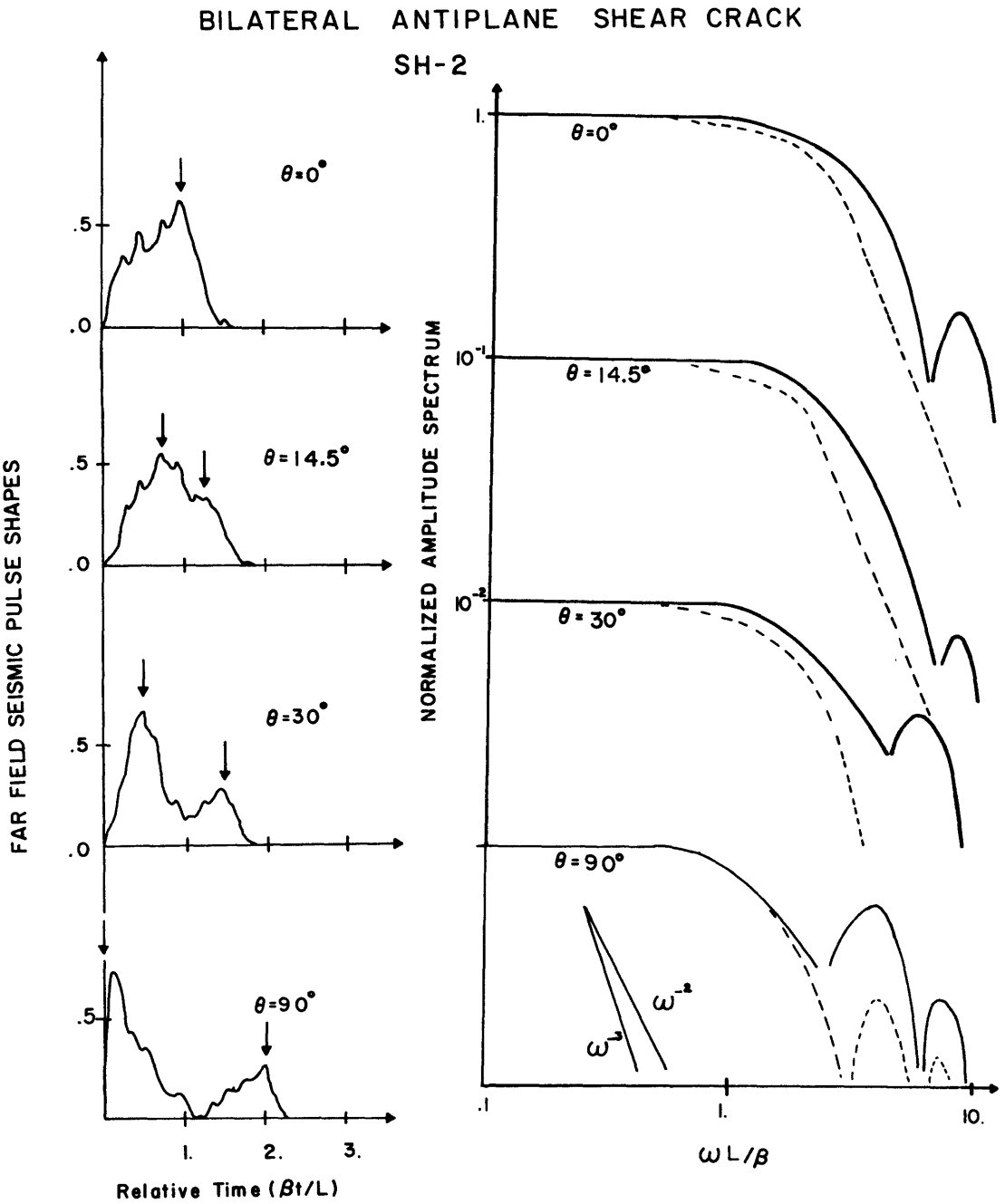

Figure 4.16. Same as Figure 4.14 but for case SH-2.

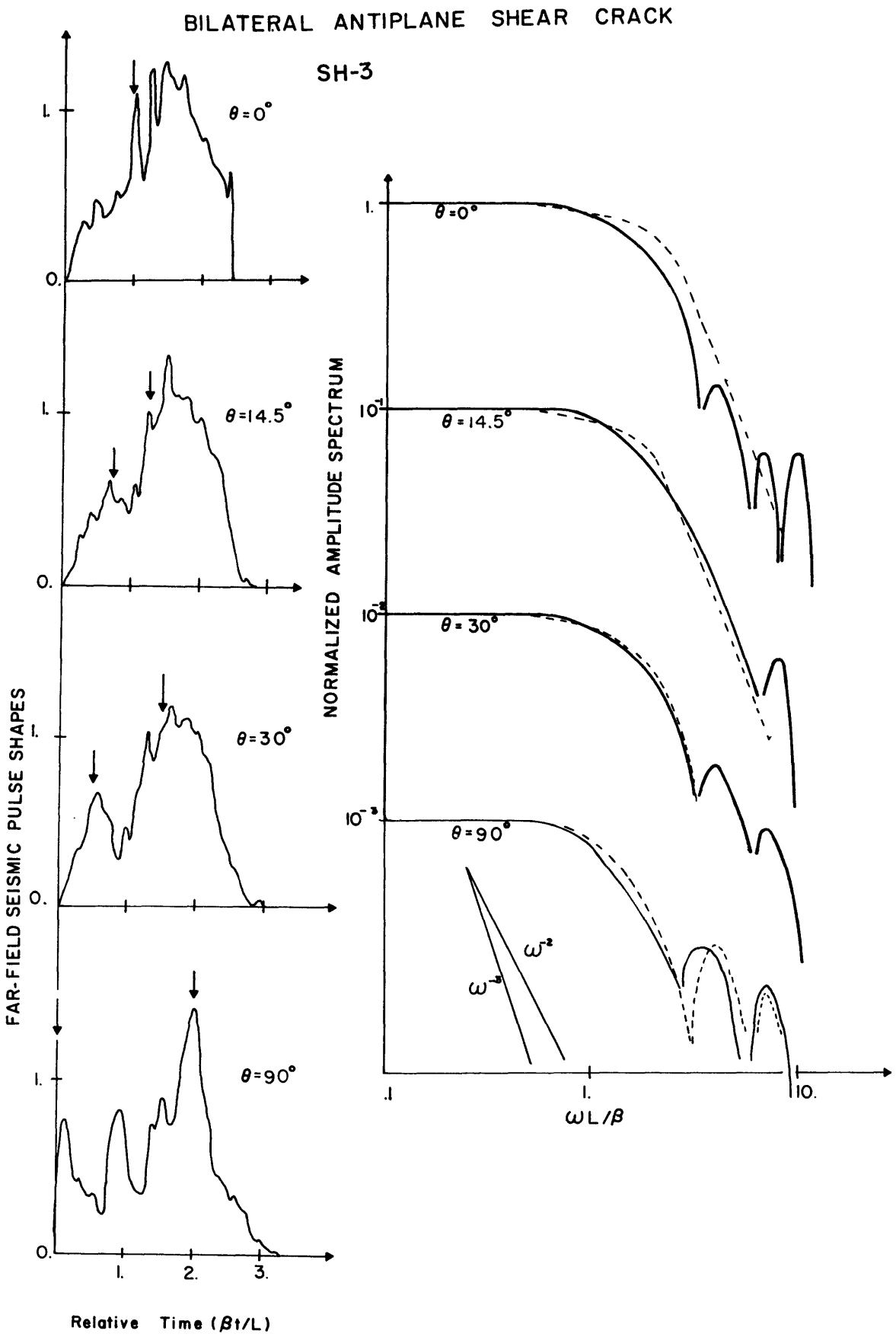

Figure 4.17. Same as Figure 4.14 but for case SH-3.

Table IV lists the corner frequencies in radians, in the unit of β/L, L being the crack half-length, for different θ measured from the spectral curves shown in Figure 4-14 through 4-17.

TABLE IV

	SH-O	SH-1	SH-2	SH-3
0°	1.9	2.3	2.	1.35
14.5°	1.55	2.1	1.55	1.2
30°	1.3	1.5	1.1	1.1
90°	.76	.7	.5	.72

In a few cases, the high-frequency asymptote was not clearly definable and in these cases the value of the corner frequency in Table IV is approximate.

Note that the corner frequencies for a given θ are not significantly different among the cases SH-O, SH-1 and SH-2. Thus, if we try to find the length of a fault from these corner frequencies (Brune, 1970) we would get the same length in all these three cases, the length for case SH-1 and SH-2 being the total length of the whole region of rupture. We

shall return to this point in a later section where we discuss comparison with observations on rock bursts in a deep mine.

It is found that the high frequency decay of the far-field spectra depend on the azimuth. At $\theta = 0$ and 14.5 the decay is clearly proportional to ω^{-2} for all cases. At $\theta = 30°$ and 90° a segment of the high frequency asymptote that decays as $\omega^{-3/2}$ is also seen for SH-0 and SH-3. For SH-1 and SH-2 the high frequencies for $\theta = 30°$ decay as $\omega^{-3/2}$ but as ω^{-1} for $\theta = 90°$. On the other hand, the corner frequency is higher at $\theta = 0°$ than at $\theta = 90°$, for all four cases. This is due to the well-known $\frac{\sin x}{x}$ effect (Ben-Menahem, 1961) where $x = \omega L \left(\frac{1}{V_{cr}} - \frac{\sin\theta}{\beta}\right)$, V_{cr} being the rupture velocity, which has smoothing effect on high frequencies due to destructive interference between waves coming from a finite source. The smoothing effect is weakest in the direction of rupture propagation ($\theta = 90°$) and becomes stronger as θ decreases. We note that the case SH-3 generally has more structure at frequencies between $\omega = 5\beta/L$ and $\omega = 10\beta/L$ than the other cases for the same θ. This is expected because these intermediate frequencies are affected both by the temporary stopping by obstacles and by their eventual breaking.

Brune (1970) has suggested an existence of a segment of source spectra which decays as ω^{-1} between the flat part and the high-frequency asymptote when the stress drop is not uniform and coherent in space. The ω^{-1} dependence comes from an assumption that in the case of partial stress drop, the

stress on the fault drops below the final stress (static friction) during slipping. He models this by applying an initial shear stress pulse σ say, instantaneously over the whole fault plane and after a short time, applies a reverse stress pulse $(1 - \epsilon)\sigma$ over the whole fault plane. This leads to the existence of the ω^{-1} decay in the far-field spectrum. This behavior of the stress on the fault-plane is not found in our results. We found that the stress drop on the crack plane can overshoot because of stick-slip arrest but never reverse the sense of change. Our results show that no ω^{-1} decay is found in the spectra for small θ but, for large θ such a behavior is seen in cases of SH-1 and SH-2. We shall return to this point again in the discussion of the unilateral, in-plane shear crack.

The left sides of Figure 4.14, 4.15, 4.16 and 4.17 show the far-field waveforms $u(\theta,t)$ for the four cases under study, for θ = 0°, 14.5°, 30° and 90°. Time is measured relative to the arrival from the center of the fault and the arrows show the theoretical arrival times of waves radiated from the nearer and farther tips of the fault. The time intervals between the first arrival from the center of the fault and the arrival of stopping phases from the nearer and farther ends are given by

$$t' = L\left(\frac{1}{V_{cr}} \mp \frac{\sin\theta}{\beta}\right)$$

where L = half length of fault, V_{cr} is the rupture velocity, + refers to the farther end, - to the near end.

The figures show that for the SH-0 case the far-field wave form has a triangular shape at $\theta = 0°$, progressively gets wider at the top as θ increases and takes trapezoidal shapes and is almost rectangular at $\theta = 90°$. A comparison of the four different cases shows that width of the pulse at the base depends on the time of duration of the whole rupture process, so that the pulses for SH-0 and SH-3 are wider than that for SH-1 and SH-2. $u(\theta, t)$ as defined in (4.1) and (4.3) only gives the shape of wave form. The actual amplitude of the displacements are dependent on the radiation pattern, the geometrical spreading and material properties of the medium. For the anti-plane shear crack the radiation pattern is given by $\cos\theta$ which is maximum at $\theta = 0°$ and zero at $\theta = 90°$, so that we would never actually be able to observe the wave forms and spectra plotted for $\theta = 90°$. Comparison of the wave forms for four cases SH-0, SH-1, SH-2 and SH-3 shows that the complexity of rupture process is well reflected in the complexity of far-field wave form.

However, we note that for the bilateral, antiplane shear crack, the corner frequency alone cannot always distinguish between the case of simple and complex rupture. The length of the crack inferred from these corner frequencies for a rupture with obstacles [by the use of a formula applicable to a smooth rupture] was the total length of the rupture propagation including the unbroken portions.

Next, we consider unilateral propagation of an in-plane shear crack in an infinite medium which is homogeneous and linearly elastic everywhere off the crack plane. The crack is initially of length L/10, L being the final crack length. We shall consider the following six cases:

Case P-SV-0: Smooth propagation without obstacles

Case P-SV-1: One obstacle on fault plane, which never breaks

Case P-SV-2: Two obstacles on fault plane, which never breaks

Case P-SV-3: Two obstacles on the fault plane which break eventually

Case P-SV-4: One obstacle on the fault plane which breaks eventually

Case P-SV-5: An obstacle of four grids long in the center of the crack which never breaks

Figures 4.18, 4.19, 4.20 and 4.21 show the distribution of normalized critical stress jump (1 + S) assigned to the fault, for the six cases under consideration. The corresponding normalized parallel displacements, under the condition that the slip stops when the particle velocity reverses sign, are shown in the figure. The normalizing factor for the displacement is $L(\tau_o - \tau_f)/\mu$, L being the <u>total</u> length of the fault. The normalizing factor for the slip velocities is now $\alpha(\tau_o - \tau_f)/\mu$ where α is the P-velocity. Figures 4.22, 4.23, 4.24, 4.25, 4.26 and 4.27 show contour plots of the amplitude spectrum $\mu B(k,\omega)/\alpha(\tau_o - \tau_f)$ in the $k-\omega$ space for the six cases under study. The region $k \leq \omega/\alpha$ and $k \leq \omega/\beta$ indicate the region of $k-\omega$ space which determines the far-field spectra of

Figure 4.18. Same as Figure 4.7 but for cases P-SV-0 and P-SV-1.

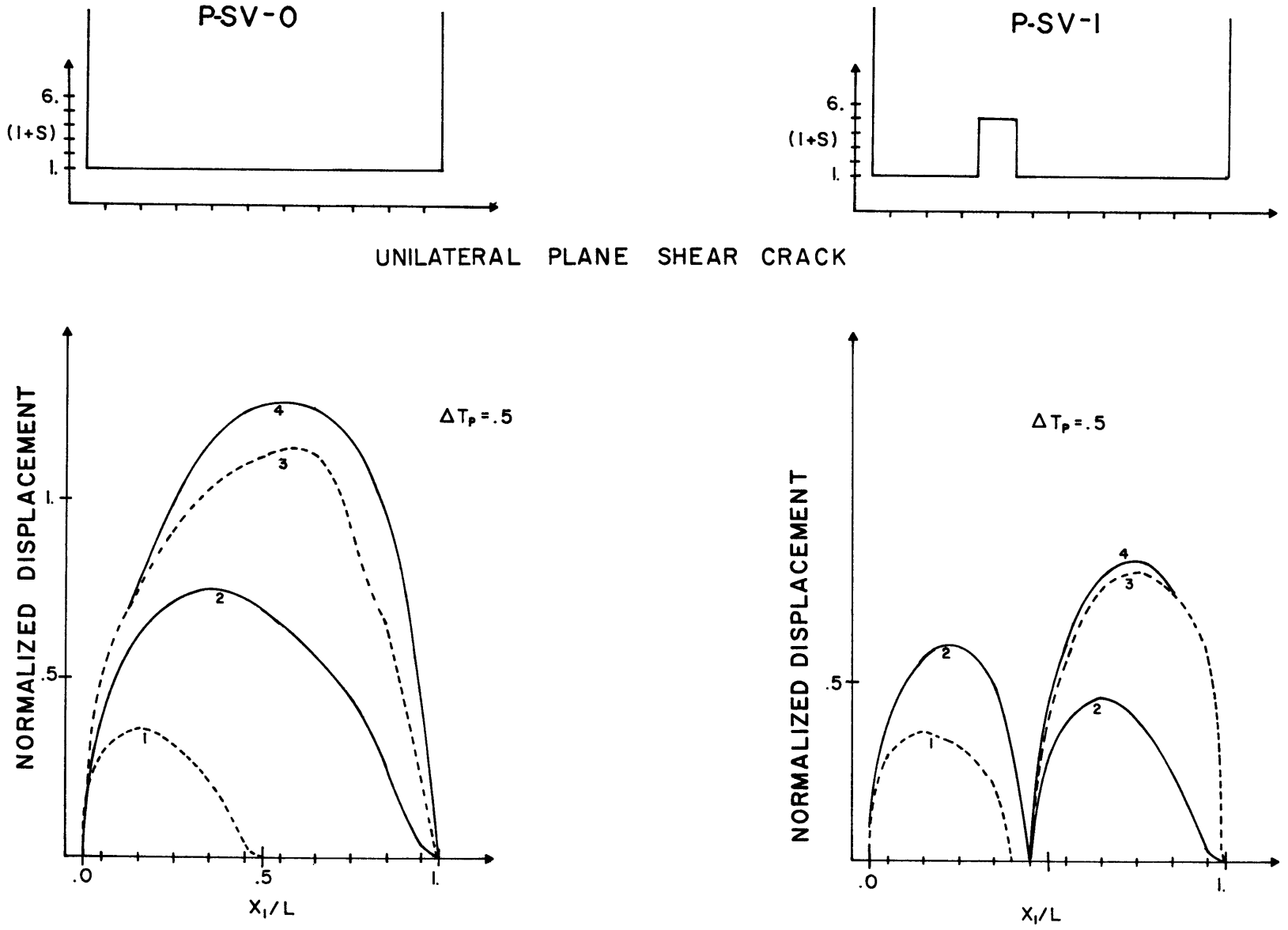

Figure 4.19. Same as Figure 4.7 but for cases P-SV-2 and P-SV-3.

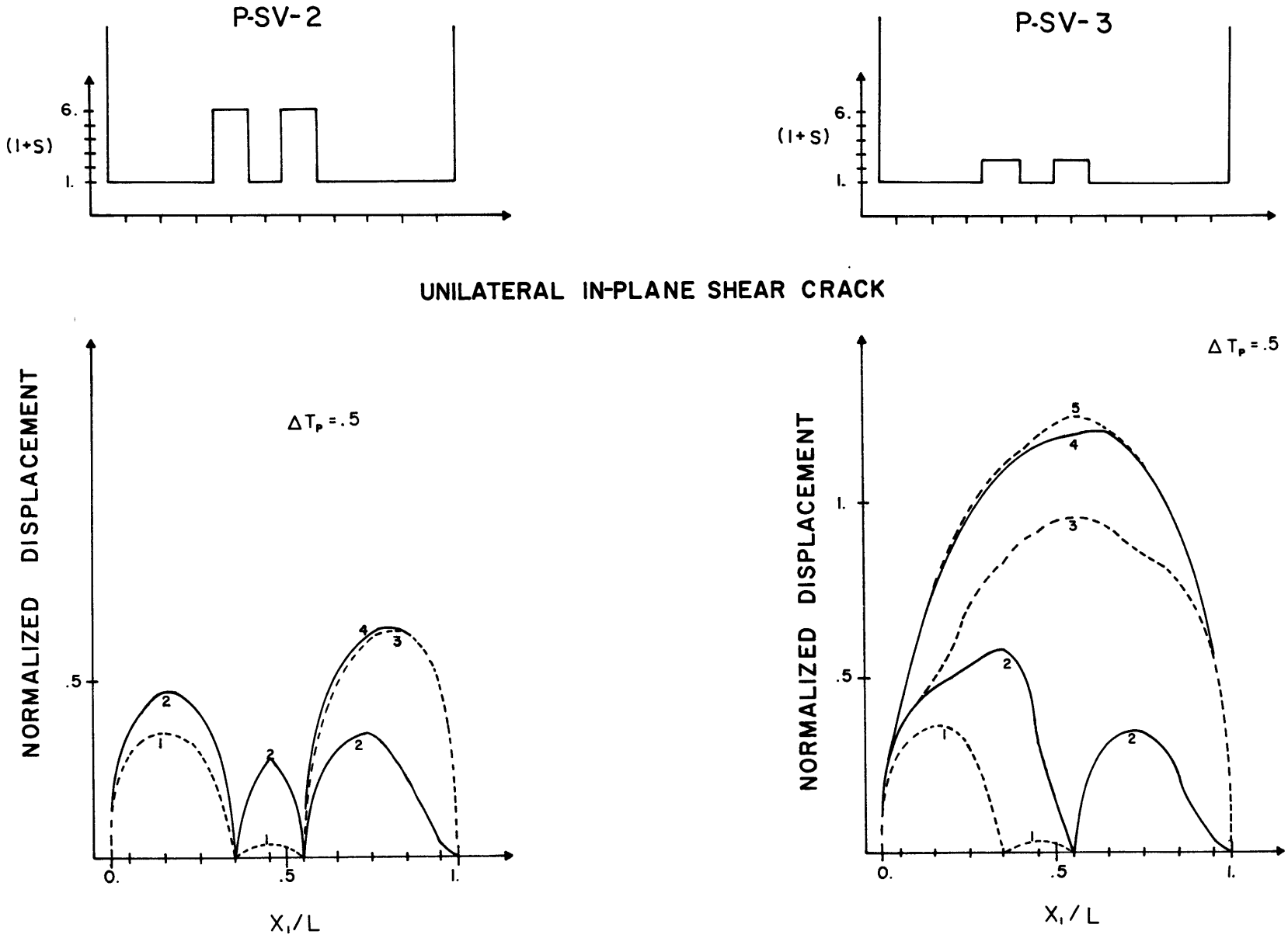

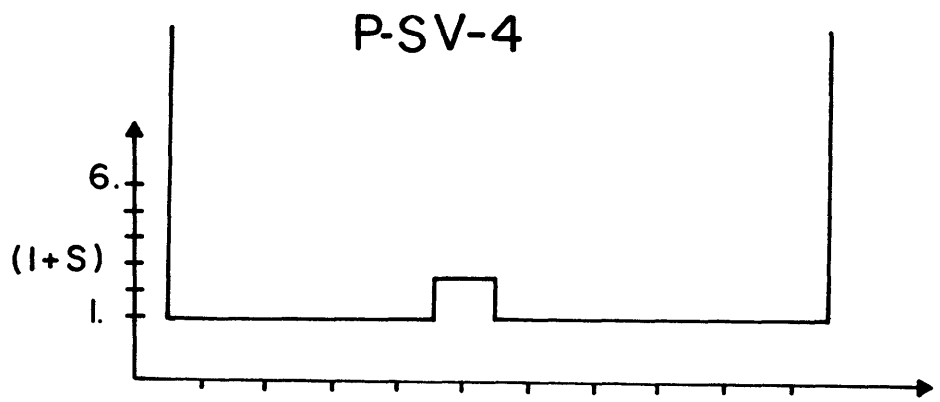

UNILATERAL IN-PLANE SHEAR CRACK

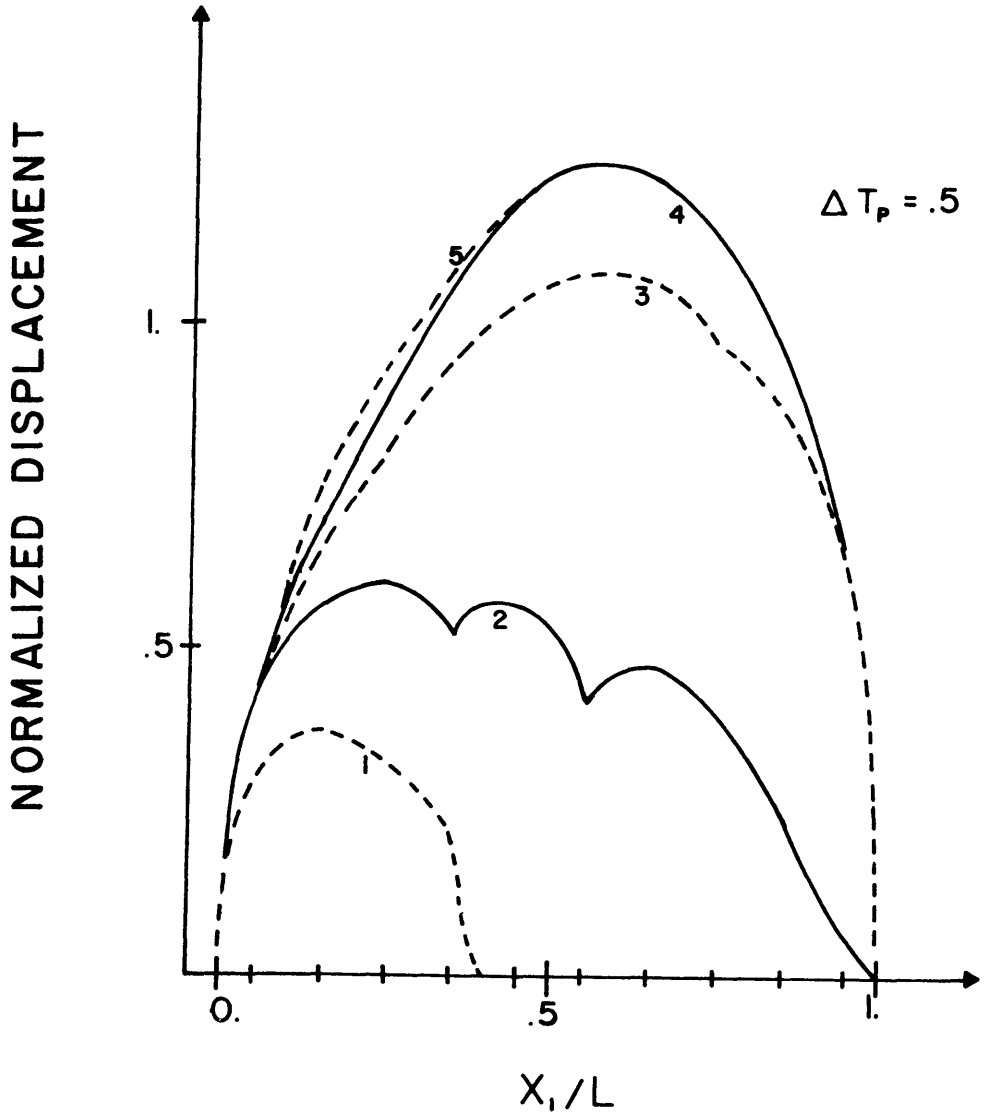

Figure 4.20. Same as Figure 4.7 but for case P-SV-4.

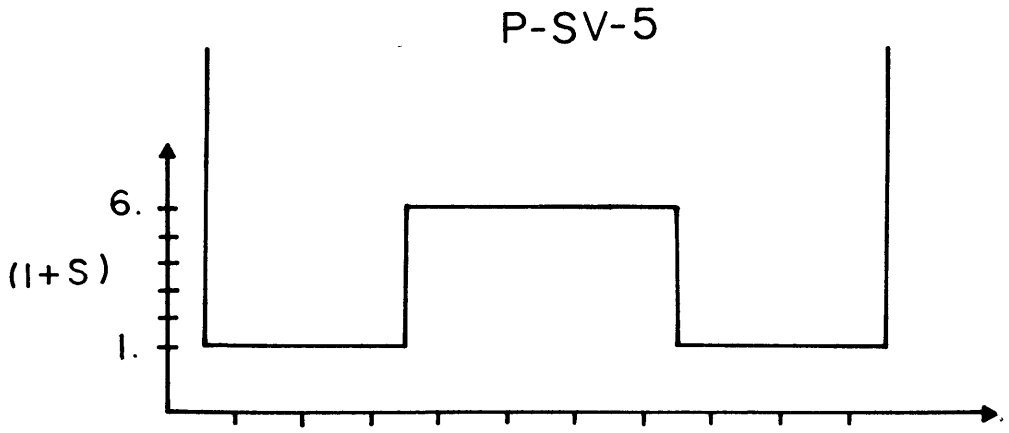

Figure 4.21. Same as Figure 4.7 but for case P-SV-5.

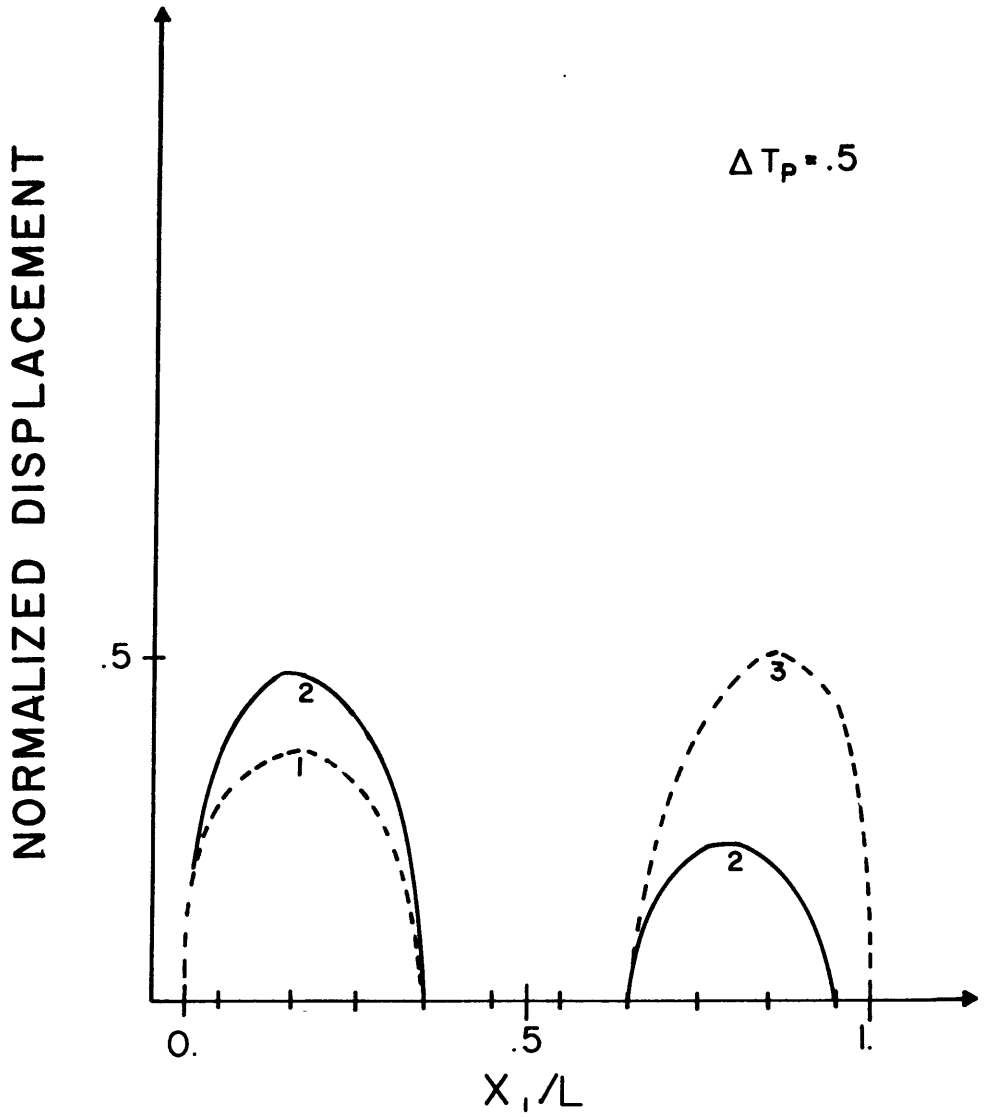

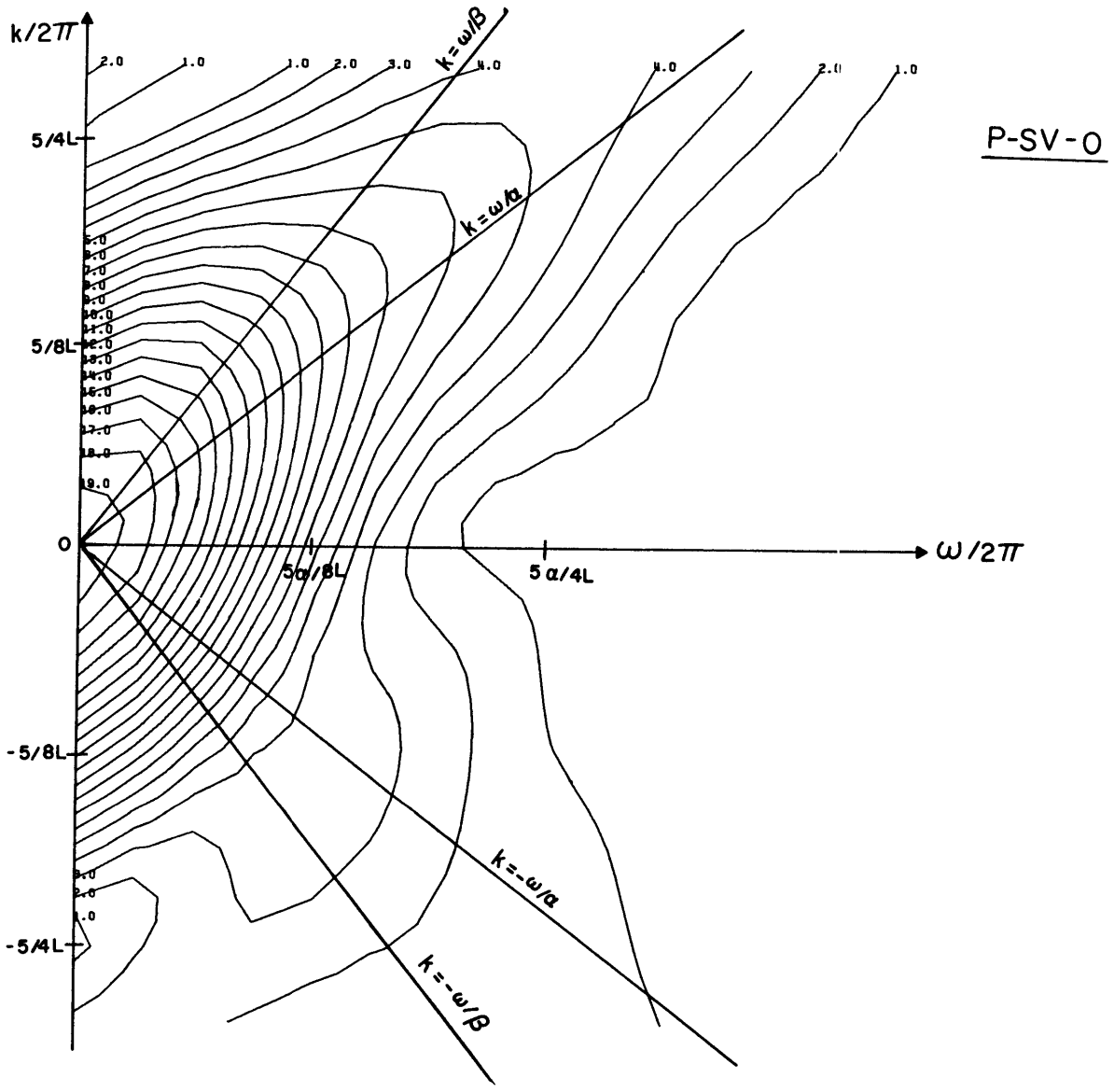

Figure 4.22. Same as Figure 4.10 but for case P-SV-0.

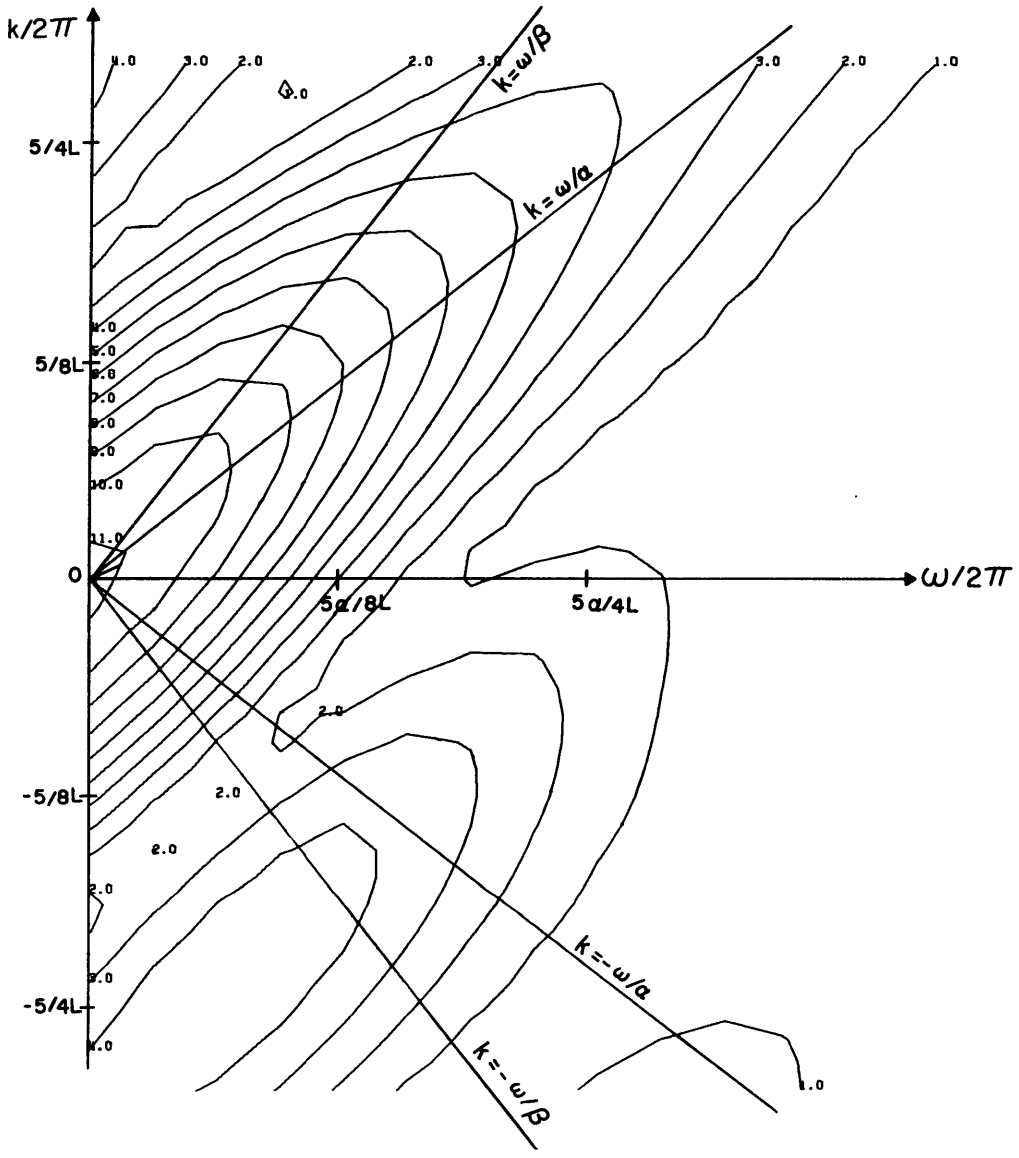

Figure 4.23. Same as Figure 4.10 but for case P-SV-1.

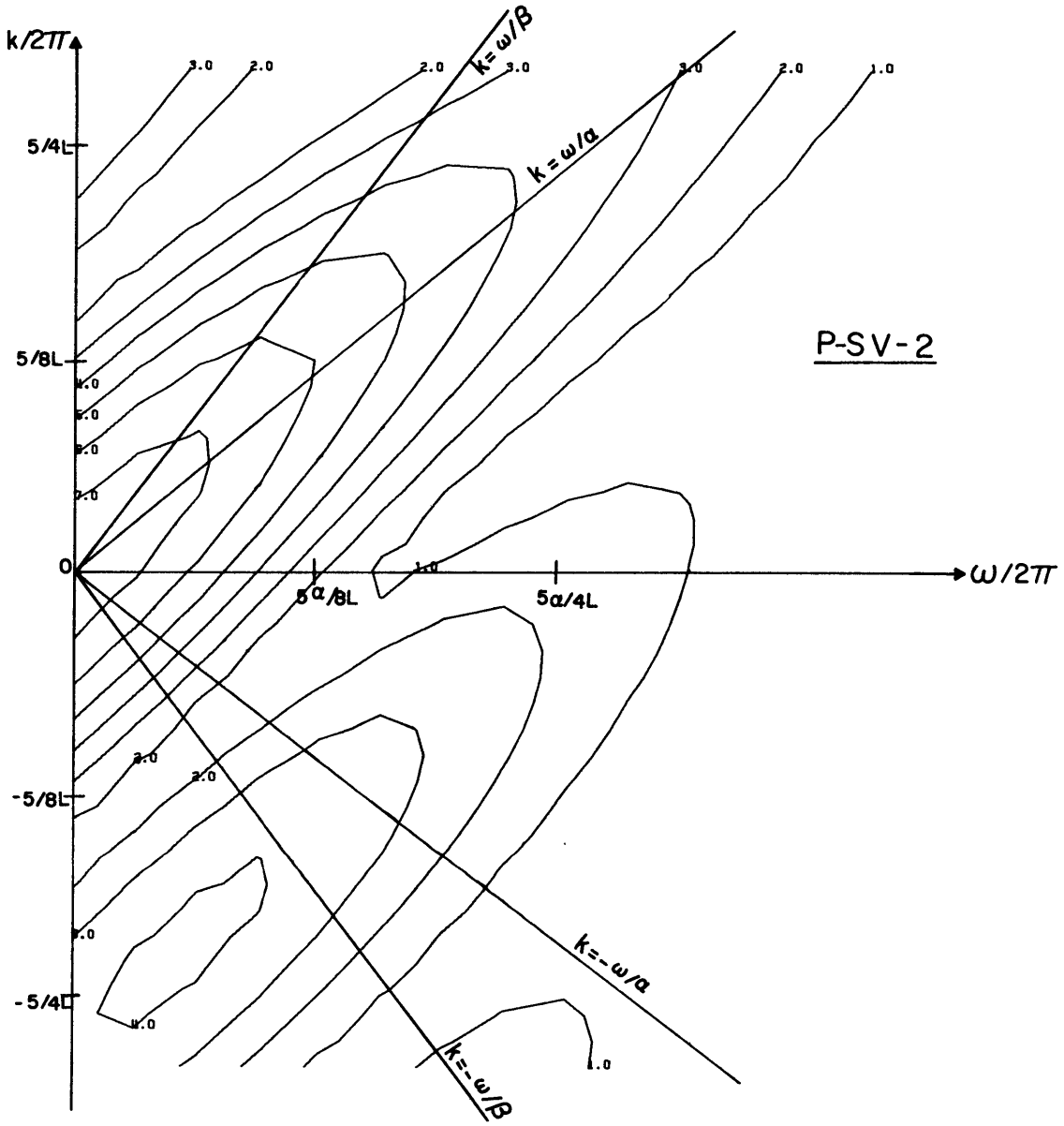

Figure 4.24. Same as Figure 4.10 but for case P-SV-2.

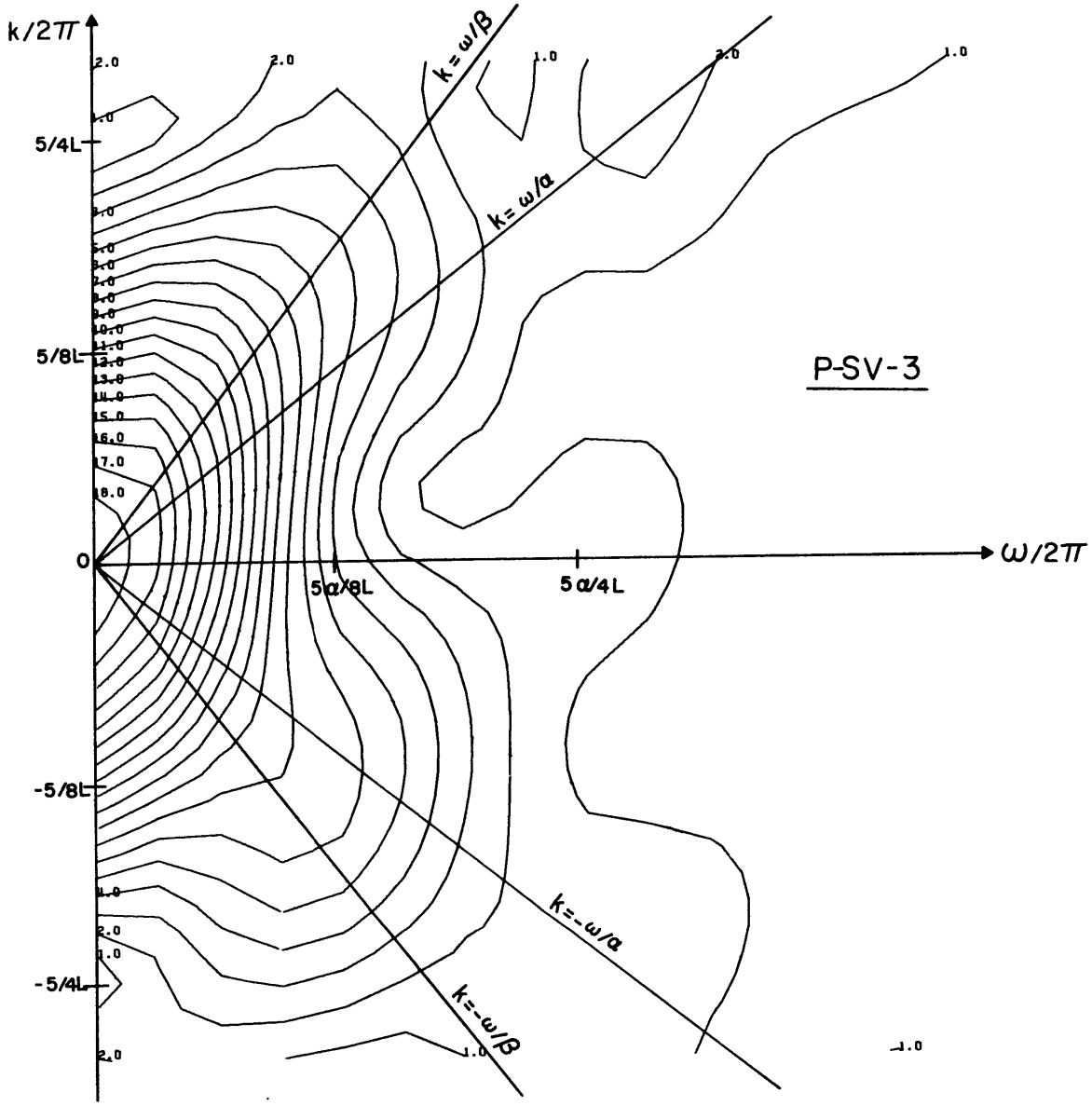

Figure 4.25. Same as Figure 4.10 but for case P-SV-3.

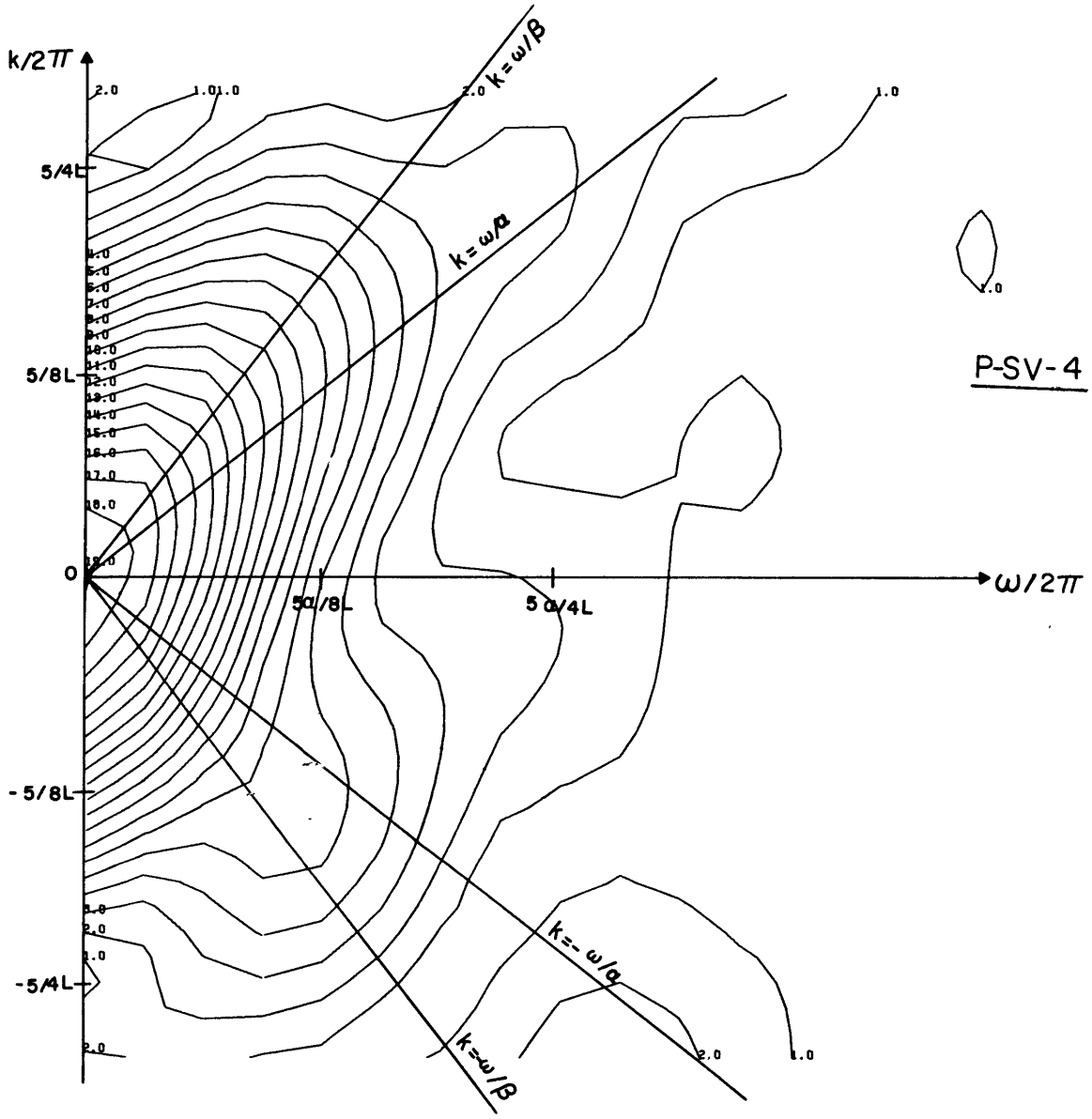

Figure 4.26. Same as Figure 4.10 but for case P-SV-4.

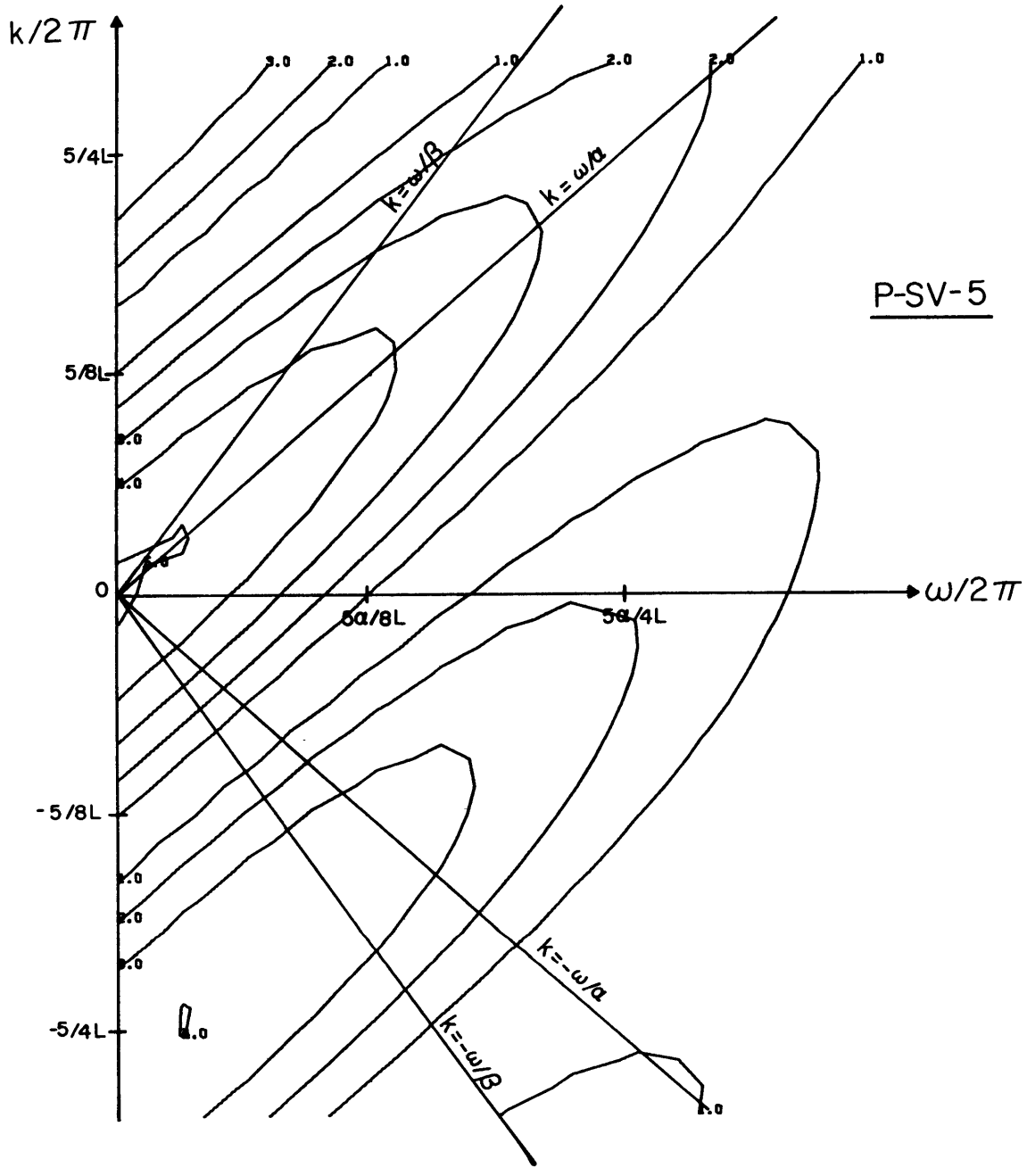

Figure 4.27. Same as Figure 4.10 but for case P-SV-5.

P- and S- waves. The far-field spectrum at angle θ is proportional to $B(k,\omega)$ along the line $k = \omega \sin\theta/c$.

Figures 4.28, 4.29, 4.30, 4.31, 4.32, and 4.33 show the normalized P-wave spectra $B(\omega \sin\theta/c, \omega)/B(0,\omega)$ and far-field wave-forms $u(\theta,t)$ for the six cases at $\theta = -90°$, $-30°$, $-14.5°$, $14.5°$, $30°$ and $90°$ and the S-wave spectra and pulse shape at $\theta = 0°$. Negative values of θ indicate observation points in a direction opposite to the direction of propagation. Points at azimuths $\theta = 0°$, $\pm$ 14.5°, $\pm$ 30°, $\pm$ 90° at which the spectra and wave forms are plotted are equidistant from the final end of the fault.

In figures showing cases P-SV-1, P-SV-2, P-SV-3, P-SV-4, P-SV-5 we have also indicated by dotted lines the spectra for P-SV-0 for comparison. As in the antiplane case, we have plotted the spectra up to $\omega L/\alpha = 10.0$ which corresponds to a wavelength of 6d, d being the grid-length in our integral equation (2.16) and is thus well within the limit of accuracy of our numerical scheme.

We see that for small $|\theta|$, the corner frequencies for the five cases P-SV-0, P-SV-1, P-SV-2, P-SV-3, and P-SV-4 are almost unchanged. For P-SV-5 the corner frequency for small $|\theta|$ is effected more than the other five cases, but still the change is small. For large $|\theta|$, the corner frequency is more affected but still small for all cases except P-SV-5 where it is significantly changed.

The high-frequency decay is, in most cases, proportional

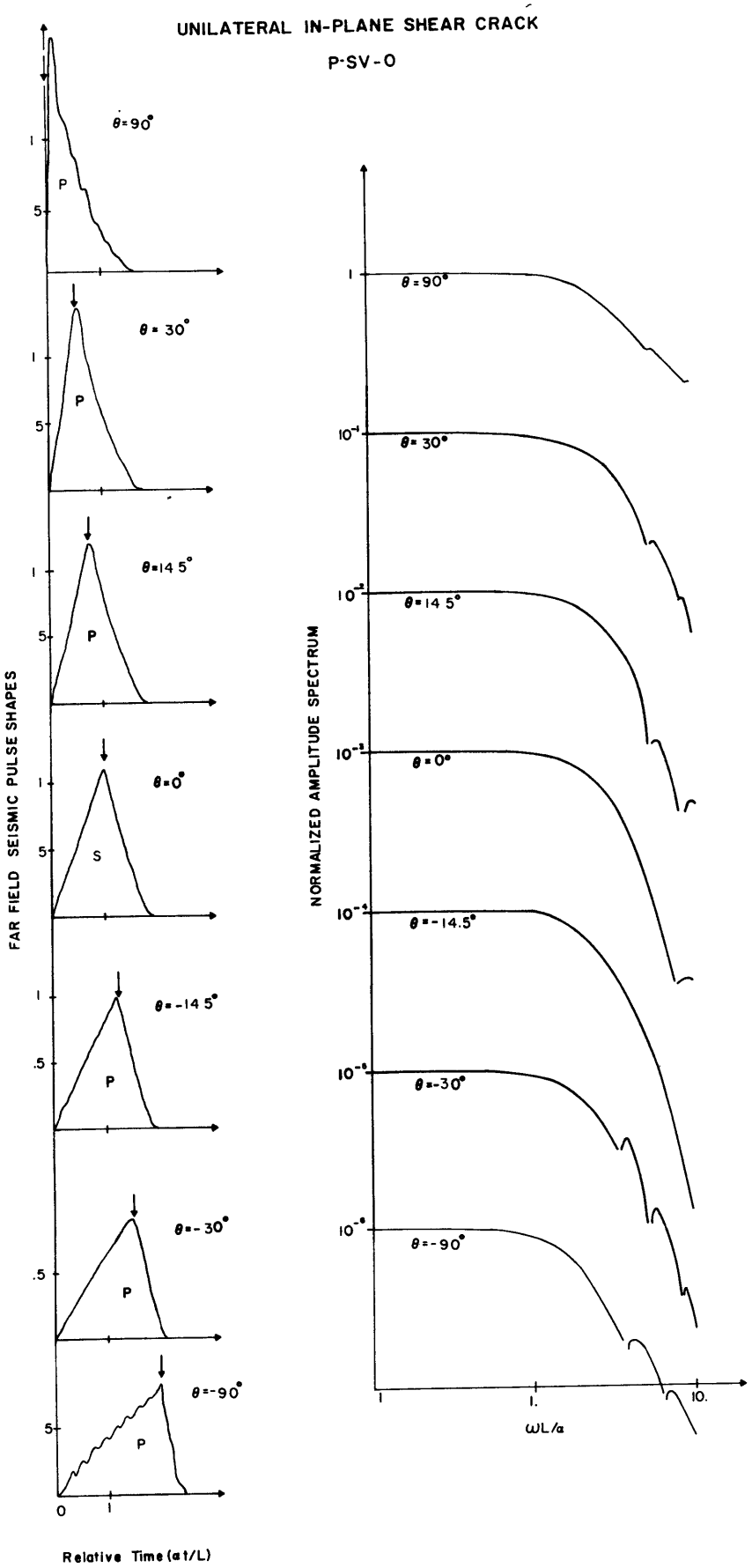

Figure 4.28. Same as Figure 4.14 but for case P-SV-O.

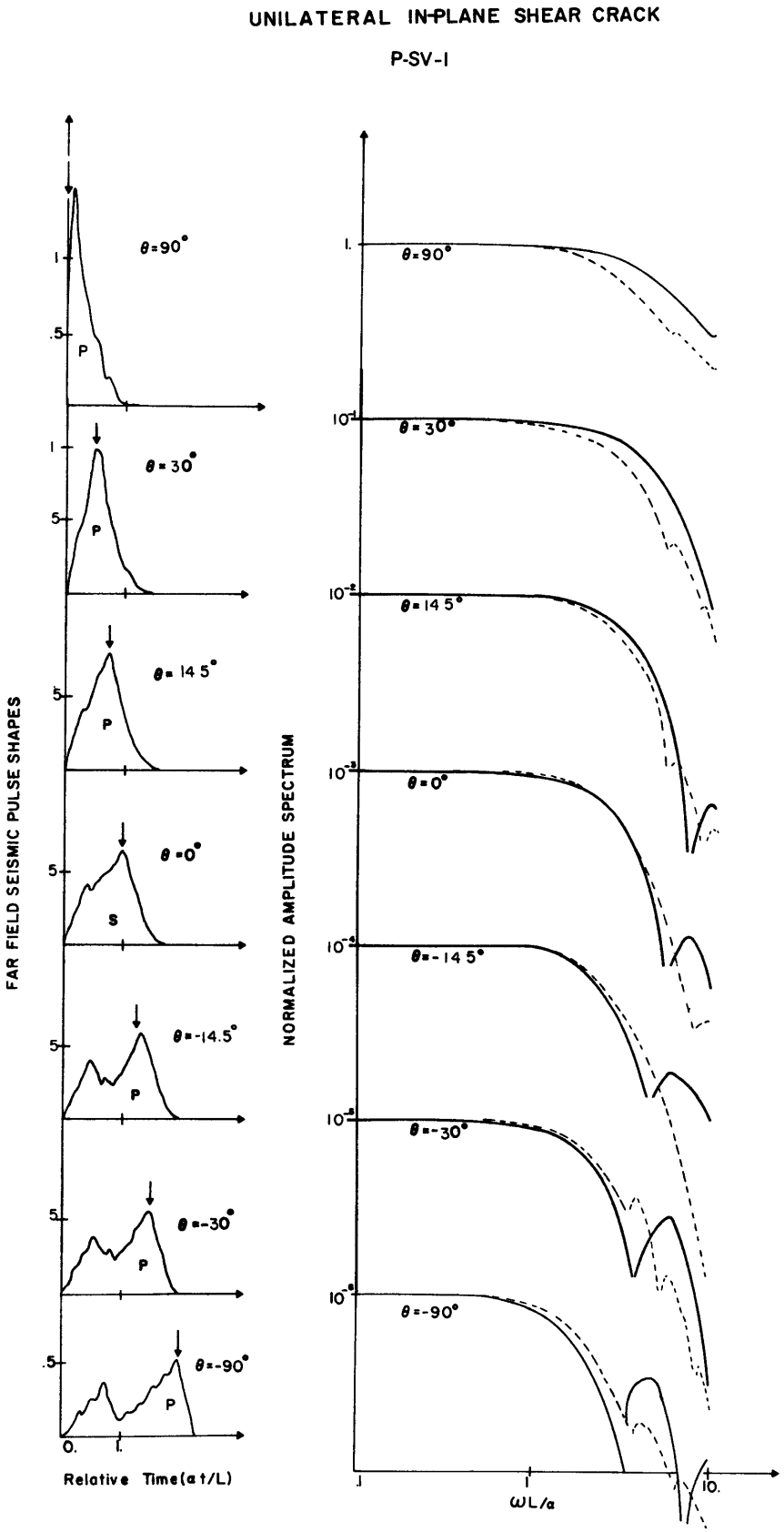

Figure 4.29. Same as Figure 4.14 but for case P-SV-1.

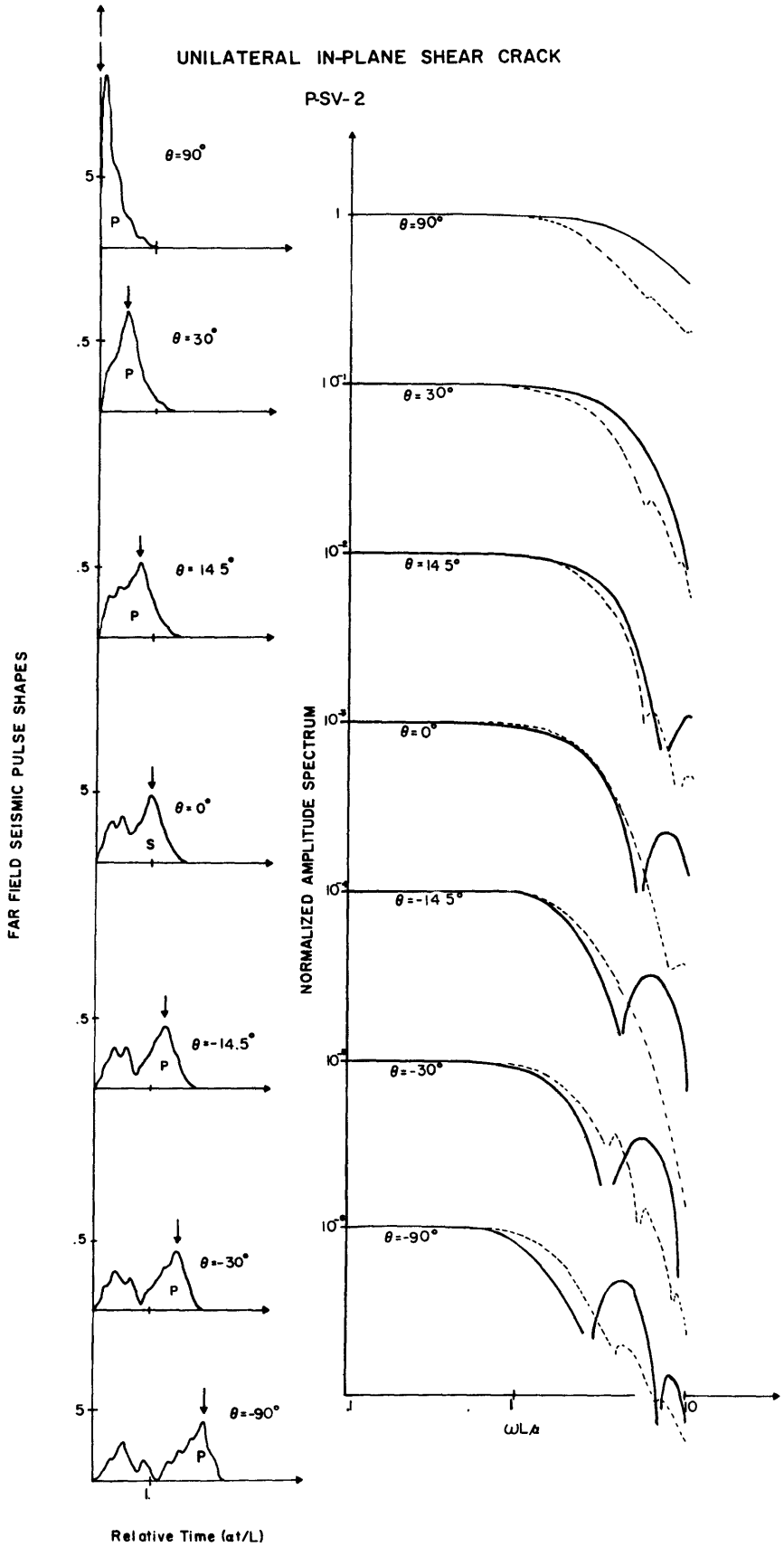

Figure 4.30. Same as Figure 4.14 but for case P-SV-2.

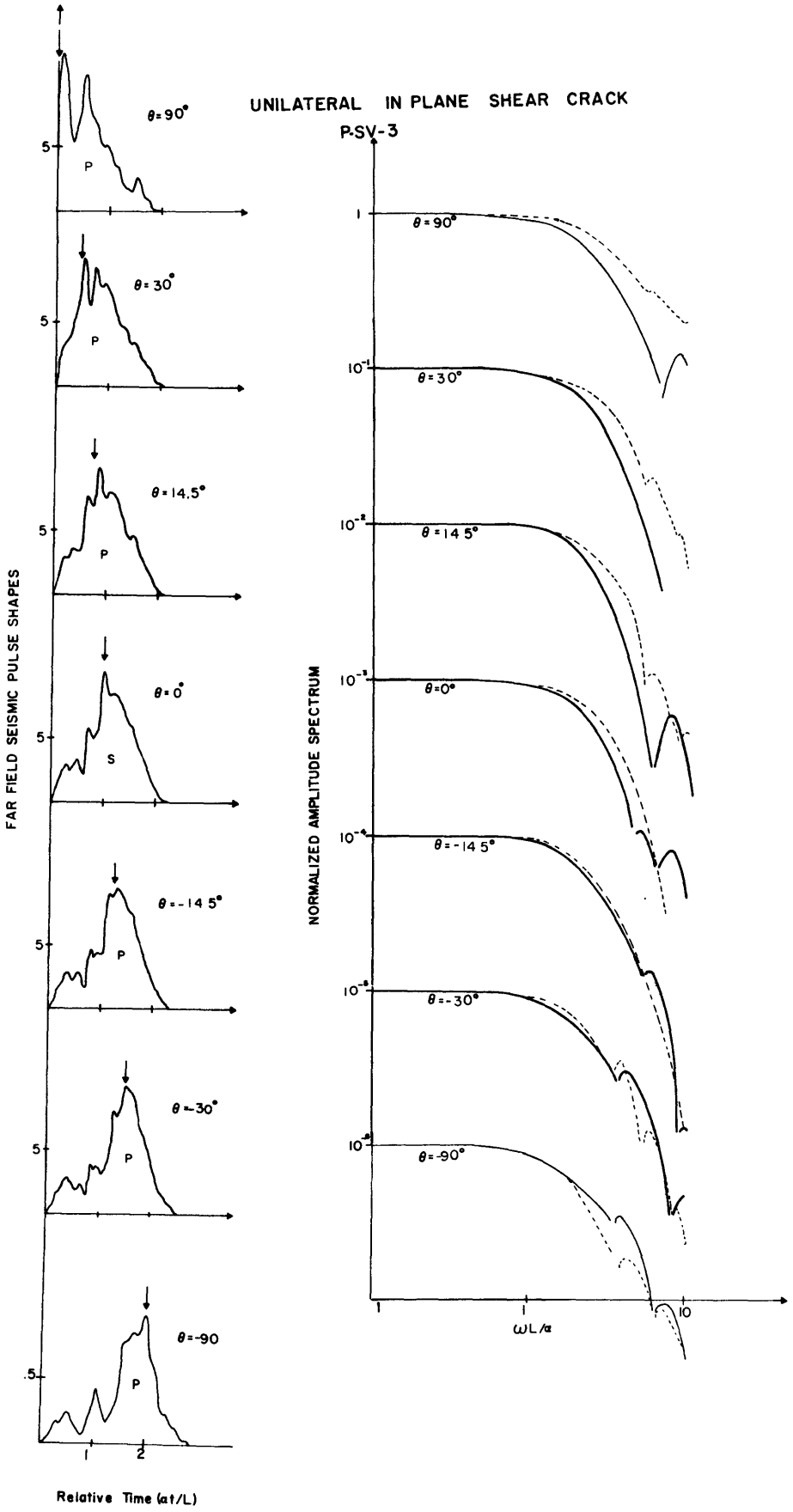

Figure 4.31. Same as Figure 4.14 but for case P-SV-3.

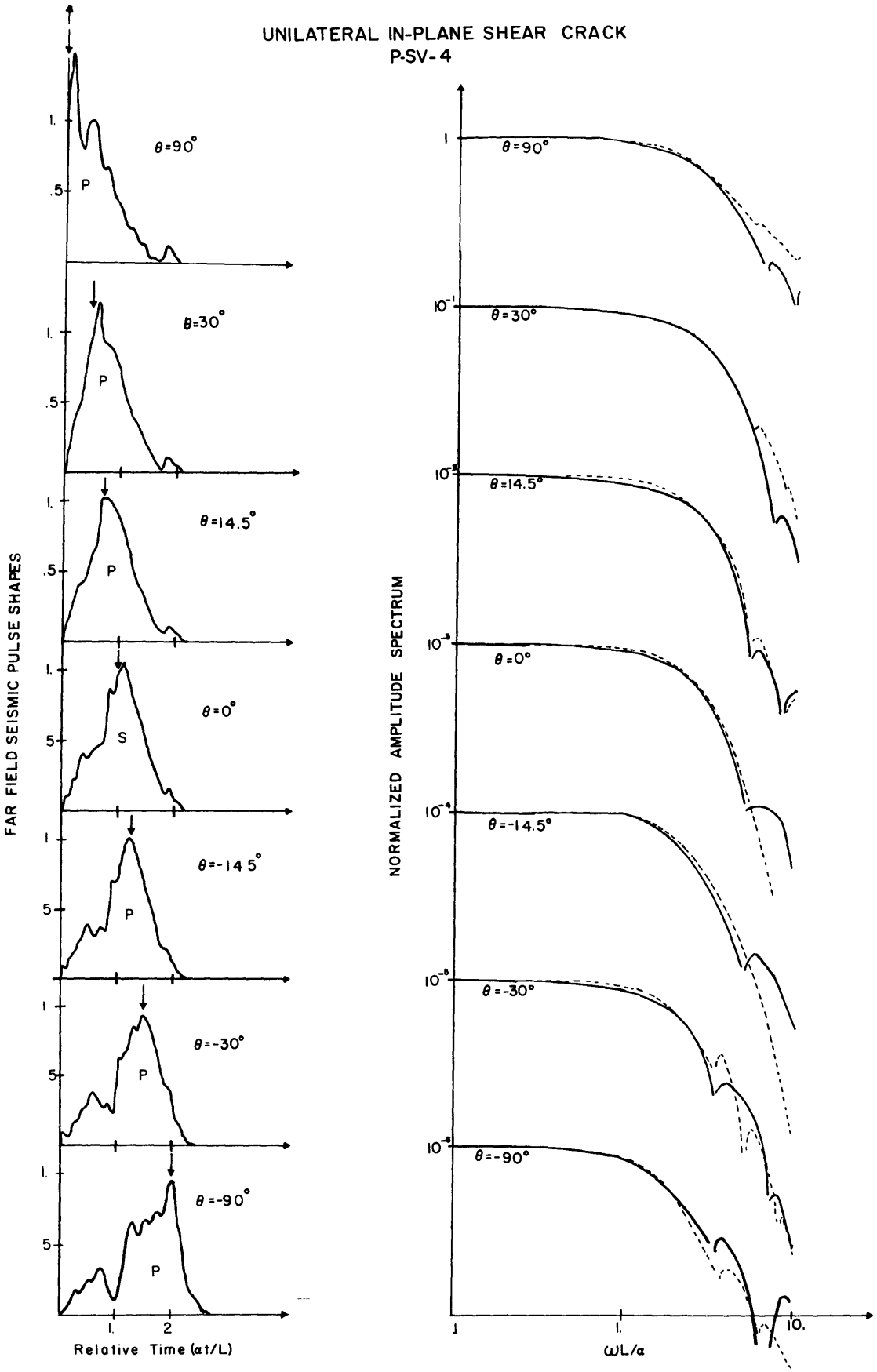

Figure 4.32. Same as Figure 4.14 but for case P-SV-4.

UNILATERAL IN-PLANE SHEAR CRACK

P-SV-5

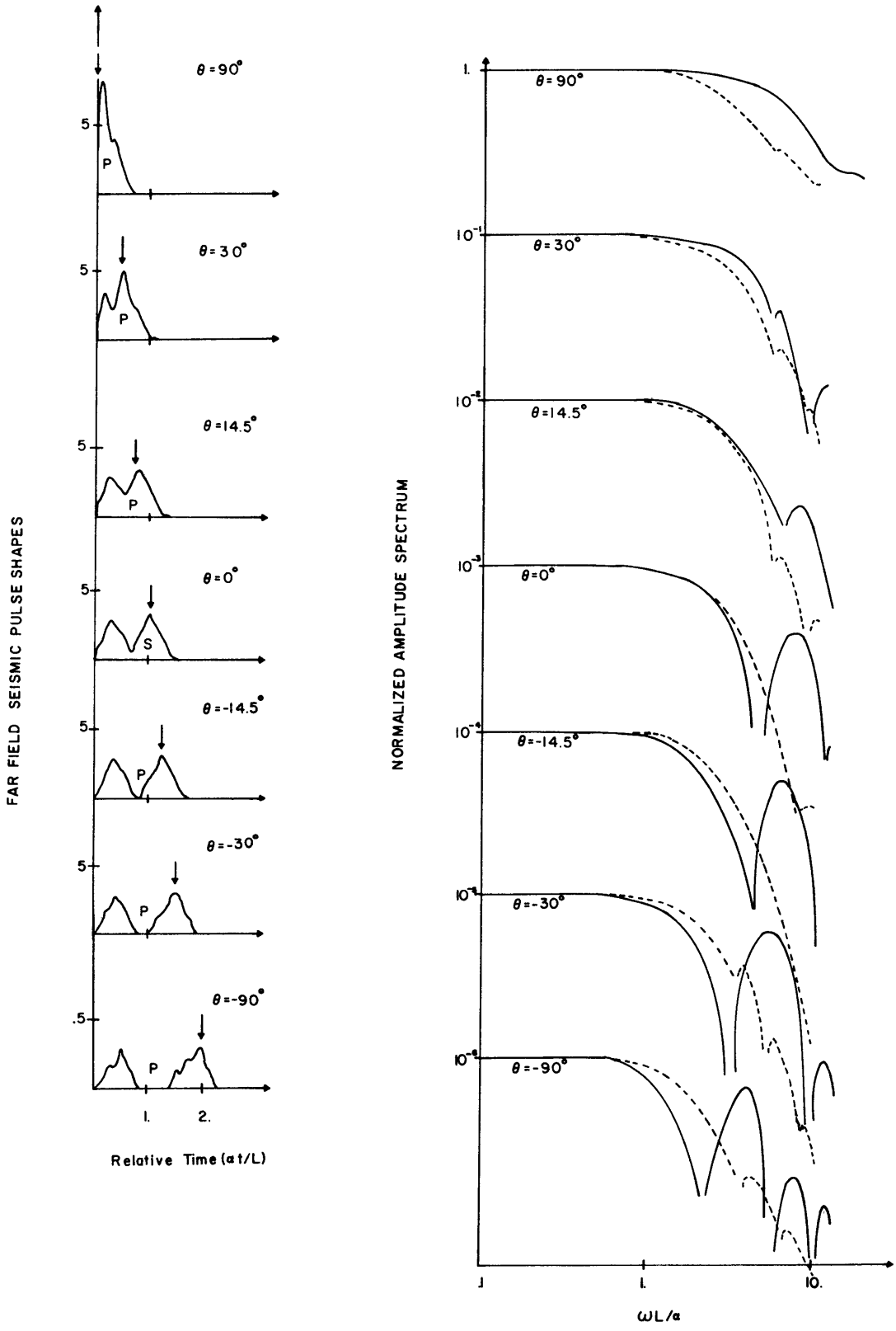

Figure 4.33. Same as Figure 4.14 but for case P-SV-5.

to ω^{-2} but segments of ω^{-1} or $\omega^{-3/2}$ can be recognized sometimes, especially for $|\theta| \simeq 90°$. The general features of the spectra are similar to the corresponding cases of bilateral antiplane crack studied before. The unilateral propagation, however, has the effect of sharpening the pulse shape in the direction of propagation and widening it in the opposite direction. This is due to the later arrival of the stopping phase at negative θ from the moving tip. These times are shown by arrows in the figures for the far-field pulse shapes. The pulse is thus narrowest at $\theta = 90°$ and widest at $\theta = -90°$.

So we see that for unilateral propagation of in-plane shear crack, the corner frequency is not significantly different for small $|\theta|$ between cases with and without obstacles. For large $|\theta|$, an intermediate range of frequencies where the spectrum decays proportionally to ω^{-1} is found, but for small $|\theta|$, no such behavior is seen. We shall now compare these theoretical results with some observational results associated with rock bursts in a deep mine.

Spottiswoode and McGarr (1975) studied the far-field displacements and amplitude spectra for many tremors originating in a mining area near Johannesburg, South Africa, using a network of stations on the surface and underground. McGarr (1971) showed that these tremors were due to shear failure due to normal faults. The tremors occurred at depths of about 3.2 km below the stations and had magnitudes ranging

from 0 to 3. The medium was assumed to be homogeneous and isotropic. Attenuation effects were neglected. The free surface was accounted for by dividing the measured ground displacement by 2.

After corrections for instrumental response and average radiation pattern, Figure 4.34 shows the ground displacements and corresponding spectra at a surface station for selected events. For most cases, the high frequency portion of the spectra decay as ω^{-3} but a few cases where it decays as ω^{-2} or $\omega^{-3/2}$ are also found. Using the corner frequencies determined from these spectra, they found the fault-length for many events. They used Brune's (1970) relation between the corner frequency of the S-wave spectra and the fault radius for a circular fault, and Trifunac's (1972) relation for the corner frequency and fault radius for the P-spectra to determine the fault radius. The relation between corner frequencies and radius determined by Brune and by Trifunac differ from those determined by Madariaga (1976) by a factor of 2. (We find that our relation (Table IV) between corner frequency and fault-length is in agreement with Madariaga's). Thus, the fault-lengths determined by Spottiswoode and McGarr will differ from those determined using Madariaga's relations by a factor of 2. From underground in-situ observations in the mines, they actually measure the total extent of the damaged zone for some of the events. In particular, for the event of February 4, 1972 at 22h50m

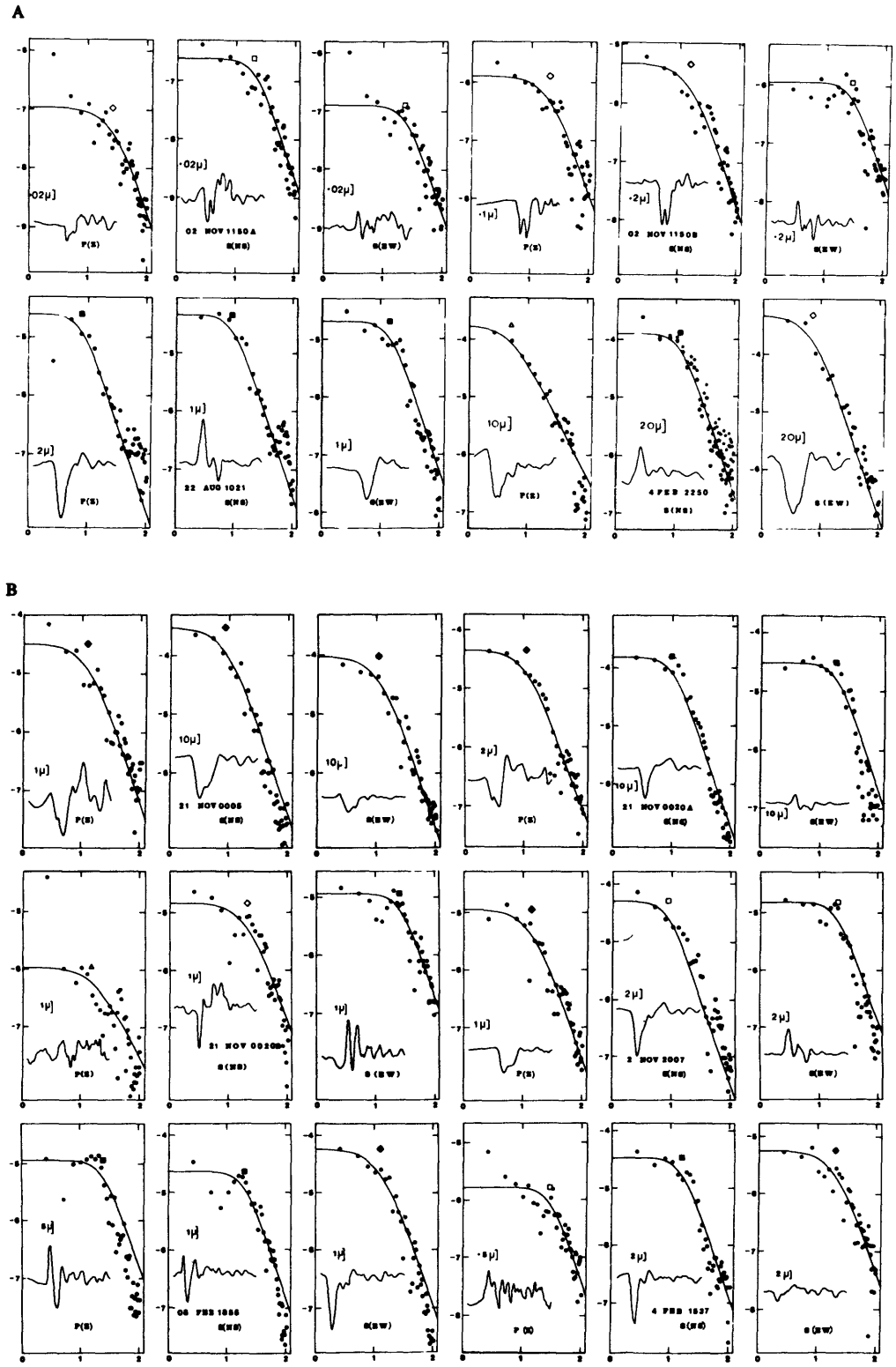

Figure 4.34. Spectra and displacement for ten events studied by Spottiswoode and McGarr (1975), for P (vertical), S (north-south, and east-west) waves.

(South African Standard Time), it was found that there were four sections, each 5-20 meters long, where damage occurred in widely separated regions between which no damage occurred. They appear as if the rupture propagated through the entire length leaving a fracture only in weak regions and no scar in strong parts (just as predicted by our cases SH-1, -2, P-SV-1, -2, -5). The total extent of the damaged region was observed from the field measurements to be about 1/2 km. Using Brune's formula and the S-wave corner frequency, Spottiswoode and McGarr determined the fault radius to be 310 meters and using Trifunac's formula and the P-corner frequency, they found the fault radius to be 350 meters. If we use Madariaga's relation, we would get the fault radius to be about 150-180 meters long.

Madariaga's relation between corner frequency and fault radius is for bilateral propagation of an in-plane shear crack with rupture velocity $.9\beta$. From figure 4.28 we can find the relation between corner frequency and fault length for smooth unilateral propagation of an in-plane shear crack with rupture velocity . This relation is found to be approximately

$$\frac{\omega^P L}{\alpha} \approx 2.0$$

where ω^P = P-corner frequency, L = <u>total</u> length of fault. Using this we would get the same result for the fault length as found by Madariaga's relation. However, if the rupture

propagation for the rockburst was bilateral, and had the speed α, then we would get the fault length to be the same as that found by Brune's formula and by Trifunac's formula. Since in that case the corner frequency-fault length relation would be the same as that found by Trifunac. Spottiswoode and McGarr concluded that the total extent of the underground damaged zone was found to be about the same as that deduced from the corner frequencies. If the rockbursts are regarded as bilaterally propagating in-plane shear crack with rupture velocity α, then this conclusion is justified.

The fault-plane solutions for rockbursts were not given by Spottiswoode and McGarr so we cannot find $|\theta|$ at the station for the events. Comparison of the shapes of the P-pulses in Figure 4.34 with that for the case P-SV-5 which most closely resembles the event of 4 February at 22h50m indicates that $|\theta|$ could not have been very large for this event, at the station under consideration. (Also, note that due to the double-couple radiation pattern, no P-wave is seen at $\theta = 0°, \pm 90°$, which reinforces the argument that θ cannot be too close to +90° or -90°.

Spottiswoode and McGarr have pointed out that they did not find any intermediate segment, in the far-field spectra, with ω^{-1} decay as Brune (1970) suggested for complex ruptures (multiple events). Our computed results agrees with this observation. We have noted earlier that except for large $|\theta|$, the segments with ω^{-1} decay are not seen in any case.

Thus, we find that two important conclusions of our theoretical results are in harmony with the observations of Spottiswoode and McGarr.

(i) When rupture propagates through a region of variable strength, it propagates through the entire region, leaving a fracture in the weak zones and no scar in the strong zones.

(ii) No segment of spectral curve with ω^{-1} decay is seen except for the $|\theta|$ near 90°.

From our theoretical results, we conclude that corner frequency alone cannot distinguish between a rupture with and without obstacles that never break. However, the far-field wave forms can easily distinguish them. Examination of the P wave form for several events including that of February 4 at 2250 (Figure 4.34) show a marked resemblance with the wave-form calculated for $\theta = \pm 14.5°$ in the cases P-SV-1, P-SV-2 and P-SV-5. We also conclude that the corner frequency is related to the length of time required for rupture rather than fault length.

4.3 Arrest Mechanism for Rupture Propagation

A very important problem in seismology is the understanding of how rupture propagation stops. Husseini et al. (1975) have suggested two mechanisms by which a semi-infinite antiplane shear crack can stop. In one of them, a crack-tip stops propagating by encountering a region of higher fracture energy. This is called the "fracture energy barrier" arrest mechanism. The other is called "seismic gap" arrest mechanism and is that the initial stress is confined in a finite region, and once the tip propagates into regions where the pre-stress doesn't exist, it will slow down and eventually stop. For a semi-infinite antiplane shear crack, Husseini et al. found the stopping position of the crack-tip for various cases. We shall study the same cases for finite, shear cracks and compare our results with those of Husseini et al.

Let us first discuss in more detail, the "seismic gap" arrest mechanism. Husseini et al. have considered a two-dimensional, semi-infinite antiplane shear crack, as shown in Figure 4.35. The tip of the crack is at x', say, at time t. The specific surface energy γ, along the crack plane is taken as a constant. To simulate the finiteness of the available strain energy, they limit the region of stress drop $T(x_1)$ to the region (-a,b). The regions outside this interval are not able to supply any stress drop to the crack-tip as the tip moves through it. Husseini et al. have shown that

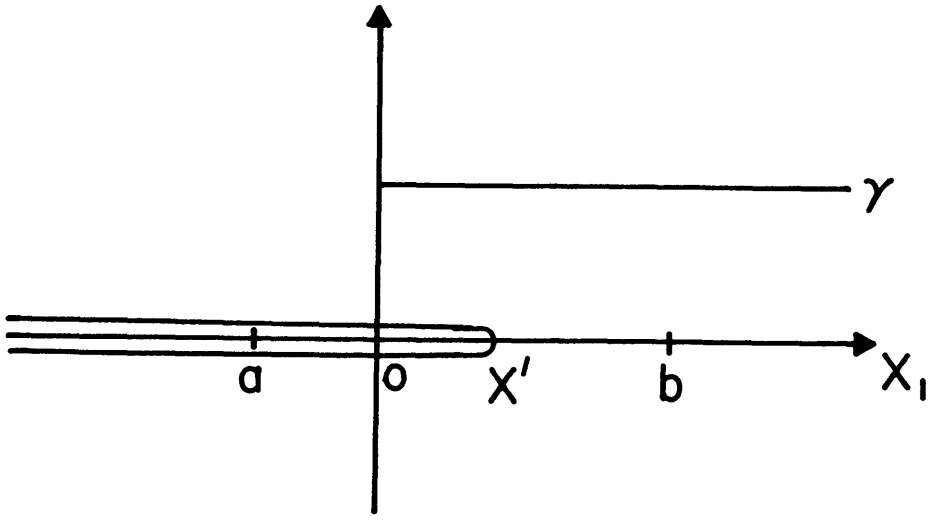

Figure 4.35. Seismic gap arrest mechanism. The initial stress is limited to the region $-a<x_1<b$. γ, the specific surface energy, is a constant.

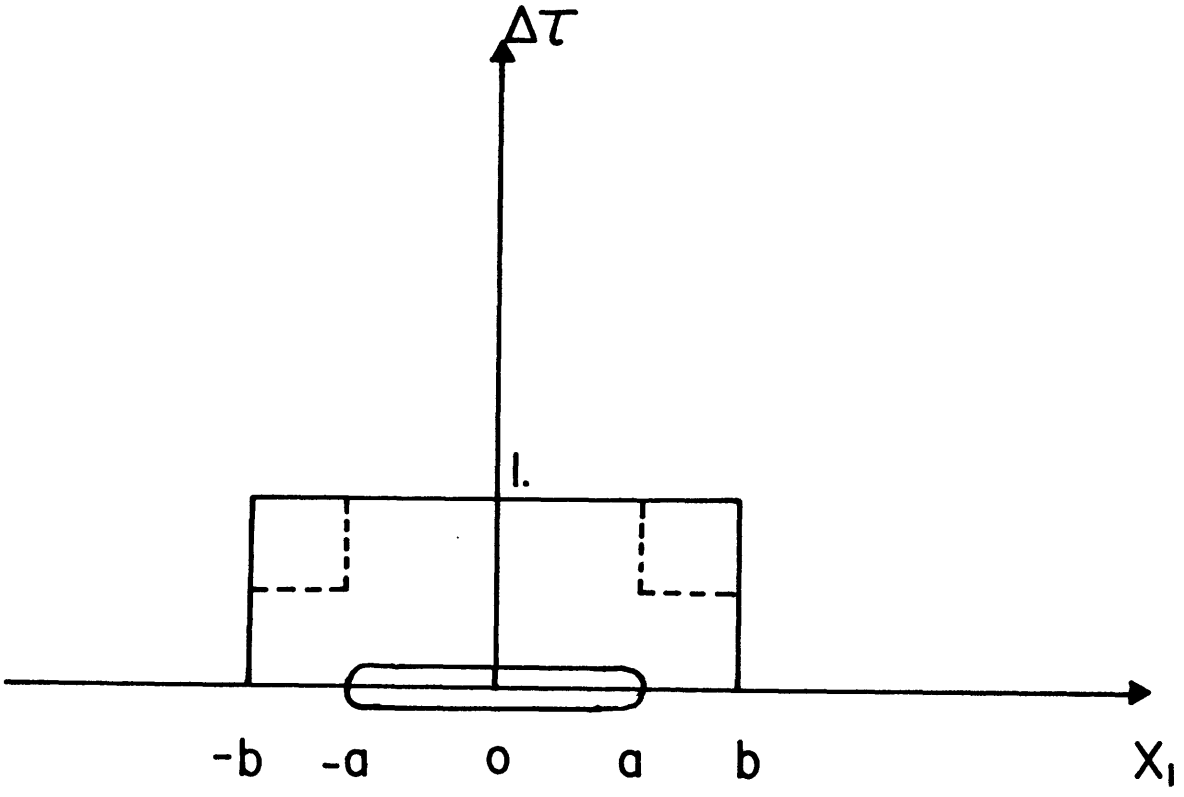

Figure 4.36. Crack geometry and initial stress distribution for the cases U (solid line) and L (dotted line).

the tip will pass the point $x_1=b$ and continue to propagate for some distance through the region free of stress-drop before it eventually stops. The stopping position of the tip depends on the distribution of the stress drop $T(x_1)$. Husseini et al. have considered the following three forms of $T(x_1)$.

(i) Uniform box-car loading "U".

$$T(x_1) = T_o, \quad -a<x_1<b$$
$$= 0 \qquad \text{outside this interval,}$$

To being a constant.

(ii) Linearly decreasing load "L"

$$T(X_1) = 0 \qquad x_1<-a$$
$$= T_o \qquad -a<x_1<o$$
$$= T_o(1 - x_1/b), \quad o<x_1<b$$
$$= 0 \qquad x_1>b$$

(iii) Parabolically decreasing load: "P"

Same as case (ii) except in the interval $o<x_1<b$ where $T(X_1) = T_o(1 - x_1^2/b^2)$

Consideration of a semi-infinite crack gives an approximation to unilateral propagation of finite crack without taking into account the multiple reflections from the crack tips. The motion of the crack-tip is determined using the equation of motion (3.11) together with (3.9) and (3.10). They use Griffith's fracture criterion, i.e. γ is assumed to be the material constant, as their fracture criterion.

For the case of uniform box-car loading, they find an analytical expression for the stopping position given by

$$x_R = \frac{(a+b)^2 T_0^2}{2\pi\mu\gamma} + \frac{b-a}{2} + \frac{\mu\pi\gamma}{8 T_0^2}$$

where μ = modulus of rigidity. For the other two cases, they are unable to find exact expressions for x_R, but give an approximate expression for the case when $b \gg a$,

$$x_R = C\, b^2 T_0^2 / \pi\mu\gamma$$

where C = 1/2 for uniform box-car loading

= 1/8 for linear loading

= 2/9 for parabolic loading.

In all cases, they find that the tip "overshoots" into the unstressed region before it stops. This is a very interesting property of the crack-tip which has no inertia but is able to overshoot into regions free of prestress.

Let us study the "seismic gap" arrest mechanism for bilateral propagation of finite anti-plane and in-plane shear crack. We shall consider the case of uniform box car loading "U" and linearly decreasing loading "L". The crack geometry and the positions a and b are shown in Figure 4.36. Thus 2a is the initial crack length and 2b is the length of the prestressed region. Let us solve the problem for the case S = 1.0, where $S = \frac{\tau_u - \tau_0}{\tau_0 - \tau_f}$, τ_u being the limiting rupture

stress, τ_f = final stress on crack, and τ_o = initial stress on crack.

We shall use the method described in Chapter II and Chapter III to solve the problem. Since we are studying bilateral crack properties we do not expect to get the same stopping position as they did for the antiplane crack. However we would like to compare for both modes of crack properties, the general features of the solution — in particular, the overshoot of the crack-tip into the unstressed region, the two cases, "U" and "L".

The initial crack length is taken as the critical crack length required for the crack to start propagating for a given S. Table III shows this critical crack-length as a function of S for the in-plane shear crack. For S=1, $2L_c/d$ = 2.80. We take the closest higher integer for the number of grids to represent critical crack length, so that $2L_c/d = 3$. For the antiplane case, we find also the same critical crack length $2L_c/d = 3$ for S=1. We take the total length of the prestressed region (which by the principle of superposition discussed in Chapter II, is the same as the region supplying stress-drop to the crack-tip) 2b = 2L/d = 5. In Figure 4.36, the form of $T(x_1)$, the normalized stress-drop, for the case of uniform box-car loading (U) is shown by the solid line and for the linearly decreasing load, (L) by the dashed line. Figure 4.37 shows the position x_1/d of the right crack-tip (the left one moves in exactly the

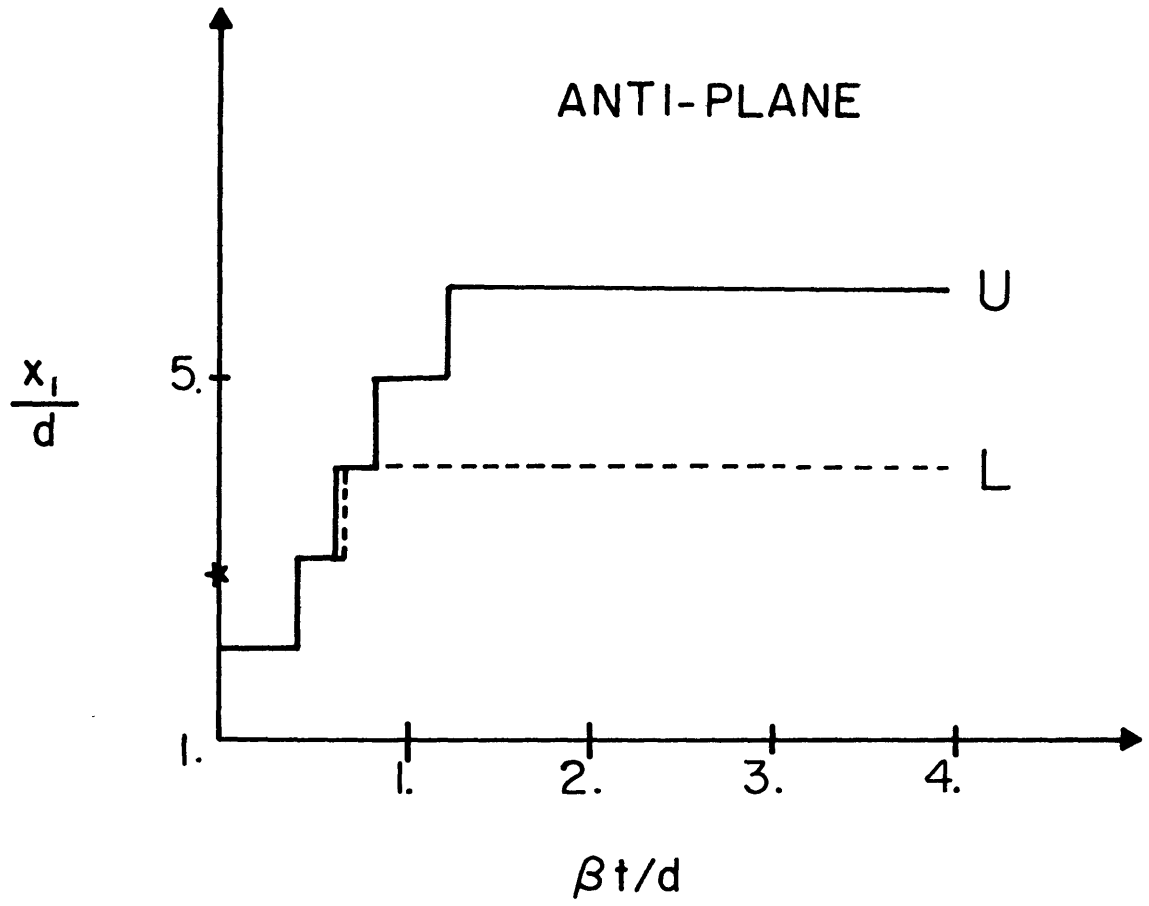

Figure 4.37. Position of the crack-tip as a function of time for the cases U and L for the bilateral, antiplane shear crack, starting from the Griffith critical length.

same way as the right one, in the opposite directions) as a function of time $\beta t/d$, for the antiplane shear crack, for the cases U and L. For both cases, the tips overshoots and move into the unstressed region for some distance before they come to a stop. For the case U, the tips travel farther into the unstressed region than for the case L, in agreement with Husseini et al. Figure 4.38 shows the same problem solved for the finite, in-plane crack. The time-axis is now $(\alpha t/d)$. Again the crack-tips exhibit overshoot and travel further into the unstressed region for the form of stress-drop given by U than that given by L.

Thus, the "seismic gap" arrest mechanism of Husseini et al. holds for finite cracks as well and the tips exhibit overshoot. However, their stopping positions are only very approximate so that their "strong" relation between fracture energy, stress-drop and fault-radius (which they take as approximately equal to x_R, and which is only valid for $b \gg a$) is also a rough approximation. On the other hand, using our method of solution we can find the stopping position of the crack-tips for all values of a and b, without the restrictive condition $b \gg a$, for unilateral and bilateral propagation of truly "finite" in-plane and antiplane shear cracks.

Let us now consider the "fracture energy barrier" arrest mechanism. Husseini et al. have shown that for a semi-infinite antiplane crack if the fracture energy Υ increases in the form of a step-function, the initial stress distribution being

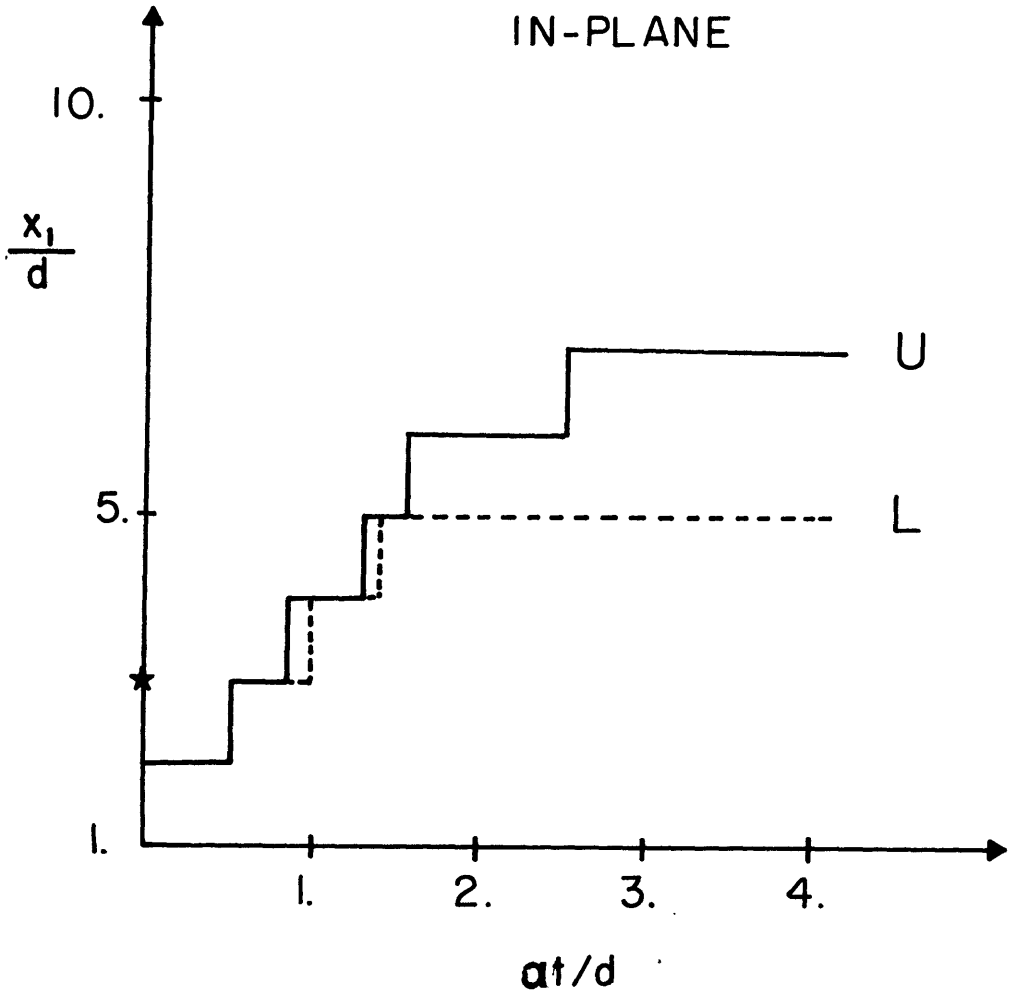

Figure 4.38. Same as Figure 4.37 for the in-plane shear crack.

uniform over the crack-plane, then either the crack tip velocity immediately becomes zero at that point, or continues to propagate indefinitely. Figure 4.39 shows the crack, the region of stress drop $T(x_1) = T_o\, H(x_1 + a)$ and the point $x_1 = b$ at which there is a jump in γ equal to $\gamma+\Delta\gamma$. If the condition

$$\frac{\mu\pi}{2T_o}\left(\gamma+\Delta\gamma\right) \geq (a+b)$$

is satisfied, the tip will stop immediately at b. Otherwise, it will never stop.

For fixed a and b, the jump $\Delta\gamma$ will determine if the tip stops immediately or goes for ever. If $\Delta\gamma$ is very large, the tip will stop. (Note that the reason why the crack-tip is able to stop immediately is because it has no inertia. This is in contrast to a moving dislocation which has an "effective mass").

We shall study the "fracture energy barrier" arrest mechanism for bilateral, propagation of finite, in-plane shear crack, the initial stress distribution being uniform. Andrews (1976) gives the relation for the Griffith critical length L_c required for a crack to start propagating for a given γ. In Table III (section 3.5) we determined the values of $2L_c/d$ for different S. This relation gives the <u>static</u> critical length, i.e. the loading is applied quasi-statically. For the case when the loading is applied in a finite time (dynamically)

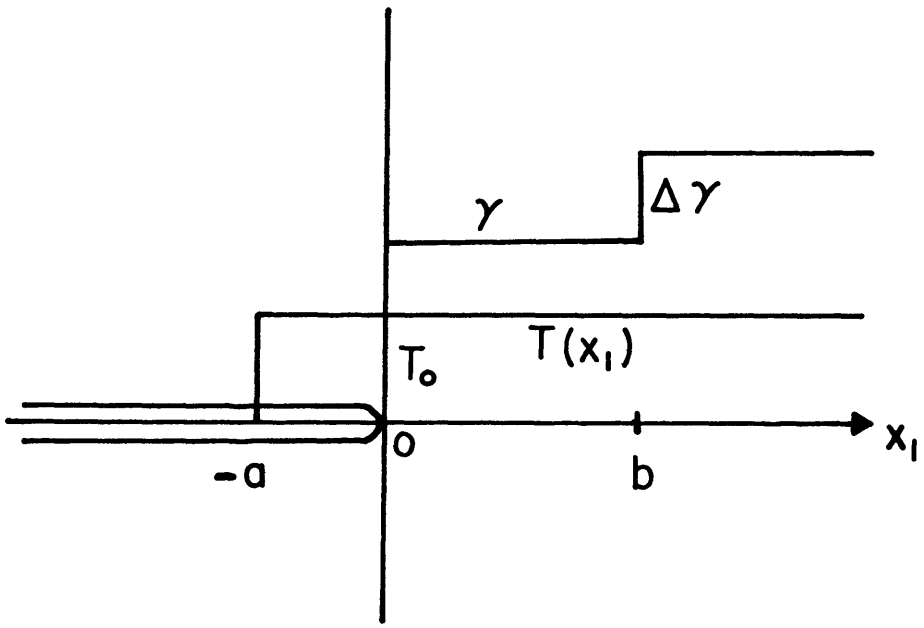

Figure 4.39. Fracture energy barrier arrest mechanism. The initial stress distribution is uniform and there is a jump in Υ to $\Upsilon+\Delta\Upsilon$ at $x_1=b$.

e.g. when a stress wave is made to impinge on the crack, we find dynamic critical length by making trial runs on the computer, using Hamano's criterion which is equivalent to Irwin's criterion as well as to Griffith's for zero rupture velocity (Chapter III). This dynamic critical length is shown in Table V for various values of S.

Table V

S	$2L_c/d$
1	3
2	6
3	13

We find a good agreement between $2L_c/d$ found in Table III (section 3.5) and Table V. Figure 4.40 shows the value of L_c/d against S for the dynamic case. The curve joining these points give the criterion for a crack to stop or continue propagating, from the consideration of whether or not the stress-intensity factor is high enough to cause rupture. Let us consider that S changes along the fault-plane. We plot this value of S as a function of distance from the crack-tip in Figure 4.40. Then if this curve lies above the L_c/d vs. S curve, the crack will stop and if it lies below, the crack will propagate. As a test of this criterion, we ran three cases A, B, C shown in Figure 4.40. As expected, for case A the crack does not stop while for cases B and C it stops.

Figure 4.40. Plot showing L_c/d versus S.

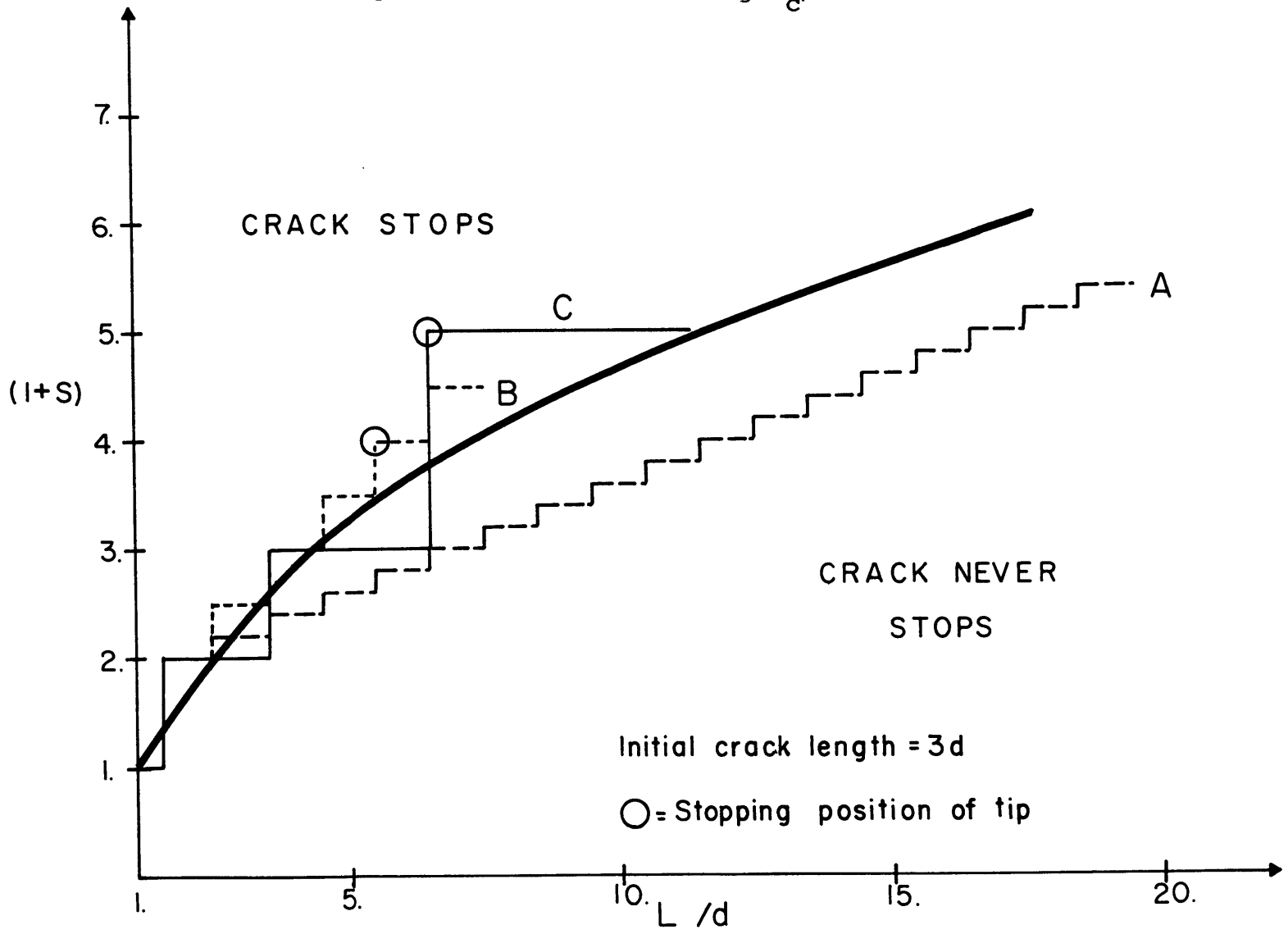

It is found that when the crack stops, (case B and C), it stops immediately. Qualitatively, our result agrees with that of Husseini et al. For a given initial crack length and position at which there is a jump in S, the magnitude of the increase in S determines whether the crack stops or not. Since our criterion is for a finite (in-plane shear) crack, we believe it to be more useful in actual application to stopping of faults in the earth, than that of Husseini et al.

In order to study the effect of two stopping mechanisms discussed above on the slip functions, we compare the following two cases:

Case (a): bilateral propagation of in-plane shear crack along the fault in which the parameter S = 1. The appropriate initial crack length $2L_c$ is 3d (Table III), d being the grid length. The initial stress distribution is taken as shown by the dotted line (case L) in Figure 4.36, i.e. the stress decreases linearly.

Case (b): The crack is made to stop abruptly by making the strength parameter S very large, when the crack reaches the same length as the final crack length of case (a), the initial stress distribution being uniform over the fault-plane. For both cases, we implement the frictional arrest of sliding, so that slip stops when the particle velocity reverses sign. The parallel component of displacement at the tip is shown in Figure 4.41 for the

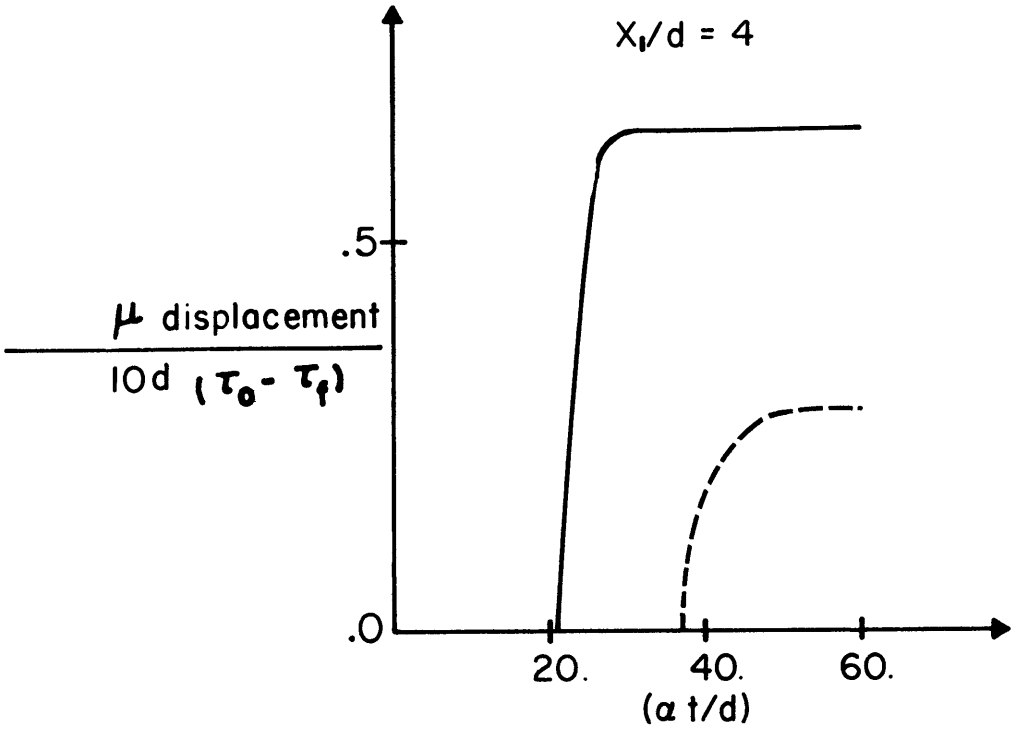

Figure 4.41. Parallel component of displacement as a function of time at the crack tip for the case of when the crack-tip stops abruptly (solid line) and when it stops gradually (dotted line).

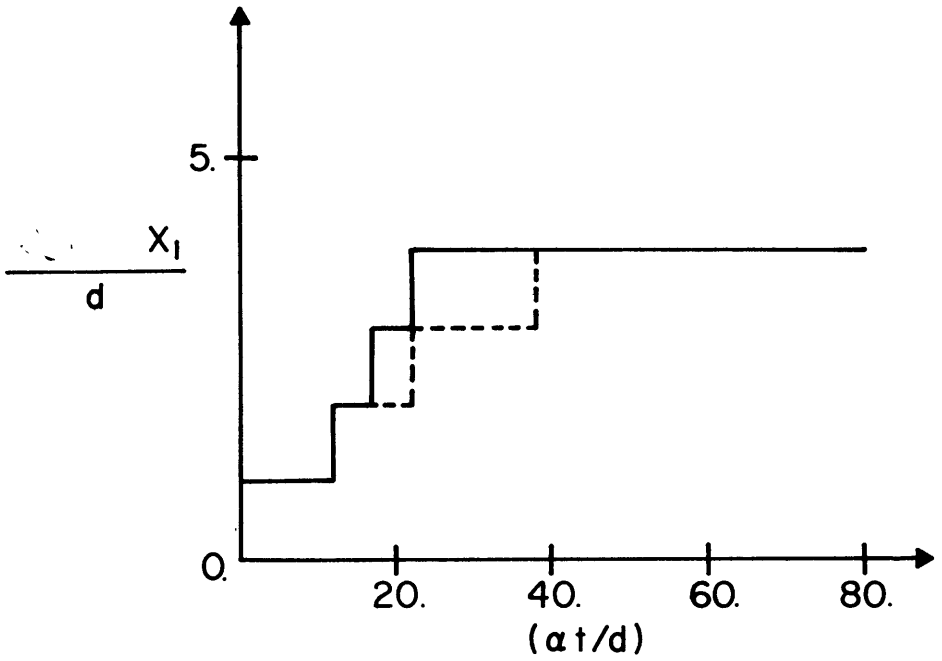

Figure 4.42. Position of the crack tip as a function of time when the tip stops abruptly (solid line) and when it stops gradually (dotted line).

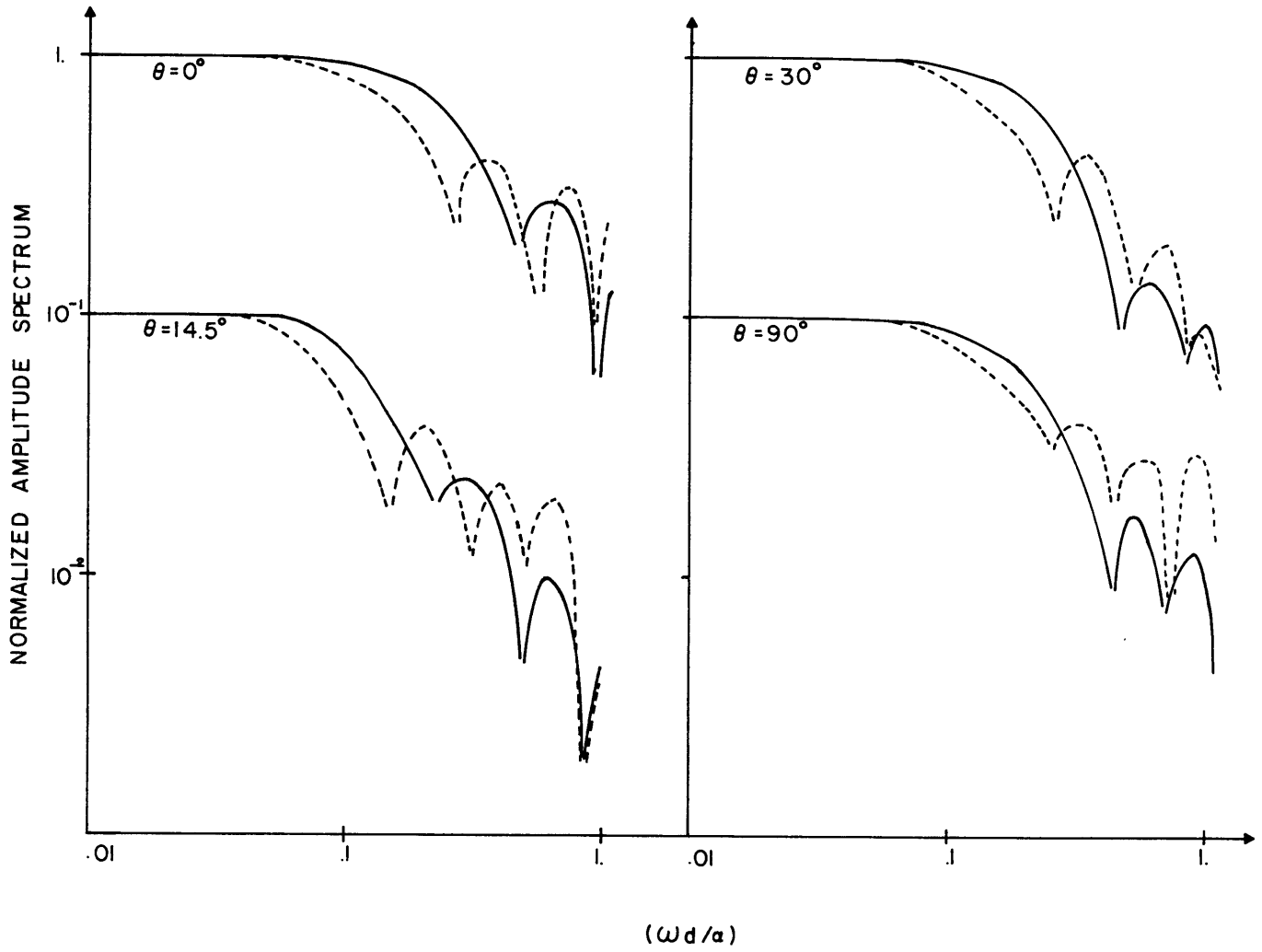

Figure 4.43. Far-field spectra for the case when the tip stops abruptly (solid line) and when it stops gradually (dotted line) for different values .

two cases. For the case of abrupt stopping, the parallel displacement at the tip rises steeply and then stops. For the case when the tip decelerates and stops, the parallel displacement at the tip rises gradually and levels off slowly to its final value. The final value of the parallel displacement for abrupt stopping of the crack is higher than that when the tip decelerates and stops. Near the center of the crack, the two different stopping mechanisms do not affect the parallel displacement significantly. Figure 4.42 shows the position of the crack-tip as a function of time for the two cases . We find that in the case (a) i.e. when the initial stressed region is finite (dotted line in figure) the fault propagation tends to become irregular before it stops, as compared to the case of abrupt stopping (solid line in figure) where it propagates smoothly before suddenly stopping. Figure 4.43 shows the far-field spectra for the two cases, the solid line being for the case of abrupt stopping and the dotted line for the case of gradual stopping. Since the final value of the slip is different for the two cases, the normalizing factor for the amplitude spectra are different. The high frequency asymptote of the spectra for the case of abrupt stopping falls off as ω^{-2}. For the case of gradual stopping, the spectra fall off as ω^{-1}. We find that the same amount of high frequencies are generated in both cases, but the source of the high frequencies for the two cases are different. When the crack propagation is smooth with abrupt stopping, the

stopping phase is the source of the high frequencies. On the other hand, when the crack tip decelerates and repeatedly stops and / goes before coming to a final stop, the irregular rupture propagation generates more high frequencies. It is also found that in the case of gradual stopping, the corner frequency is lowered since the rupture process takes a longer time. The lowering of corner frequency and increased high frequency contents give rise to a wide frequency range over which the spectrum decays as ω^{-1}.

CHAPTER V

Conclusions

In this thesis, we have described a numerical technique to study the displacement and stress-field due to unilateral and bilateral propagation of two-dimensional in-plane and antiplane shear cracks in an infinite medium, which is homogeneous and linearly elastic everywhere off the crack plane. We have shown agreement of our results with available solutions. We incorporated the use of fracture criterion into the method and showed that our "finite stress" fracture criterion is equivalent to Irwin's fracture criterion. For the in-plane shear crack starting from the Griffith critical length, we determined the terminal crack velocity as being sub-Rayleigh or super-shear depending on the strength of the material along the fault. From the sub-shear rupture velocity observed for large earthquakes, we found the value of the apparent surface energy for large earthquakes to be of the order of 10^{10} ergs/cm^2.

We applied our method to the study of the spontaneous propagation of finite unilateral in-plane shear cracks. We found that the displacement field for the unilateral case is more complex than that for the bilateral case. We compared our results with experimental results of unilateral shear crack propagation in foam-rubber and found good agreement.

We also applied our method to study the effect of obstacles on the fault plane. We found that with the corner

frequency alone we could not distinguish between rupture propagation with and without obstacles. However, using the far-field wave-forms for different distribution of obstacles on the fault plane we can distinguish easily between rupture propagation with and without obstacles. For small angle θ between the normal to the fault plane and the direction of wave radiation the fault length deduced from the observed corner frequencies gives the total fault length, including the unbroken parts. The high-frequency asymptote of the displacement spectrum, in most cases, has a ω^{-2} decay, but segments of ω^{-1} or $\omega^{-3/2}$ sometimes exist, especially for $|\theta| \approx 90°$.

Finally, we use our method to study the arrest mechanism of faults for finite, shear cracks. We determine a criterion for stopping of rupture propagation when the strength of the material varies along the crack-plane. For the case where the prestressed region is limited, we find that the crack-tip "overshoots" into the unstressed region for some distance. The stopping is, however, immediate when the greater strength of material acts as a barrier.

It is found that when the rupture propagation stops abruptly, the high frequency spectra falls off as ω^{-2} while when the crack-tip decelerates and slowly stops, there are a wide range of frequencies in which spectra decay as ω^{-1}. The corner frequency is lowered in the latter case simply because the rupture process takes a longer time.

From our studies of the effect of obstacles on the fault plane and of the arrest mechanism of faults, we found that corner frequency is related to the length of time required for the rupture process rather than to the fault length.

This thesis can be extended by solving the problem of a spontaneous rupture propagation for a three-dimensional shear crack and incoporating in the solution the effects of a free surface near or in the path of the propagating crack. Since the computation of Green function for a point source is not a complex problem, the extension to a three-dimensional problem would be straight-forward although time-consuming on computer.

References

Abe, K. (1974a). Seismic displacement and ground motion near a fault: the Saitama earthquake of September 21, 1931. J. Geophys. Res., 79, 4393-4399.

Abe, K. (1974b). Fault parameters determined by near- and far-field data: the Wakasa Bay earthquake of March 26, 1963. Bull. Seismol. Soc. Am., 64, 1369-1382.

Achenbach, J.D. (1973). On dynamic effects in brittle fracture, Mechanics Today, Pergammon Press, New York.

Aki, K. (1968). Seismic displacements near a fault. J. Geophys. Res., 72, 1217-1231.

Andrews, D.J. (1976). Rupture velocity of plane-strain shear cracks, J. Geophys. Res., in press.

Archuleta, R.J. and J.N. Brune (1975). Surface strong motion associated with a stick-slip event in a foam rubber model of earthquakes, Bull. Seismol. Soc. Am., 65, 1059-1071.

Atkinson, C. and J.D. Eshelby (1968). The flow of energy into the tip of a moving crack, Int. J. Fracture Mech., 4, 3-8.

Barenblatt, G.I. (1959). The formation of equilibrium cracks during brittle fracture. General ideas and hypotheses. Axially symmetric cracks, J. Appl. Math. Mech. (PMM), 23, 434-444.

Barenblatt, G.I. (1962). The mathematical theory of equilibrium cracks in brittle fracture, Adv. Appl. Mech., 7, 55-129.

Brace, W.F. and J.B. Walsh (1962). Some direct measurements of the surface energy of quartz and orthoclase, Amer. Mineralogist, 47, 111-1122.

Brune, J.N. (1970). Tectonic stress and the spectra of seismic shear waves from earthquakes, J. Geophys. Res., 75, 4997-5009.

Brune, J.N. (1973). Earthquake modelling by stick-slip along pre-cut surfaces in stressed foam rubber, Bull. Seismol. Soc. Am., 63, 2105-2119.

Burridge, R. (1969). The numerical solution of certain integral equations with non-integrable kernels arising in the theory of crack propagation and elastic wave diffraction, Phil. Trans. Roy. Soc. London, A265, 353-381.

Burridge, R. (1973). Admissible speeds for plane-strain self-similar shear cracks with friction but lacking cohesion, Geophys. J. Roy. Astron. Soc., 35, 439-455.

Burridge, R. and G.S. Halliday (1971). Dynamic shear cracks with friction as models for shallow focus earthquakes, Geophys. J. Roy. Astron. Soc., 25, 261-283.

Boore, D.M., K. Aki, and T. Todd (1971). A two-dimensional moving dislocation model for a strike-slip fault, Bull. Seismol. Soc. Am., 61, 177-194.

Eaton, J.P. (1967). The Parkfield-Cholame, California earthquakes of June-August, 1966, Instrumental seismic studies, U.S. Geol. Survey Profess. Paper, 579, 57-65.

Eshelby, J.D. (1949). Uniformly moving dislocations, Proc. Phys. Soc. Lond., 62A, 307-314.

Eshelby, J.D. (1957). The determination of the elastic field of an ellipsoidal inclusion and related problems, Proc. Roy. Soc., A241, 376-396.

Evvard, J.C. (1950). Use of source distributions for evaluating theoretical aerodynamics of thin finite wings at supersonic speeds, N.A.C.A., Report No. 951.

Filson, J.R. and T.V. McEvilly (1967). Love wave spectra and the mechanism of the 1966 Parkfield sequence, Bull. Seismol. Soc. Am., 57, 1245-1257.

Freund, L.B. (1972). Energy flux into the tip of an extending crack in an elastic solid, Jour. Elasticity, 2, 341-349.

Fukao, Y. (1970). Focal processes of a deep focus earthquake as deduced from long period P and S waves, Bull. Earthq. Res. Inst., 48, 707-727.

Goodier, J.N. (1968). Mathematical theory of equilibrium cracks, in Fracture, Volume II, Academic Press, New York, 1968.

Hamano, Y. (1974). Dependence of rupture-time history on the heterogeneous distribution of stress and strength on the fault plane, (abstr.), EOS (Am. Geophys. Union, Trans.), 55, 352.

Hanson, M.E., A.R. Sanford and R.J. Shaffer (1974). A source-function for a dynamic brittle unilateral shear fracture, Geophys. J. Roy. Astron. Soc., 38, 365-376.

Haskell, N., (1964). Total energy and energy spectral density of elastic wave radiation from propagating faults, 2. A statistical source model, Bull. Seismol. Soc. Am., 56, 125-140.

Husseini, M.I., D.B. Jovanovich, M.J. Randall and L.B. Freund, (1975). The fracture energy of earthquakes, Geophys. J. Roy. Astron. Soc., 43, 367-385.

Ida, Y. (1973). Cohesive force across the tip of a longitudinal-shear crack and Griffith's specific surface energy, J. Geophys. Res., 77, 3796-3805.

Irwin, G.R. (1958). Fracture mechanics, in, Handbuck der Physik, 79, 551-590, Springer-Verlag, Berlin.

Kanamori, H. (1970a). Synthesis of long-period surface waves and its application to earthquake source studies - Kurile Islands earthquakes of October 13, 1963, J. Geophys. Res., 75, 5011-5027.

Kanamori, H. (1970b). The Alaskan earthquake of 1964 - Radiation of long-period surface waves and source mechanism, J. Geophys. Res., 75, 5029-5040.

Kanamori, H. (1971). Seismological evidence for a lithospheric normal faulting. the Sanriku earthquake of 1933, Phys. Earth Planet. Inter., 4, 289-300.

Kanamori, H. (1972). Determination of effective tectonic stress associated with earthquake faulting. The Tottori earthquake of 1943, Phys. Earth Planet. Inter., 5, 426-434.

Knopoff, L. and A.F. Gangi (1959). Seismic reciprocity, Geophysics, 24, 681-691.

Kostrov, B.V. (1966). Unsteady propagation of longitudinal shear cracks, J. Appl. Math. Mech. (PMM), 30, 1241-1248.

Kostrov, B.V. (1975). On the crack propagation with variable velocity, Int. J. Fracture, 11, 47-56.

Lamb, H. (1904). On the propagation of tremors at the surface of an elastic solid, Phil. Trans. Roy. Soc. London, Ser. A., 203, 1-42.

Madariaga, R. (1976). Dynamics of an expanding circular fault, Bull. Seismol. Soc. Am., 66 (3), 639-666.

Niazy, A. (1975). An exact solution of a finite, two-dimensional moving dislocation in an elastic, half-space with application to the San Fernando earthquake of 1971, Bull. Seismol. Soc. Am., 65, 1797-1826.

Richards, P. (1976). Dynamic motions near an earthquake fault: a three-dimensional solution, Bull. Seismol. Soc. Am., 66, 1-32.

Spottiswoode, S.M. and A. McGarr (1975). Source parameters of tremors in a deep-level gold mine, Bull. Seismol. Soc. Am., 65, 93-112.

Starr, A.T. (1928). Slip in a crystal and rupture in a solid due to shear, Proc. Camb. Phil. Soc., 24, 489-500.

Takeuchi, H. and M. Kikuchi (1973). A dynamical model of crack propagation, J. Phys. Earth, 21, 27-37.

Tsai, Y.B. and K. Aki (1968). Simultaneous determination of the seismic moment and attenuation of seismic surface waves, Bull. Seismol. Soc. Am., 59, 275-287.

Tsai, Y.B. and H. Patton (1972). Near-field small earthquakes - dislocation motion, Semi-annual Technical Report No. 1, Texas Instruments, Inc., (prep. for Air Force Office Sci. Res. Contract F44620-72-C-0073).

Trifunac, M.D. (1972). Stress estimates for the San Fernando, California, earthquake of February 9, 1971; Main event and thirteen aftershocks, Bull. Seismol. Soc. Am., 62, 721-750.

Ward, G.N. (1955). Linearized theory of steady high-speed flow, Cambridge Monographs on Mechanics and Applied Mathematics, Cambridge University Press.

Willis, J.R. (1967). A comparison of the fracture criteria of Griffith and Barenblatt, J. Mech. Phys. Solids, 15, 151-162.

Wu, F.T. and H. Kanamori (1972). Source mechanism of February 4, 1965, Rat Island earthquake, J. Geophys. Res., 78, 6082-6092.

Fossum, A.F., and Freund, L.B. (1975). Non-uniformly moving shear crack model of a shallow focus earthquake mechanism, J. Geophys. Res., 80, 3343-3347.

APPENDIX I

Derivation of equation for balance of rates of energies at the tip of a crack.

We shall derive Equation (3.8) following Achenbach's (1973) derivation. Let us consider brittle fracture of a homogeneous, isotropic, elastic solid. Let V be a region of this solid which contains a crack, the tip of which is extending. The volume V is bounded by the external surface S_e, the crack surface S_c and the fracture surface S_f. S_f varies with time but S_e and S_c are fixed. The surface S_c is assumed to be far enough from S_f for all time under consideration, so that the fracture surface S_f does not penetrate S_e.

The displacement and velocity components at a point P in (or on the boundary of) V at time t is given by $u_i(P,t)$ and $\dot{u}_i(P,t)$. The kinetic energy K(t) at time t in V is then

$$K(t) = \frac{1}{2} \int_V \rho u_i(P,t)\ \dot{u}_i(P,t)\ dV,$$

where ρ is the density, and summation extends over the repeated indices. The internal energy U (assuming adiabatic change) at time t is

$$U(t) = \frac{1}{2} \int_V \tau_{ij}(P,t)\ \varepsilon_{ij}(P,t)\ dV\ ,$$

where τ_{ij} and ε_{ij} are the components of the stress and strain respectively. Let P_e be the rate of work of the surface tractions on S_e and P_V the rate of work of the body forces in V, so that the rate of work of the external forces is given by $(P_e + P_V)$.

During the fracture process, energy is extracted from the body. This is due to the fact that there exist internal (cohesive) tractions across the two sides of the crack and when the crack breaks, these cohesive tractions are released. Since the released cohesive tractions are opposite in direction to the relative displacements of the newly formed crack surfaces, their work is negative, and this accounts for the fact that the body loses mechanical energy. Then, the principle of conservation of energy states that the rate F at which mechanical energy is extracted from the region V by the fracture process is equal to the rate of work of the external forces minus the rate of increase of the total energy of V, i.e.

$$F = P_e + P_V - \frac{dK}{dt} - \frac{dV}{dt} \qquad \text{(A1)}$$

Let all the energy extracted from the body in this manner be assigned to surface energy of the newly formed free surface. Let γ_F denote the "specific fracture energy",

which is the amount of energy needed to create a unit area of free surface. The time rate of change of the surface energy can be written as

$$\frac{dD}{dt} = \frac{d}{dt} \int_{S_f} \gamma_F \, ds \ .$$

Then, balance of rates of energies states that

$$F = \frac{dD}{dt} \tag{A2}$$

This condition has to be satisfied at the start of and during rupture. It can be shown that F is the negative of the rate of work of the cohesive tractions acting on the medium in the plane of the crack as the crack propagates. Then,

$$F = - \int_{x(t-t_f)+\varepsilon}^{x(t-t_f)+\varepsilon} \tau_{2j}(x_1,0,t) \ [\dot{u}_j(x_1,0^-,t) - \dot{u}_j(x_1,0^+,t)] \ dx_1 \tag{A3}$$

where x_1 is the direction of crack propagation and x_2 is the direction perpendicular to it (Figure 2.1). $u_j(x_1,0^-,t)$ and $u_j(x_1,0^+,t)$ are the particle velocities of the fracture surfaces for $x_2 = 0^-$ and $x_2 = 0^+$, respectively, $x_1 = x(t - t_f)$ defines the position of the crack-tip as a function of time and ε is a small, positive number. The stresses are zero inside the crack, i.e. for $x_1 < x(t - t_f)$ and the difference between the particle velocities is zero outside

the crack i.e. for $x_1 \geq x(t - t_f)$. In spite of this the integral in (A3) does have a value due to the appearance of square-root singularities in the velocity and stress at $x_1 = x(t - t_f)$.

For a plane two-dimensional crack, the general form of the stress and velocity are

$$\tau_{2j}(x_1,0,t) = \frac{T_{2j}}{\sqrt{x_1 - x(t - t_f)}}$$

and

$$\dot{u}_j(x_1,0^{\pm},t) = \frac{\dot{U}_j^{\pm}}{\sqrt{x(t - t_f) - x_1}} \quad ,$$

respectively, where T_{2j} is called the stress-intensity function and $\dot{U}_j$ the velocity-intensity function. Substituting the relation,

$$\frac{H(v)}{\sqrt{v}} \cdot \frac{H(-v)}{\sqrt{-v}} = \frac{\pi}{2} \delta(v)$$

where $H(v)$ is the Heaviside step function and $\delta(v)$ is the Dirac delta function, in (A3), we get

$$F = -\frac{\pi}{2} T_{2j}(\dot{U}_j^- - \dot{U}_j^+] \qquad \text{(A4)}$$

The above relation has also been obtained by Atkinson and Eshelby (1968) and Freund (1972). In the notation of Atkinson and Eshelby, $F = vG$, where v is the instantaneous velocity of the tip and G is the energy release rate.